Dedicated to My Family

DECLARATION

I hereby declare that the matter embodied in the thesis entitled "**Optoelectronic and Electrochemical Phenomena in Materials at Different Dimensions: A Computational Study**" is the result of investigations carried out by me at the New Chemistry Unit, Jawaharlal Nehru Centre for Advanced Scientific Research, Bangalore, India under the supervision of Prof. Swapan K. Pati and that it has not been submitted elsewhere for the award of any degree or diploma.

In keeping with the general practice in reporting scientific observations, due acknowledgement has been made whenever the work described is based on the findings of other investigators.

Madhulika Mazumder

CERTIFICATE

I hereby certify that the matter embodied in this thesis entitled "**Optoelectronic and Electrochemical Phenomena in Materials at Different Dimensions: A Computational Study**" has been carried out by Ms. Madhulika Mazumder at the New Chemistry Unit, Jawaharlal Nehru Centre for Advanced Scientific Research, Bangalore, India under my supervision and that it has not been submitted elsewhere for the award of any degree or diploma.

Prof. Swapan K. Pati
(Research Supervisor)

Acknowledgements

This thesis would be incomplete without acknowledging the people whose guidance and support enabled me to complete this journey.

I would like to extend my heartfelt gratitude to my supervisor Prof. Swapan K. Pati, without whom, I could have never reached up to where I stand today. His guidance has directed me in the path of wisdom and helped me to develop a deep-rooted passion for learning. His constant encouragement has instilled in me, the power to believe in myself and push my abilities to the utmost. It is exemplary how he has always provided the best of everything, from scientific insight, to computational resources, to a warm and empathetic environment in the lab.

I am also extremely grateful to Prof C.N.R. Rao, for giving me an opportunity to begin a new life of enlightenment at JNCASR. He is always an inspiration to strive for brilliance.

I am thankful to all my course instructors at JNC, Prof. S. Balasubramanian, Prof. H. Ila, Dr. Meher K. Prakash, Prof. M. Eswaramoorthy, Dr. Sridhar Rajaram, Prof. T.K. Maji, Prof. Ranjani Vishwanatha, Dr. Sarit Agasti, Prof. Kanishka Biswas, Prof. Jayanta Halder, Prof. U.V. Waghmare, Prof. Subi J. George, Prof. Sebastian C. Peter, Prof. T. Govindaraju and Prof. Shobhana

Narasimhan, who helped me grow a passion for Science. I am also especially thankful to Dr. Premkumar Senguttuvan for enlightening me with useful concepts pertaining to my work. I would also like to acknowledge my teachers at Lady Brabourne College, especially Prof. P. Ganguly, Dr. Nabanita Karmakar and Prof. S. Chakraborty who schooled me in the various disciplines of chemistry. I thank Dr. S. Roychowdhury, Dr. A. Mitra and Dr. A. Das for their valuable teachings. I take this chance to thank the person who really introduced me to this wonderful world of Chemistry, Sir Mrinal Chakraborty. It was his perseverance and support that fuelled in me the desire to make this subject my vocation.
I cannot overlook the wisdom and counsel I have received from my seniors. My deepest gratitude to Dr. Arkamita Bandyopadhyay, Dr. Swastika Banerjee and Dr. Pralok K Samanta, for their advice and suggestions in tackling difficulties faced in my work.

I am thankful to the Academic Section, the Administration, Library, Complab and CCMS for up-keeping all the facilities here. I thank the NVSH and Student Residence staff, Dhanvantari and Dining Hall, for making my stay hospitable.

I extend warm regards to Anusooya Ma'am and Sohan who never let me feel away from home and always created cherishable moments for me.

I am grateful to all my Int. Ph.D batch-mates, Manaswee, Sreyan, Satyajit, Santu, Niloyendu, Janaky, Sukanya, Lakshay, Rajendra, and Narendra, for being in this together! I thank all my present and past companions at JNC, Sushmita, Srimayee, Arka, Anindita, Anusha, Debdipto, Rajdeep, Sourav, Nivedita, Tarak, Rana, to name a few - for creating a convivial atmosphere here, and the friends that remained - Pratyusha, Gaurav, Sauvik and Soham for those refreshing banters.

I thank my past and present colleagues at lab - Dibyajyoti, Pallavi, Swastika, Bradraj, Arkamita, Ashvini, Sukanta, Pralok, Siam, Amrit, Fransesco, Madhuri,

Nisheal, Shubhajit, Abhiroop, Neha, Sandhya, Raju, Pallavi, Navamani and Ganesh. Special thanks to Abhiroop and Shubhajit for being my pillars throughout, in moments of fun and uncertainty.

I cannot end without acknowledging my family. I extend my deepest gratitude to my grandparents, aunts, uncle and Orko for showering me with affection always. Words fall short, to thank my parents, Ma and Baba, for their endless guidance. I can never thank them enough for making everything possible.

Contents

List of Figures

1 Introduction

The interdisciplinary field of materials science has always been an exciting and rather demanding branch of scientific research ever since metallography came into practice in the late 1800s. A *material* can be any system with distinguished properties which finds use in societal or technical needs. The study of materials divulges many exquisite phenomena at all dimensions. The internal microstructure of systems is solely responsible for these phenomena and though materials at different dimensions are mutually exclusive, at the microscopic level, they are all governed by the laws of Quantum Mechanics. As the title of the thesis suggests, we are interested in studying the electronic, optical and electrochemical properties of materials at 0, 2 and 3 dimensions, computationally.

The discovery of graphene in 2004 ushered in an era of advanced nanosciene. The scientific community was fuelled to conduct research on nanosheets, nanotubes and nanoclusters of Carbon followed by diverse heterostructures. The fundamental allure in exploring these low dimensional systems lies in arriving at "Nanostructures" or pint-sized structures that have enough horsepower to undertake formidable tasks because of their highly tunable properties. Delving deep into the vortex of minutia, one finds new insights into inter-electron interactions in condensed matter systems giving rise to a host of simple to complex interesting

phenomena. From a fundamental point of view, one can achieve tunablility in catalytic, photochemical and optoelectronic properties just by changing the size, composition and morphology of these low dimensional systems.
Nanomaterials can be synthesized by top-down or bottom-up approaches. A lot of research is put into the synthesis and fabrication of nanostructure materials, in solid, liquid and vapor phases.

Low dimensional systems are generally described as systems where the motion and thus the quantum mechanical wave function of electrons is restricted, due to a reduction in the size of one or more spatial dimensions. The motion of electrons (or phonons, or photons) cannot explore the three dimensions of motion, and is confined only to the available dimensions. In the field of condensed matter physics, these systems exhibit many intriguing phenomena. The reduction in spatial dimensions is referred to as Quantum Confinement, which leads to discretization of the energy spectrum traversed by the electrons.

The Quantum Confinement effect can be easily visualised bearing the Heisenberg Uncertainty Principle in mind. The uncertainty in momentum and hence energy increases if the position of the particle becomes more precise, or spatially localised. Based on the number of dimensions confined, we can have different structures as enumerated below.

Structure	**Quantum Confinement**	**No. of free dimensions**
Bulk	0	3
Quantum Wells *superlattices*	1	2
Quantum Wire	2	1
Quantum Dots	3	0

Table 1.1: Quantum Confinement Effect and Structures

Along with dimensions, the energy levels also change from continuous to discrete as we decrease the number of free dimensions and we can define the density

of states as a function of energy as follows.

$$(a) \quad 0D : D(E) \propto E^{1}$$

$$(b) \quad 1D : D(E) \propto E^{-1/2}$$

$$(c) \quad 2D : D(E) \propto E^{0}$$

$$(d) \quad 3D : D(E) \propto E^{1/2}$$

Despite the attractions in the low dimensional world, one simply cannot ignore materials in three dimensions. They are tangible and have more multifaceted and realisable applications, varying from biological/medical equipments to sources of power and energy. Energy storage systems are of great interest nowadays, as, it is necessary to have a constant supply in today's power-hungry world.

In this thesis, optoelectronic as well as electrochemical properties of materials at different dimensions have been studied. Hence, before going into a detailed discussion of the work done, a brief idea about photophysical and electrochemical phenomena is provided.

1.0.1 Photophysical and Optoelectronic Phenomena

Optoelectronics deals with the interactions of light and particles within materials through which the light is propagating. Quantum mechanical studies of light as photons with matter reveals different kinds of electronic excitations (inter- and intraband excitations, excitons, plasmons, etc.) and excitations of phonons, polaritons, magnons, etc. Additionally, there may be localized or non-localized electronic or vibrational states that are related to defects, impurities, or the solid

surface itself. In liquids and gases too, light can induce electronic, vibrational, and rotational transitions within single molecules. If molecules or atoms become adsorbed on a solid surface, their electronic and vibrational properties change. The term photochemical is used if the radiation-induced process occurs mainly non-thermally.

The concept of optoelectronics dates back to the eras of Galileo and Newton who believed that light was "corpuscular". Planck introduced the idea of "quanta"and Einstein explained the photoelectric effect thereafter. The polarization phenomena was recognized eventually and Maxwell proved the presence of mutually orthogonal oscillating electric and magnetic fields in Light. It is not unknown that Light has a dual wave-particle behaviour and the wave equation gives free-space solutions corresponding to electromagnetic waves with a defined velocity - the velocity depending on the electric and magnetic fields. A set of sinusoidal equations may be written :

$$E_x = E_0 e^{[i(\omega t - kz)]} \qquad\qquad H_y = H_0 e^{[i(\omega t - kz)]} \tag{1.1}$$

These two equations describe a wave propagating in the $\hat{z}$ direction with electric field E_x oscillating sinusoidally (with time t and distance z) in the xz plane and the magnetic field H_y oscillating in the yz plane. The two fields are orthogonal in direction and have the same phase. The two fields must oscillate at right angles to the direction of propagation, $\hat{z}$. Electromagnetic waves are transverse waves. The frequency and wavelength of the waves are given by -

$$f = \frac{\omega}{2\pi} \qquad\qquad \lambda = \frac{2\pi}{k} \tag{1.2}$$

where ω is the angular frequency and k is the propagation constant. So,

$$c = f \times \lambda = \frac{\omega}{k} \tag{1.3}$$

The free space equation however shows that,

$$c_0 = \frac{1}{(\epsilon_0 \mu_0)^{1/2}} \tag{1.4}$$

where, ϵ_0 is the electric permittivity, and μ_0 is the magnetic permeability of free space.

The wave nature of light allows us to visualize the electromagnetic spectrum varying from low frequency ($10^3 Hz$) radio waves to high frequency ($10^{20} Hz$) Gamma waves. The visible range lies in $(7.5 - 4.3) \times 10^{14} Hz (400 - 700 nm)$. Optoelectronic devices are designed to absorb and function in specific ranges of the electromagnetic spectrum. With the increasing importance of tapping solar light to be used in photovoltaics, photocatalysts, water-splitting etc, it is customary to know the intrinsic properties of materials which would affect its interaction with light. This is where the particle nature of light grows in importance. The relationship between light and matter consists of the interaction between atoms (or molecules) and photons. An atom either absorbs/emits a single photon, or it does not. The Jablonski diagram illustrates the electronic states of a system and the various transitions involved as a result of its interaction with light. The states are arranged vertically by energy and grouped horizontally by spin multiplicity. Figure 1.1 depicts the various processes resulting from the interaction of light and matter. Here, S_i states have spin multiplicity of one and T_i states are triplet spin states.

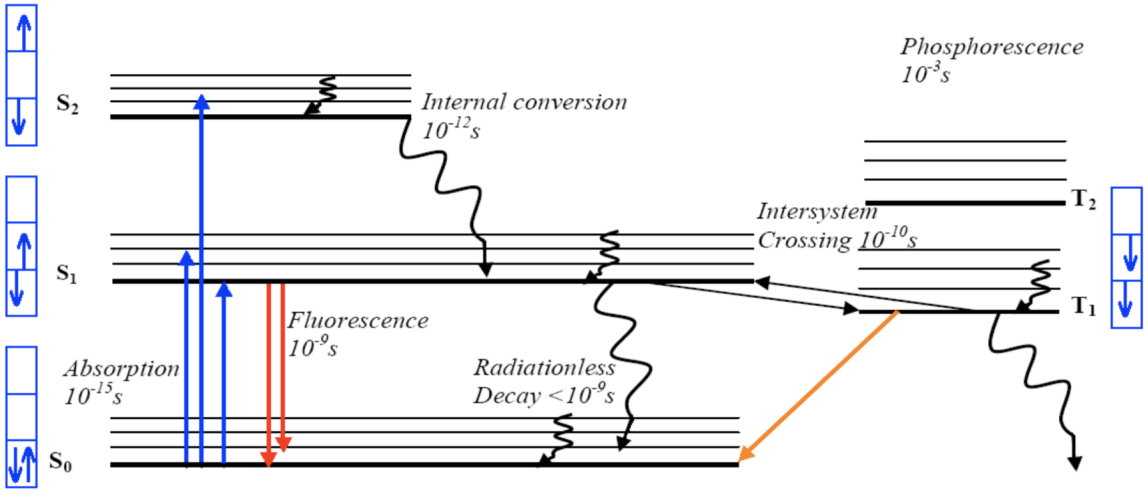

Figure 1.1: Summary of Photophysical Phenomena - The Jablonski Diagram

Absorption

Absorption is the method by which an electron is excited from a lower energy level to a higher energy level. The energy of the photon is transferred to the particular electron. That electron is then transited to a different eigenstate corresponding to the amount of energy transferred. Absorbance is a very fast transition, on the order of 10^{-15} seconds.

Vibrational Relaxation

Once an electron is excited, there are many ways of dissipating the energy. The first is through vibrational relaxation, a non-radiative process. This is indicated on the Jablonski diagram as a curved arrow between vibrational levels. Vibrational relaxation occurs when the energy transferred from the photon into the electron is further transferred to other vibrational modes as kinetic energy. This kinetic energy may stay within the same molecule, or it may be transferred to other molecules around the excited molecule, largely depending on the phase of

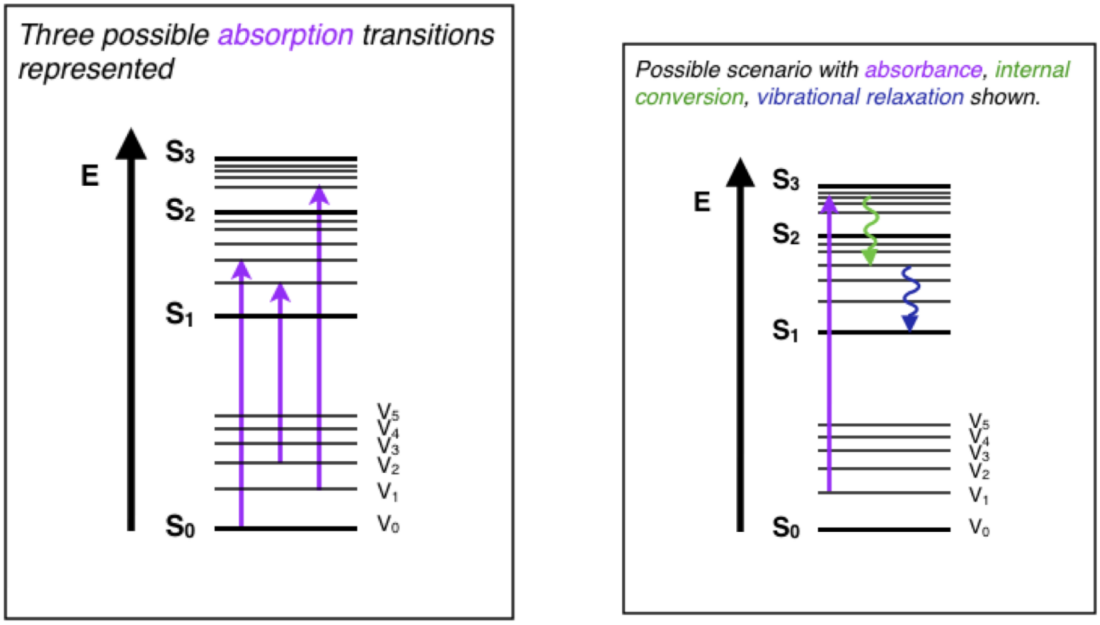

Figure 1.2: (a) Absorption (b) Vibrational Relaxation

the probed sample. This process is also very fast, between 10^{-14} and 10^{-11} seconds. Since this is a very fast transition, it is extremely likely to occur immediately following absorbance. This relaxation occurs between vibrational levels, so generally electrons will not change from one electronic level to another through this method.

Internal Conversion

If vibrational energy levels strongly overlap with electronic energy levels, a possibility exists that the excited electron can transition from a vibration level in one electronic state to another vibration level in a lower electronic state. This process is called internal conversion and mechanistically is identical to vibrational relaxation. It is also indicated as a curved line on a Jablonski diagram, between two vibrational levels in different electronic states. Both vibrational relaxation and

internal conversion occur in most perturbations, yet are seldom the final transition.

Emission

Another pathway for molecules to deal with energy received from photons is to emit a photon, radiatively or non-radiatively. Radiative emission includes **Fluorescence** and **Phosphorescence**. The former is indicated on a Jablonski diagram as a straight line going down on the energy axis between electronic states. Fluorescence is a slow process, of the order of 10^{-9} to 10^{-7} seconds; therefore, it is not a very likely path for an electron to dissipate energy especially at electronic energy states higher than the first excited state. While this transition is slow, it is an allowed transition with the electron staying in the same multiplicity manifold. Fluorescence is most often observed between the first excited electron state and the ground state for any particular molecule because at higher energies it is more likely that energy will be dissipated through internal conversion and vibrational relaxation. At the first excited state, fluorescence can compete in regard to timescales with other non-radiative processes. The energy of the photon emitted in fluorescence is the same energy as the difference between the eigenstates of the transition; however, the energy of fluorescent photons is always less than that of the exciting photons. This difference is because energy is mostly lost in internal conversion and vibrational relaxation, where it is transferred away from the electron.

In case of phosphorescence, the electron which absorbed the photon undergoes an intersystem crossing into an energy state of higher spin multiplicity. As a result, the excited electron can become trapped in the triplet state with only "forbidden" transitions available to return to the lower energy singlet state (Spin-Relaxation). These transitions are kinetically unfavored and thus progress at significantly slower

time scales. Most phosphorescent compounds can store light energy in the form of very slowly degrading excited electron states. If the phosphorescent quantum yield is high, these substances will release significant amounts of light over long time scales.

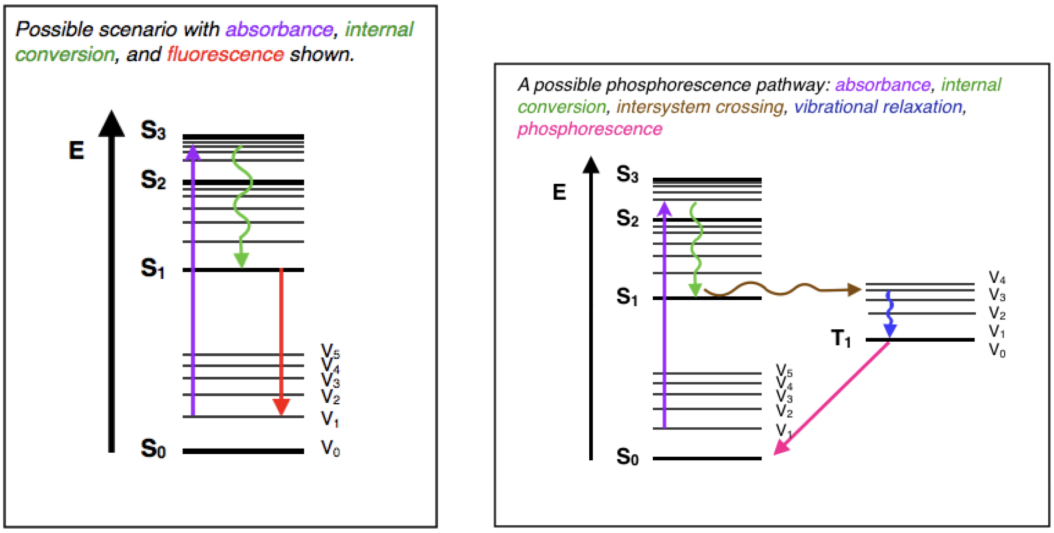

Figure 1.3: (a) Fluorescence (b) Intersystem Crossing and Phosphorescence

Intersystem Crossing

This happens when the electron changes spin multiplicity from an excited singlet state to an excited triplet state or vice versa. Spin-orbit coupling is a necessary condition to allow ISC (Intersystem Crossing). It is indicated by a horizontal, curved arrow from one column to another. This is the slowest process in the Jablonski diagram, as it is a forbidden transition. By coupling vibrational factors into the selection rules, the transition become weakly allowed and is able to compete with the time scale of fluorescence. Intersystem crossing leads to several interesting routes back to the ground electronic state. One direct transition is **phosphorescence**, where a radiative transition from an excited triplet state

to a singlet ground state occurs. This is also a very slow, forbidden transition. Another possibility is **delayed fluorescence**, the transition back to the first excited singlet level, leading to the emitting transition to the ground electronic state.

1.0.2 Optoelectronics in Nanostructures

Physics and chemistry of nanostructures or nanophysics and nanochemistry are relatively new areas of science arisen in last decade of past century after discovery of fullerenes and nanotubes. Main mechanisms of physico-chemical processes affected formation of nanostructured materials and their properties are clearly expressed, in particular, a dielectric permittivity as a principal characteristic of electric, magnetic, acoustic, optic transparency, superconducting, and other properties of nanoceramics and nanometals. Numerous applications are considered including microlasers, photonic crystals, probe microscopy, left-handed materials with negative refraction index, etc.

Generally, the physical properties of any given material can be characterized

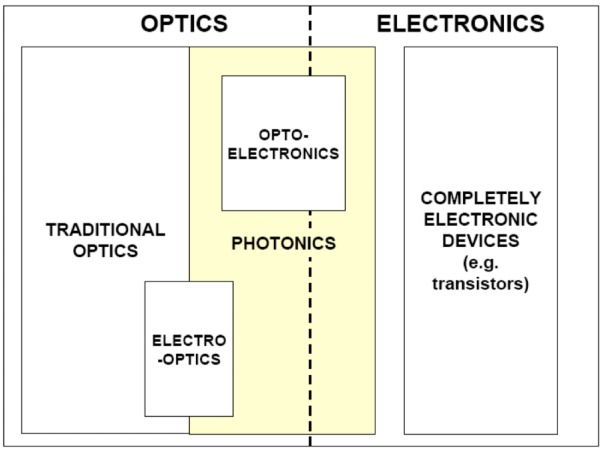

Figure 1.4: Optoelectronic Phenomena

by some critical length, e.g., thermal diffusion length and attenuation distance.

What makes nanoparticles very interesting and endows them with their remarkable properties is that their dimensions are smaller than a relevant critical length. Accordingly, the electron states of nanostructures are quantized, leading to new and usually striking electrical, thermal, magnetic, optical, and mechanical properties at the nanoscale. Thus, nanostructures are of both basic and practical interest since their physico-chemical properties can be tailored by controlling their size and shape at the nanoscale, leading to improved and novel applications.

We now divert our attention to the topic of Energy storage in higher dimensional materials. With conventional energy sources like fossil fuels, gradually running out, we can no longer overlook the need to develop alternate, reliable energy storage systems for clean and sustainable energy. Chemical energy storage systems open up new, intelligent means of interlinking the various energy supply sources for electricity, fuel, gas and heat and of exploiting their respective advantages. On such a note, we should acquaint ourselves with the concepts of Electrochemistry, the science that will help us to store and generate electric power using simple chemical means.

1.1 Electrochemistry

1.1.1 Chemistry and Electricity

The relationship between Chemistry and Electricity dates back to the late 18th century when Alessandro Volta proved the generation of electricity by placing two dissimilar metals on opposite sides of a moistened paper. Swedish chemist, Berzelius named electrified atoms as ions (Greek for travellers). Michael Faraday, was the first to show that there is a quantitative relation between the amount of electric charge and the quantity of electrolysis product.

Electrochemistry is thus defined as the branch of science that studies phenomena arising from combined electrical and chemical effects. And Nature being averse to the loss of symmetry, always succeeds in maintaining a total charge balance. The build-up of positive or negative charge in an electrochemical reaction is compensated by the flow of electricity through an external circuit, that can be quantified in terms of electrochemical potential, current and/or energy density.

Electrochemical Cell

The basic electrochemical cell is comprised by

- Electrodes - surface for Oxidation (Anode) and Reduction (Cathode) reactions,
- Electrolyte - the channel of ionic flow between electrodes and an
- External circuit connecting the electrodes to generate electric current.
- Liquid Junction - a salt-bridge or porous membrane to serve as a contact between electrodes and minimizes diffusion potential that can develop when two phases are in contact and may create interference in the cell potential.

Electrochemical cells can be of two types :

Galvanic	**Electrolytic**
Chemical energy to Electrical energy	Electrical to Chemical Energy
Spontaneous, Reversible, Thermodynamic	Non-spontaneous, Irreversible, Kinetic
Cathode (+); Anode (-)	Cathode (-); Anode (+)
$G^o < 0; E_c^o > 0$	$G^o > 0; E_c^o < 0$
Example : Dry cell, Daniel cell	Electroplating

The work done as described in the subsequent chapter is solely on galvanic cells i.e. the conventional battery.

1.1.2 Working Principle of a Battery

In electrochemical systems, the focus remains on factors and processes that affect transport of charge across the interface between chemical phases (electrodes and electrolyte). Since the electrodes are composed of materials having different electron affinity, a potential difference develops between them. The positive electrode or anode undergoes oxidation to lose electrons, which are taken up by the negative electrode or cathode for reduction. Each electrode forms a **Half Cell**. The magnitude of the half cell potential is an indication of the ease with which electrons move from a negative to positive potential. The summation of the half cell potentials of the cathode(+) and anode(-) equates to the total electromotive force (**EMF)** that can be generated from the cell. And the net free energy change (ΔG) of the two reactions determines the spontaneity of the entire cell reaction. The reference reaction is the Standard Hydrogen Electrode (SHE) which is considered to have a potential of 0 eV. All other half cell energies are just the full cell energy using the SHE as the other half of the battery. The cell potential is observed to vary with concentration of the components. So, to quantify the net potential, under non-standard conditions, the Nernst Equation is utilized.
Under ideal conditons,

$$E_0 = E_{cathode} - E_{anode} \tag{1.5}$$

The change in Gibbs Free Energy, (ΔG) is related to the Electromotive Force (E) as -

$$\Delta G = -nFE_0 \tag{1.6}$$

where n is the number of free electrons exchanged and F is the Faraday constant ($96500 C mol^{-1}$)
Kinetics of electrode reactions play an important role in determining the output of a cell. The amount of current drawn from a cell depends on

1. The rate of electron transfer between the metal and species in solution
2. The transport of material to and from the electrode interface.

The more sluggish the kinetics the lower is the current in which case, a larger activation overpotential would be needed. According to the famous Marcus Theory of electrode kinetics, there are two possible mechanisms for electron transfer (ET).

- Outer Sphere ET : two chemical species undergo a change in their oxidation states through electron hopping but there is no structural deformation.

- Inner Sphere ET : the chemical species undergo a significant geometrical/structural transformation assists the electron transfer, via breakage or formation of bonds.

The electrochemical properties of electrodes are determined by the intrinsic nature of the selected materials and current techniques include the insertion of working ions into the host lattice along certain crystallographic orientations; thus, elucidating these orientations enhances the ion transportation and the rate capability. Although the crystal structure is an inherent property of a certain material, the crystal parameters can be slightly modified by introducing dopants, that would affect cyclability and specific capacity. Since most battery materials nowadays involve transition metals, the effect of doping can influence the crystal field and induce changes in the electronic structure and electrochemical properties. Site energy, which is the contribution of the enthalpy change (H) to the process of ion intercalation is an important tool to measure the extent of electrodic reactions.

Rechargeable batteries or secondary batteries, such as Li-ion batteries, Na-ion batteries, and Mg-ion batteries, reversibly convert electrical and chemical energy via redox reactions, and store the energy as chemical potential in their electrodes. Although batteries offer a much higher energy density than electric double-layer

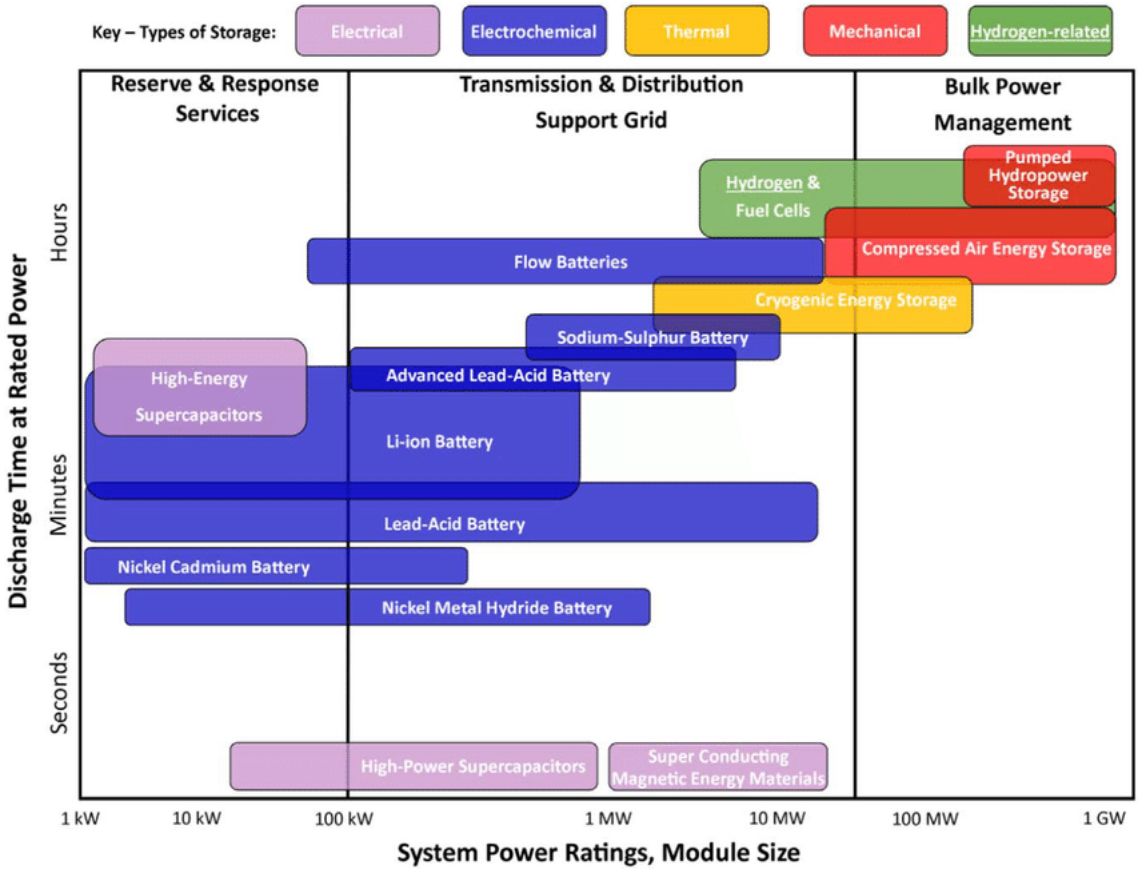

Figure 1.5: Power ratings of different Energy Storage Systems. *Adapted from Hydrogen - A sustainable energy carrier - Kasper T. Moller et al, Progress in Natural Science: Materials International .*

capacitors (EDLCs), supercapacitors, ultracapacitors, or electrochemical pseudo-capacitors, they possess relatively lower power density and shorter cyclic life. A significant number of studies have been conducted on the synthesis and characterization of various electrode materials with large specific surface area and short solid-state transport distance, that promise improved power density as well as a better cyclability.

The energy density and power density of a battery are two essential parameters to judge its practical performance, and they are commonly presented in Ragone plots. The energy density of a rechargeable battery is determined collectively by the specific capacity of electrodes and the working voltage of the cell, which is the

differential potential between the cathode and the anode. The theoretical capacity of electrode materials corresponds to the number of reactive electrons and the molar weight of the designed materials, as expressed by the following equation :

$$C = \frac{n \times F}{3.6 \times M} \tag{1.7}$$

where n is the number of active electrons per formula unit, F is Faraday's constant and M is the molar mass of the species.

Due to their high energy density, batteries have long been used in portable and stationary electronic devices. In the last two decades, after Goodenough's breakthrough, Li-ion batteries have advanced rapidly with increased energy density and long cyclic stability. Current rechargeable batteries based on ion insertion/extraction in electrodes, including Li, Na, Mg and Al ion batteries are being explored. Sadly, devices based on metallic sodium, magnesium, or aluminum have lower energy densities and operating voltages than those with lithium ions. The endeavour of the scientific community now, is to improve upon the performance of these systems to achieve longevity coupled with good performance at affordable rates.

1.2 Computational Methods

This section is devoted to providing an overview about the theoretical methods employed in our calculations. First Principles Density Functional Theory has been the indispensable tool in all calculations. Before moving on to the works done, it is beneficial to be familiarized with the rungs of the ladder of this theory for a smoother understanding[1–4].

1.2.1 The Many Electron Problem in Quantum Mechanics

The microscopic depiction of matter is indeed a complex process. In principle, the properties of a system can be obtained by solving the quantum mechanical wave equation governing the system dynamics. Non-relativistically, this equates to solving the time-independent Schrödinger equation, to get the total energy of the system.

$$\hat{H}\Psi = E\Psi \tag{1.8}$$

where $\hat{H}$ is the Hamiltonian operator of the system, Ψ is the total wavefunction and E is the total energy eigenvalue. For an n-electron system, where each particle has a spatial coordinate of r_i, the time-independent, non-relativistic Schrodinger equation is -

$$\hat{H}\Psi(r_1, r_2, ..., r_i, ...r_n) = E\Psi(r_1, r_2, ..., r_i, ...r_n) \tag{1.9}$$

In real systems of N_e electrons and N_n nuclei, the total Hamiltonian would look like :

$$\hat{H} = \hat{T}_e(r) + \hat{T}_N(R) + \hat{V_{ext}}(r, R) + \hat{V_{ee}}(r) + \hat{V_{NN}}(R) \tag{1.10}$$

Expanding which,

$$\hat{H} = -\frac{\hbar^2}{2}\sum_{i=1}^{N_e}\nabla_i^2 - \frac{\hbar^2}{2}\sum_{I=1}^{N_n}\frac{\nabla_I^2}{M_I} - \sum_{i=1}^{N_e}\sum_{I=1}^{N_n}\frac{Z_I e^2}{|r_i - R_I|} + \sum_{i=1}^{N_e}\sum_{j>1}^{N_e}\frac{e^2}{|r_i - r_j|} + \sum_{I=1}^{N_n}\sum_{J>1}^{N_n}\frac{Z_I Z_J e^2}{|R_I - R_J|} \tag{1.11}$$

where, $\hbar$ is the Planck's constant, m and M are the masses of electrons and nuclei respectively, ∇_i^2 and ∇_I^2 are the Laplacians of the coordinates of the i^{th} electron

and I^{th} nucleus. Z_I and Z_J are the atomic numbers of the I^{th} and J^{th} nuclei. r_i and R_I are the spatial coordinates of the i^{th} electron and I^{th} nucleus. r_j and R_J are the spatial coordinates of the j^{th} electron and J^{th} nucleus. e is the electronic charge.

The first two terms describe the kinetic energies of the electrons and nuclei respectively. The third term is the Coulomb attraction term between electrons and nuclei. The fourth and fifth terms describe inter-electron and inter-nuclear Coulomb repulsions respectively.

In practice, this amounts to a formidable task as one has to take into account all the electrons and nuclei involved and the inter-particle electrostatic interactions too. The numerical solution is achievable for a very small number of particles. The difficulty is understandable as we are dealing with a multi-component many-body system, where each component obeys a particular statistics. The full Schrödinger's equation cannot be decoupled into a set of independent equations. Thus, it is necessary to resort to some sensible approximations, so that the Hamiltonian can be solved with more ease.

1.2.2 The Adiabatic Born-Oppenheimer Approximation

The $\hat{V_{ext}}(r, R)$ term prevents us from separating $\hat{H}$ into nuclear and electronic parts, which would otherwise have allowed us to write the molecular wavefunction as a product of independent nuclear and electronic parts. The Born-Oppenheimer Approximation helps to treat electronic and nuclear motions as exclusive processes. It is made possible through the observation that the motion of nuclei is infinitely slower than that of electrons as the nuclear mass is very large compared to the electronic mass. The physical idea is that the light, fast-moving electrons readjust to nuclear displacements instantaneously. This is the reason the approximation produces an electronic Schrödinger's equation for each possible geometrical

arrangement of the nuclei in the molecule. The need is only to know the instantaneous positions of the nuclei, and not how they are moving, in order to find an electronic wavefunction. It is thus, almost accurate to say that the nuclei remain fixed at their coordinates while the electrons explore the charge field created by the nuclei. Now, the entire wavefunction can be decomposed into two parts :

$$\Psi(r, R) = \Psi(r) \times (R)$$

The second ($\hat{T_N}$) and fifth ($\hat{V_{NN}}$) terms of the total Hamiltonian are thus approximated out and we have a "***clamped***" Schrödinger's equation as follows -

$$\hat{H}_e(r, R)\Psi_e = E_e\Psi_e, \tag{1.12}$$

$\hat{H}_e$ being the electronic Hamiltonian :

$$\hat{H}_e = \hat{T}_e(r) + \hat{V_{ee}}(r) + \hat{V_{ext}}(r, R) \tag{1.13}$$

i.e. ,

$$\hat{H}_e = \sum_{i=1}^{N_e} -\frac{\hbar^2}{2m}\nabla_i^2 + \sum_{i=1}^{N_e}\sum_{j>i}^{N_e}\frac{e^2}{|r_i - r_j|} + \hat{V_{ext}} \tag{1.14}$$

The B-O approximation helps to reduce the number of degrees of freedom to deal with, but for real systems, it is still difficult to tackle all the inter-electron interactions. Further approximations are hence required. It was Hartree, in 1928, who first postulated that the many-electron wave function can be written as a product of one-electron wave functions.

$$\Psi(R,r) = \prod_i \psi(r_i) \tag{1.15}$$

It is worth realizing that though solving the Schrödinger's equation is the most fundamental aspect in quantum mechanics, the wave function for a set of coordinates cannot be directly observed. What can be observed and quantified, is in fact, the ***probability*** that n electrons are at a particular set of coordinates. This probability is equal to $\psi^*(r_1...r_n)\psi(r_1....r_n)$, where ψ^* indicates a complex conjugate. Since electrons are indistinguishable particles, the quantity of interest is really the probability that n electrons in any order have the coordinates $(r_1....r_n)$. In other words, we are looking at the density of electrons at a particular position in space :

$$\rho(r) = \psi^*(r_1...r_n)\psi(r_1....r_n)$$

Herein, the many-body wavefunction which was a function of 3n coordinates is intelligently written as a function of only 3 coordinates, $\rho(r)$! Each one particle Schrödinger's equation considers an effective potential that treats the interaction with the other electrons in a mean field approach.

$$-\left(\frac{\hbar^2}{2m}\nabla^2 + V_{eff}^{(i)}(R,r)\right)\psi_i(r) = \epsilon_i\psi_i \tag{1.16}$$

where

$$V_{eff}^{i}(R,r) = V(R,r) + \int \frac{\sum_{j\neq i}^{N}\rho_j(r')}{|r-r'|}dr' \tag{1.17}$$

and

$$\rho_j(r) = |\psi_j(r)|^2 \tag{1.18}$$

The second term is a classical electrostatic potential generated by the charge dis-

tribution $\sum_{j\neq i}^{N} \rho_j(r)$, which does not include the charge associated with particle i. So, the Hartree approximation is self-interaction free. But this effective potential wrongly counts the electron-electron interaction twice, So the correct expression for energy is -

$$E_H = \sum_{n=1}^{N} \epsilon_n - \frac{1}{2}\sum_{i\neq j}^{N} \iint \frac{\rho_i(r)\rho_j(r^{'})}{|r - r^{'}|} dr dr^{'} \tag{1.19}$$

The next step is to minimize the energy with respect to a set of variational parameters in a trial wave function or, alternatively, by recalculating the electronic densities in equation (1.15) using the solutions of equation (1.13), then cast them back into the expression for the effective potential (equation 1.14), and solve again the Schrödinger equation. This procedure can be repeated several times, until self-consistency in the input and output wave function or potential is achieved. This procedure is called **self-consistent Hartree approximation.**

If one has to include the Pauli Exclusion principle to treat electrons as Fermions, the wave function becomes anti-symmetrized and complicated. But it can be expressed as a Slater determinant and this approximation is called **Hartree-Fock** or self-consistent field (SCF). It is fairly reliable for atomic systems, despite ignoring many body correlations.

Thomas and Fermi also proposed that the full electron density was the fundamental variable of the many body problem and derived differential equations for the same. But it was crude and did not include exchange and correlation effects. But it did pave the way for the development of the most successful electronic structure theory - the Density Functional Theory.

1.2.3 The Density Functional Theory

This ground-breaking theoretical approach towards quantum modelling of real systems rests on the framework built by two theorems given by **Walter Kohn**

and **Pierre Hohenberg** in mid-1960.

Hohenberg-Kohn Theorems -

Theorem 1

"*The ground state energy from Schrödinger's equation is a unique functional of the electron density.*"

This means that there is a one-to-one mapping between the ground state wave function and the ground state electron density. A functional is simply a function of another function defining a single number from the parametric function. Mathematically, the Ground state energy,

$$E = E[\rho(r)]$$

Theorem 2

"*The electron density that minimizes the energy of the overall functional is the true electron density, corresponding to the full solution of the Schrödinger's equation.*"

The condition for the correct ground state electron density is described in the second theorem, such that it minimizes the energy functional.

The Schrödinger's equation is now rewritten as

$$E[\rho] = \hat{F}[\rho] + \int dr V_{ext}(r)\rho(r) \tag{1.20}$$

where, ρ is the electron density and $\hat{F}[\rho]$ is the universal functional of density. The next step is to minimize $E[\rho]$. with respect to ρ. A pioneering achievement here was the proposal given by **Walter Kohn** and **Lu Jeu Sham**. According to this, the intractable many-body problem of interacting electrons in a static external potential is reduced to a tractable problem of non-interacting electrons moving in an **effective potential**. The effective potential includes the external

potential and the effects of the Coulomb interactions between the electrons, i.e. the **exchange and correlation interactions** Then,

$$E[\rho] = \hat{T}[\rho(r)] + \frac{1}{2}\int \frac{\rho(r)\rho(r^{'})}{|r_i - r_j^{'}|} dr dr^{'} + \int \rho(r) V_{ext}(r) dr + E_{xc}[\rho(r)] \tag{1.21}$$

The first three terms are the electron kinetic energy, Coulomb interactions between electron pairs and the external potential created by the nuclei. The last term is the **Exchange Correlation** term. The formidability of the initial problem is now reduced largely. The Kinetic energy term is solved as :

$$T[\rho(r)] = -\frac{\hbar^2}{2}\sum_{i=1}^{N} \int \Psi_i^*(r) \nabla^2 \Psi_i(r) dr \tag{1.22}$$

From equation (1.18) a set of differential equations can be obtained which are referred to as the **Kohn-Sham** equations.

$$\left[-\frac{\hbar^2}{2m}\nabla^2 + V_h + V_{ext} + V_{xc} \right] \Psi_i(r) = \varepsilon_i \Psi_i(r) \tag{1.23}$$

V_h is the Hartree potential as described in equation (1.16); V_{ext} is the external potential and V_{xc} is the exchange-correlation term. The wave function $\Psi_i(r)$ corresponds to the Kohn-Sham orbitals. The Hartree potential includes a self-interaction contribution because the electrons described in the KS equations is a part of the total electron density. This unphysical self-interaction is taken care of in the V_{xc} potential. V_{xc} defines exchange and correlation contributions to the single electron equations. It is the functional derivative of the exchange-correlation energy.

$$V_{xc}(r) = \frac{\delta E_{xc}(r)}{\delta \rho(r)} \tag{1.24}$$

For the exact functional, and thus exact local potential, the KS orbitals yield the exact ground state density via equation(1.15) and exact ground state energy via equation(1.20). The Kohn-Sham equations have the same structure as the Hartree-Fock equations with the non-local exchange potential replaced by the local exchange-correlation potential. The KS equations are solved iteratively.
Walter Kohn was awarded the Nobel Prize in Chemistry in 1998 for the development of DFT.

The Exchange Correlation Functional

Despite simplifying the complex many body Schrödinger's equation, one must admit the difficulty in defining the exchange correlation energy(E_{xc}) precisely. The uniform electron gas is the only case where E_{xc} can be known where the electron density is constant at all points. To find the E_{xc}, which is the difference between the exact energy and other contributions, some more approximations are needed. The two most important functionals used in this case are :

Local Density Approximation (LDA)

It is a simple approximation, that uses only the local density to define the approximate XC functional.

$$E_{xc}^{LDA}[\rho(r)] = \int d^3\epsilon_{xc}\big(\rho(r)\big).\rho(r) \tag{1.25}$$

where $\rho(r)$ is the local electron density, and ϵ_{xc} is the exchange and correlation energy per electron of a homogenous electron gas of charge density ρ. Since the density is believed to vary smoothly in space, a summation of local exchange-correlation energy in all regions of space, would give the total ϵ_{xc}. The LDA works well for bulk systems, but fails in cases where electron density is not smooth. LDA has a tendency to under-estimate the exchange energy and over-estimate

the correlation energy.The errors due to the exchange and correlation parts tend to compensate each other to a certain degree. To correct for this tendency, it is common to expand in terms of the gradient of the density in order to account for the non-homogeneity of the true electron density. The LDA also helps in the construction of more sophisticated approximations.

Local Spin Density Approximation (LSDA)

It is a straightforward generalization of the LDA to include electronic spin.

$$E_{xc}^{LSDA}[\rho\uparrow,\rho\downarrow] = \int d^3\epsilon_{xc}\big(\rho\uparrow,\rho\downarrow\big).\rho(r) \tag{1.26}$$

Generalized Gradient Approximation (GGA)

The GGA attempts to incorporate the effects of inhomogeneities by including the gradient of the electron density; as such it is a semi-local method. The GGA XC functional can be written as -

$$E_{xc}^{GGA}[\rho(r)] = \int d^3\epsilon_{xc}\big(\rho,\vec{\nabla}\big)\rho(r) \tag{1.27}$$

GGA gives very good results for molecular geometries and ground state energies. There are 3 basic classes of GGA functionals :

1. Ab-Initio Based : Exchange and correlation parts are calculated individually. eg. **PBE** (Perdew, Burke-Ernzerhorf), **PW91** (Perdew-Wang 1991)

2. Atom Based : Exchange and correlations are calculated separately. But the functional parameters are fitted based on close shell atomic properties. eg. **Becke's** GGA for exchange and **Lee, Yang, Parr's** functional for correlation.

3. Empirical : Exchange and correlation are treated as a whole and parameters are fitted on both atomic and molecular properties. eg. **HCTH** (Hamprecht-Cohen-Tozer-Handy) functional.

There are functionals that are more accurate than GGA and these are :

- Meta-GGA : It includes the second order derivative of the electron density. Examples are **Minnesota functionals**, **TPSS** (Tao-Perdew-Staroverov-Scuseria).

- Hybrid Functionals : A combination of Hartree-Fock exchange and DF correlations are used. $E_{xc}^{hybrid} = \alpha E_x^{HF} + E_c$

  α is a parameter that can be chosen to satisfy some criteria. A very common example is the **B3LYP** functional (Becke -3 - Lee - Yang - Parr) which is widely used in computations. It uses three adjustable parameters to fit values to a molecular database.

Science always succumbs to the temptation of more room for improvement. B3LYP is like a magic functional having one of the greatest contributions in computational chemistry. But it is unsuccessful in applications like polarizability in long chains, excitations using Time-Dependent Density Functional Theory (TDDFT) and also Charge Transfer excitations. This is because, at long range, the exchange potential behaves as $-0.2r^{-2}$ instead of the exact value r^{-1}. Tsuneda et al; worked on this deficiency through an Ewald split of r^{-12} into :

$$\frac{1}{r_{12}} = \frac{1 - erf(\mu r_{12})}{r_{12}} + \frac{erf(\mu r_{12})}{r_{12}} \tag{1.28}$$

such that the first term accounts for short range interactions and the second term treats long range interactions. Yanai, Tew and Handy developed the Coulomb

Attenuating Method - B3LYP (**CAM-B3LYP**) by using two parameters as :

$$\frac{1}{r_{12}} = \frac{1 - [\alpha + \beta.erf(\mu r_{12})]}{r_{12}} + \frac{\alpha + \beta.erf(\mu r_{12})}{r_{12}} \tag{1.29}$$

with the conditions : $0 \leq \alpha + \beta \leq 1; 0 \leq \alpha \leq 1; 0 \leq \beta \leq 1$.

The CAM-B3LYP functional comprises of 0.19 Hartree-Fock (HF) plus 0.81 Becke 1988 (B88) exchange interaction at short-range, and 0.65 HF plus 0.35 B88 at long-range. The intermediate region is smoothly described through the standard error function with parameter 0.33.

The Heyd-Scuseria-Ernzerhof **(HSE)** density functionals are popular for their ability to improve the accuracy of standard semilocal functionals such as Perdew-Burke-Ernzerhof (PBE), particularly for semiconductor band gaps. They also have a reduced computational cost compared to hybrid functionals. These functionals are defined by an overall fraction of Fock exchange and a length scale for exchange screening.

$$E_{xc}^{HSE} = \frac{1}{4}E_x^{SR}(\mu) + \frac{3}{4}E_x^{PBE,SR}(\mu) + E_x^{PBE,LR}(\mu) + E_c^{PBE} \tag{1.30}$$

(SR : short range ; LR : long range)

It cannot be claimed that there is a systematic approach to the exact functional but it is clear that improvements are being made in the underlying functional form which reflects in the description of ground state properties. To summarize, DFT covers a wide range of functionals. The development of approximations to the exchange-correlation functionals over the past 20 years has improved the performance of DFT calculations, which can be schematically represented using the Jacob's ladder (Figure 1.6) and will continue until energy differences can be determined to within 1 kcal/mol ("chemical accuracy"). The numerical cost increases as one climbs, and this may not necessarily bring more information. Most prob-

lems in "computational nanoscience"are performed part way up the ladder, and this situation will probably remain true for some time.

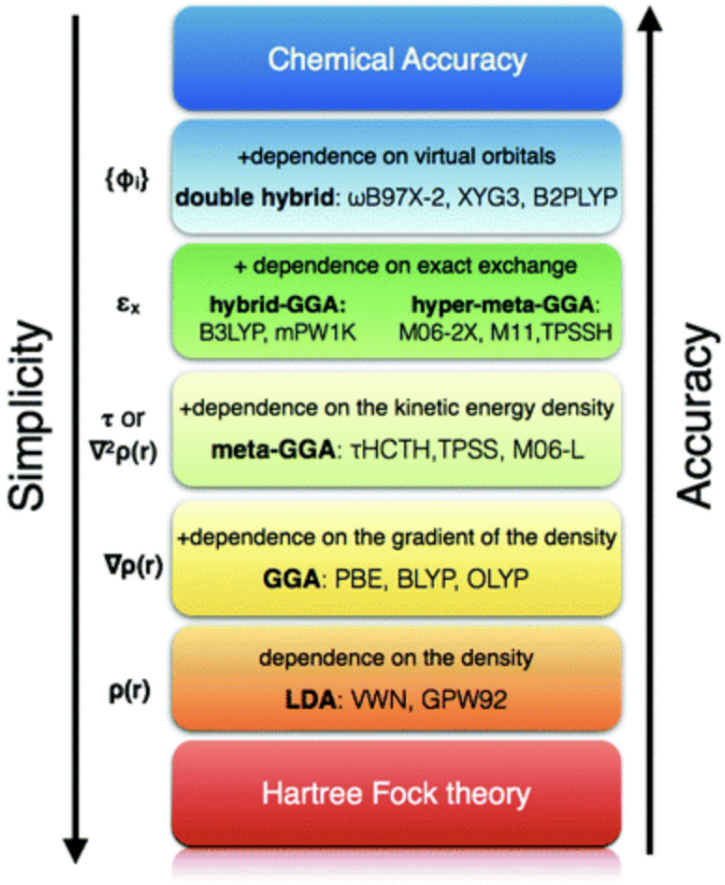

Figure 1.6: Jacob's Ladder of DFT Schemes. *Adapted from : Q.Peng et al, Chem. Soc. Rev., 2016, 45*

1.2.4 Time-Dependent Density Functional Theory

TD-DFT(Time-Dependent Density Functional Theory) is a universal approach to solve the dynamical many-body problem at time-dependednt potentials. It extends the basic ideas of ground-state density-functional theory (DFT) to the

treatment of excitations or more general time-dependent phenomena. TDDFT can be viewed as an alternative formulation of time-dependent quantum mechanics but, in contrast to the normal approach that relies on wave-functions and on the many-body Schrödinger equation, its basic variable is the one-body electron density, $\rho(r,t)$. The advantages are clear: The many-body wave-function, a function in a 3N-dimensional space (where N is the number of electrons in the system), is a very complex mathematical object, while the density is a simple function that depends solely on 3 variables, x, y and z. The standard way to obtain $\rho(r,t)$ is with the help of a fictitious system of non-interacting electrons, the Kohn-Sham system. The final equations are simple to tackle numerically, and are routinely solved for systems with a large number of atoms. These electrons feel an effective potential, the time-dependent Kohn-Sham potential. Two regimes can be observed: If the time-dependent potential is weak, it is sufficient to resort to linear-response theory to study the system. In this way it is possible to calculate, e.g. optical absorption spectra. It turns out that, even with the simplest approximation to the Kohn-Sham potential, spectra calculated within this framework are in very good agreement with experimental results. On the other hand, if the time- dependent potential is strong, a full solution of the Kohn-Sham equations is required. A canonical example of this regime is the treatment of atoms or molecules in strong laser fields. In this case, TDDFT is able to describe non- linear phenomena like high-harmonic generation, or multi-photon ionization.

Prerequisites

We first consider a system of N electrons with coordinates $r = (r_1....r_N)$ to obey the time dependednt Schrödinger's equation :

$$i\frac{\delta}{\delta t)}\Psi(r,t) = \hat{H}(r,t)\Psi(r,t) \tag{1.31}$$

The total Hamiltonian of this system would be :

$$\hat{T}(r) + \hat{W}(r) + \hat{V_{ext}}(r,t) \tag{1.32}$$

where $\hat{T}(r)$ is the Kinetic energy term, $\hat{W}(r)$ is the Coulomb repulsion between electrons (as have been described in previous sections) and $\hat{V_{ext}}(r,t)$ is the time-dependent potential. The **Runge-Gross Theorem** is the cornerstone of TD-DFT. It can be said to be the time-dependent analogue of the Hohenberg-Kohn theorem. The R.G theorem postulates that, for a given initial wavefunction, there is a unique mapping between the time-dependent external potential of a system and its time-dependent density. $\hat{V_{ext}}(r,t) \leftrightarrow \rho(r,t)$ This implies that the many-body wavefunction, depending upon 3N variables, is equivalent to the density, which depends upon only 3, and that all time evolving properties of a system can thus be determined from knowledge of the density alone.

$$\rho(r,t) = N \int d^3r_2 .... \int d^3r_N |\Psi(r_1, r_2 ... r_N, t)|^2 \tag{1.33}$$

Unlike in DFT, there is no general minimization principle in time-dependent quantum mechanics. The idea is to solve the time-dependent Schrödinger equation of a noninteracting system that produces the same density as the interacting system. The many-body wave function of such a system is easy to deal with as it can be written as a Slater determinant :

$$\Phi(r_1, ...r_N, t) = \frac{1}{\sqrt{N}} det[\phi_j(r_j, t)] \tag{1.34}$$

and thus the time-dependent Schrödinger's equation becomes

$$i\frac{\delta}{\delta t} = \left[-\frac{\nabla^2}{2} + V_s[\rho](r,t) \right] \tag{1.35}$$

The above equation is termed as the time-dependent Kohn Sham equation. The KS orbitals reproduce the exact density of the interacting system. The effective single-particle potential V_s causes the noninteracting system to reproduce the exact density.

$$V_s(r,t) = V(r,t) + \int d^3r' \frac{\rho(r',t)}{|r-r'|} + V_{xc}(r,t) \tag{1.36}$$

It should be noted that the time-dependent Kohn-Sham system is not meant to reproduce the full many-body wave function of the interacting system, but only its single-particle density. Mathematically speaking, the ground state KS equation is :

$$\left[-\frac{\nabla^2}{2} + V_s^0[\rho_0](r) \right] \phi_j^0(r) = \epsilon_j \phi_j^0(r) \tag{1.37}$$

where the static effective potential V_s^0 only depends on the ground state density $\rho_0](r)$, and the time-evolved KS equation is just

$$i\frac{\delta}{\delta t} = \left[-\frac{\nabla^2}{2} + V_s[\rho](r,t) \right] \tag{1.38}$$

Evidently, one has to proceed iteratively from a static KS ground state at initial time ($t = t_0$) where the orbital $\phi_i(r,t_0) = \phi_j^0(r)$ to a final time ($t = t_i$) where $\rho(r,t) = \sum_{j=1}^{N} |\phi_j(r,t)|^2$. The time evolution of the orbitals necessarily gives the time-dependent densities.

Needless to say, the exchange correlation potential also does not remain static as described in equation (1.21). The time-dependent xc potential $V_{xc}[\rho](r,t)$ has many features and exact properties that are analogous to those of the static xc potential: for instance, it must be self-interaction free, it must have the correct asymptotic $-1/r$ behaviour, and it must exhibit an overall discontinuity upon change of particle number. However, there are also features that have no counterpart in static DFT and are truly dynamic. The most important one is that the time-dependent xc potential has a memory:

$V_{xc}[\rho](r,t)$ at time t depends on densities $\rho(r^{'},t^{'})$ at earlier times, where $t^{'} \leq t$. This memory is, in principle, infinitely long-ranged. An adiabatic approximation is normally used for the time-dependent xc potential, to ignore the memory effects.

$$V_{xc}^{adia}(r,t) = V_x c^{0,approx}[\rho_0](r)|_{\rho_0(r)\to\rho(r,t)} \tag{1.39}$$

An approximate potential from static DFT, $V_{xc}^{0,approx}$ is calculated with the instantaneous time-dependent density. This is convenient, because we can simply use our favourite approximation from static DFT in TDDFT. A widely used example is the adiabatic local-density approximation (ALDA).
TD-DFT is extremely powerful in situations where the dynamics of the interacting system is qualitatively similar to the corresponding non-interacting system. The adiabatically approximated exchange correlation functional also works well

- In linear-response calculations of the excitation spectrum of the system, whenever the spectral features are dominated by single-particle excitation processes. This is because such processes will find a counterpart in the spectrum of the noninteracting Kohn-Sham system. The dynamical xc potential then does not need to create any new spectral features, and merely adjusts and corrects the features that are already there.

- For strongly excited systems under the influence of high-intensity fields, whenever the external field dominates over the electron-electron interactions. In this case, highly nonlinear multiphoton processes are prevalent, such as multiple ionization or high-harmonic generation.

TD-DFT however faces challenges when the electron dynamics of the interacting system is highly correlated. In particular, multiple excitations (e.g., double excitations) are notoriously difficult to capture with TDDFT, because they require

xc functionals beyond the adiabatic approximation. Also, for highly delocalized, long-ranged excitation processes, problems may arise.

1.2.5 Basis Sets

Another indispensable ingredient in DFT calculations is the basis set, which is a set of functions used to represent the electronic wave function. Generically, a basis set is a collection of vectors spanning a space in which a problem is solved. In quantum chemistry, the basis set usually refers to the set of (non-orthogonal) one-particle functions used to build molecular orbitals. The one-particle wave function is expanded as -

$$\Psi_i(r) = \sum_{j=1}^{N_b} C_{i,j} g_i(r) \tag{1.40}$$

where $C_{i,j}$ depicts the coefficients of expansion, $g_i(r)$ are the basis functions and N_b is the basis size. Basis sets are a tool to convert the KS equations into one particle matrix notations. Diagonalizing this matrix yields eigenvalues and eigen vectors. When molecular calculations are performed, it is common to use a basis composed of atomic orbitals, centred at each nucleus within the molecule. The physically best motivated basis set are Slater-type orbitals (**STO**'s), which are solutions to the Schrödinger's equation of hydrogen-like atoms, and decay exponentially far away from the nucleus. The computation of STO's is difficult and they are thus replaced by **GTO'**s (Gaussian Type Orbitals).

Basis sets have also been hierarchically developed with increasing size to obtain more accuracy coupled with higher computational cost. **Minimal basis sets** are those in which, on each atom in the molecule, a single basis function is used for each orbital in a Hartree-Fock calculation on the free atom. Examples are STO-3G, STO-6G. **Split Valence Basis sets** are used to represent valence orbitals that take part in bonding (corresponding to each valence atomic orbital are va-

lence double-zeta, triple-zeta, quadruple-zeta, and so on.) Correlation-consistent and Polarization-consistent basis sets move further into higher levels of computation.

The above basis sets are mainly localized. To treat quantum mechanical systems obeying **PBC** (Periodic Boundary Conditions), **plane-wave basis sets** are used. The choice of the plane wave basis set is based on a cutoff energy. The plane waves in the simulation cell that fit below the energy criterion are then included in the calculation.

1.2.6 Pseudopotentials

After establishing a solid theoretical framework for treating quantum systems, one needs to look for ways that would ease the computational burdens of calculations. Until now, all electrons in the system were being taken into account. And it is known that the motions of the core (non-valence) electrons and the nucleus have complicated effects, which would needlessly toughen our calculations as the prime focus will usually be on the valence electrons that participate in bonding. The pseudopotential is an effective potential (V_{PP}), constructto replace the atomic all-electron potential (full-potential) such that the core states are eliminated and the valence electrons are described by pseudo-wavefunctions with significantly fewer nodes. The core states are assumed to be "*frozen* "and thus the basis set is reduced in size. The concept of Pseudopotentials was first introduced by Hans Hellmann in 1934.

If the set of core states is represented as $\{|\chi_n\}|$ and the core eigen values as $\{E_n\}$, the valence state ψ can be replaced by a smoother state ϕ and a term that includes all the core states.

$$|\psi\rangle = |\phi\rangle + \sum_{n}^{core} a_n |\chi_n\rangle \tag{1.41}$$

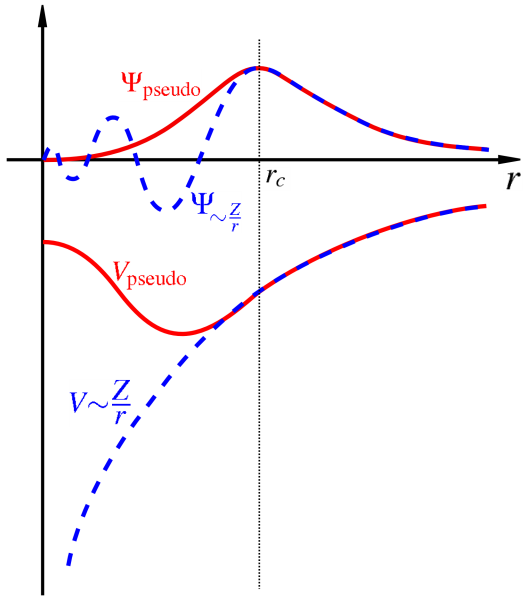

Figure 1.7: Relationship between all-electron and pseudo-potentials and wave-functions. (*Image Courtesy : www.wikipedia.org*)

The valence state is orthogonal to the core states, so

$$\langle\chi|\psi\rangle = \langle\chi|\phi\rangle + \sum_{n}^{core} a_n \langle\chi_m|\chi_n\rangle = 0 \tag{1.42}$$

The Hamiltonian for such a system is :

$$\hat{H}|\phi\rangle + \sum_{n}^{core}(E - E_n)|\chi_n\rangle\langle\chi_n|\phi\rangle = E|\phi\rangle \tag{1.43}$$

In this way, the smooth, pseudo wavefunction satisfies an effective equation with the same eigen energy of the real valence wavefunction From an atomic reference state, it is believed that the pseudo- and all-electron valence eigenstates have the same energies and amplitude (and thus density) outside a chosen core cut-off radius r_c. PP's having larger r_c are *soft* and converge sooner (smooth) but less accurate in obtaining realistic features and less transferable. Smaller r_c would mean good transferability but less smooth. A balance is thus required to construct a "good"

PP.

Commonly used pseudopotentials may be :

- **Norm-conserving (NCPP)** : NCPPs have lower cut-off r_c and allow proper numerical convergence having good transferability.

- **Ultrasoft Pseudopotentials** : They have larger r_c and they relax the norm-conserving constraint to reduce the necessary basis-set size further, and have lower transferability.

1.3 Outline of Thesis

In the subsequent chapters, Density Functional Theory as implemented in Quantum Espresso 6.0, SIESTA 3.2 and Gaussian16 set of codes have been extensively used to study materials at 0, 2 and 3 dimensions. Chapters 2 and 3 deal with Optoelectronic studies on zero and two dimensional systems. Chapter 4 focuses on electrochemistry of some three dimensional NASICON systems.

Quantum confined nanoclusters of Black Phosphorene and Arsenene have been investigated in Chapter 2, with the prime focus on their optical properties the effects of size and composition.

In Chapter 3, 2-dimensional Nanosheets of Germanane and Arsenene have been studied with respect to electronic properties and charge transfer phenomena.

The fourth chapter deals with electronic and electrochemical properties of systems belonging to NMV(Na-transition metal-vanadium) phosphate class of NASICON cathode materials, with the intention of designing efficient electrodes for Sodium Ion Batteries.

References

[1] Introduction to Quantum Mechanics by David J. Griffiths.

[2] Density Functional Theory: A Practical Introduction by David Sholl, Janice A Steckel

[3] Density Functional Theory: Basics, New Trends and Applications by J. Kohanoff and N.I. Gidopoulos, Volume 2, in Handbook of Molecular Physics and Quantum Chemistry (edited by Stephen Wilson)

[4] An Introduction to Density Functional Theory by N. M. Harrison.

2

Photophysical Properties of A Few Zero Dimensional Quantum Dots*

The history of QDs (Quantum Dots) begins with their first discovery in glass crystals in 1980 by Russian physicist Ekimov. Since then research has progressed through various metallic and non-metallic quantum dots like Cd, Si, C etc. Quantum dots typically have dimensions in nanometers, containing about 1,000 to 100,000 atoms and their size dependent properties are beautifully captured through various experimental and theoretical techniques. It is possible to adjust the electronic and photonic properties of quantum dots according to their purpose of use which makes them greatly advantageous. A rich variety of physical and chemical methods have been developed for fabricating 0D NMSs with well-controlled dimensions. As discussed previously, there can be top-down and bottom-up approaches for nanoparticle synthesis. (a) Top-down approach : a bulk material is restructured (i.e. partially disman-

**Contents of this chapter will appear as "Phosphorene Quantum Dots" , Pratap Vishnoi, Madhulika Mazumder, Manaswee Barua, Swapan K. Pati, C.N.R. Rao, *Chem.Phys.Lett.*, 2018.

tled, machined, processed or deposited) to form nanomaterials. Challenges increase as device size is reduced and as the desired component designs become larger and more complex. Also, the top-down assembly of nanocomponents over large areas is difficult and expensive.
(b) Bottom-up approach : nanomaterials are assembled from basic building blocks, such as molecules or nanoclusters. The basic building blocks, in general, are nanoscale objects with suitable properties that can be grown from elemental precursors.

Quantum Confinement

The unique properties of quantum dots arise almost solely because of size regime in which they exist. QDs are confined in all three dimensions, allowing them to exist only in the zero dimensional space. Unlike bulk systems, their electronic states are not continuous but discrete, which becomes more pronounced with a decrease in size. The magnitude of quantum confinement can be predicted by solving Schrödinger's equation assuming the barriers to be along all three dimensions (which amounts to a particle in a 3-D box with infinite potential barriers). The energy of such a system is given by -

$$E_{n,m,l} = \frac{\pi^2\hbar^2}{2m^*}\left(\frac{n^2}{L_z^2} + \frac{m^2}{L_y^2} + \frac{l^2}{L_x^2}\right) \tag{2.1}$$

where $n, m, l = 1, 2, 3$ - the quantum confinement numbers, Lx, Ly and Lz are the confining dimensions and m^* is the effective mass of the confined particle. When a photon of sufficient energy (close to the gap) strikes a quantum dot, it can excite an electron from the valence band to the conduction band, leaving behind a positive hole. Generation of an electron-hole pair (exciton) is a common phenomenon in semiconducting materials; however, in a quantum

dot, the average exciton size (the exciton Bohr radius) is smaller than the size of the quantum dot, producing a confinement energy as the exciton is squeezed into the material.

Optical properties are affected by Quantum confinement. The effect of changing size on the band gap is reflected in the equation :

$$a_b^* = a_b \epsilon_r \left(\frac{m}{\mu} \right) \tag{2.2}$$

where a_b^* is the Bohr exciton radius, a_b is the Bohr radius (0.53), and ϵ_r is the dielectric constant of the semiconductor, which varies as a function of size. Recently, a wide variety of 0D QDs have been synthesized in different morphologies, such as uniform particles arrays (quantum dots), heterogeneous particles arrays, coreshell quantum dots, onions, hollow spheres and nanolenses, to name a few[1].

Applications

One of the most obvious applications of quantum dots lies in electronic displays. Because of their bright and narrow emission spectra, quantum dots are obvious choices to replace OLED and LCD screens. By exciting various sizes of QDs, a full spectrum of colours can be produced. They have also created a stir in biological fields as specially designed QD drugs bear a huge potential in efficient delivery and functionalization.

In this chapter, 0D quantum dots of two materials have been studied for their optoelectronic properties - Black Phosphorene and Arsenene QDs.

2.1 Black Phosphorene and Arsenene Quantum Dots

Elemental Phosphorus is known to exist in many allotropes, like white, red, violet and black, out of which black phosphorus is thermodynamically stable at room temperature and pressure, having a heat of formation of -39.3kJmol^{-1}. It resembles Graphite in physical appearance, has a flaky texture and shows semiconducting properties. Discovered by Bridgman in 1914, this allotrope remained unexplored for almost a century, until its rediscovery in 2014 [2,3] as a member of the low dimensional elemental semiconducting family.

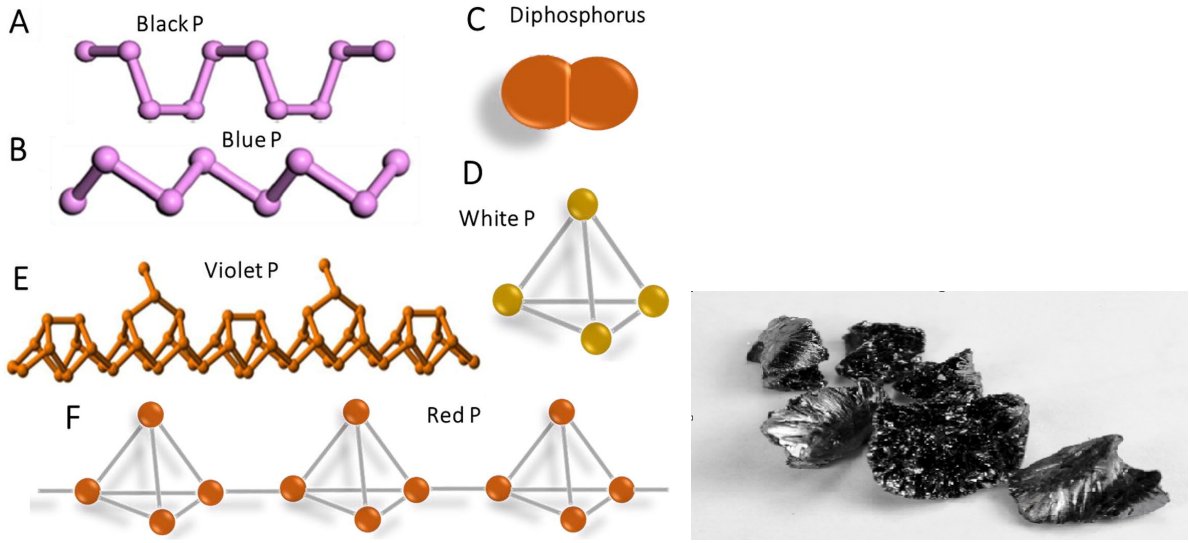

Figure 2.1: (a) Allotropes of Phosphorus. b) Black Phosphorus Crystal.

In addition to layered structures, Black Phosphorene has also been studied as Quantum Dots . Liquid Exfoliation of the Black Phosphorus crystal gives rise to these quantum dots. It is still a difficult challenge to prepare soluble black Phosphorene quantum dots (BPQD's), though Zhang et al, [4] and Xu [5], have successfully synthesized BPQD's, by mechanical exfoliation and solvothermal methods. Lee et al [6] were the first to synthesize BPQD's that

are blue-emitting and have a high fluorescence quantum yield.

The usefulness of Phosphorene can be majorly attributed to its unique structural arrangement. The strong in-plane covalent network and weaker interlayer interactions make it suitable for mechanical exfoliation. The interlayer distance (3.21 Å to 3.73 Å) varies with the type of stacking present. Three possible stacking orders of bilayer phosphorene are known and have been studied[7] - namely, **AA, AB** and **AC** - stacking. In the AA-form, the top layer is directly stacked over the bottom layer. For AB-stacking, the bottom layer is shifted by half of the cell length along a or b directions, which brings the edge of the puckered hexagon of the top layer in the centre of the puckered hexagon of the bottom layer. In the AC type stacking, top and bottom layers are mirror images of each other. Evidently, the lattice parameters also vary with the type of stacking (see Table 2.1) This in turn affects the band gap and related properties, making bilayer Phosphorene a top candidate with solar cell donor material applications.

Stacking Order	**a(Å)**	**b(Å)**	$\mathbf{d_{int}}$**(Å)**	$\mathbf{E_g}$**(eV)**
AA	4.550	3.326	3.495	0.97
AB	4.526	3.331	3.214	1.04
AC	4.535	3.324	3.728	0.78

Table 2.1: Effect of Stacking on Structure and Electronic Properties.

Arsenic is known to have three common allotropes, grey, yellow and black. Grey arsenic is the stablest and the most abundant form. It has a layered Rhombohedral structure (Space group $R\overline{3}m$) Similar to Phosphorene, Arsenene can also form monolayer and bilayer buckled honeycomb (β) and puckered washboard (α) structures with the former being more thermodynamically stable under standard conditions of temperature and pressure. Kamal and Ezawa[8] were the first to completely optimize both structures computa-

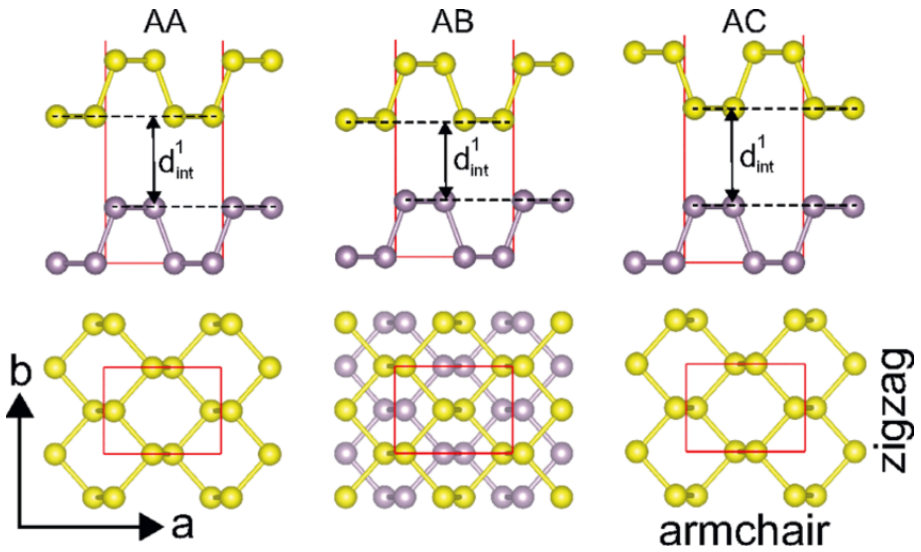

Figure 2.2: Types of stacking in Black Phosphorene

Figure 2.3: (a) Grey Arsenic crystal (b) Yellow Arsenic crystal

tionally and perform electronic calculations on them. Theoretical calculations have also been carried out to study the effect of strain on the layered structures.

2.2 Computational Methods

In the study of BPQDs, first principles based Density Functional Theory calculations have been performed in SIESTA (Spanish Initiative for

Electronic Simulation with Thousands of Atoms) Package[9] and Gaussian 16[10] suite of codes. A split valence Double Zeta Polarized basis set was used and calculations were performed within an energy cutoff of 400 Ry. Norm-conserving Troullier-Martins[11] pseudopotentials were used to treat interactions between core electrons and nucleus. Electronic correlations and exchange were treated with PBE(Perdew-Burke-Ernzerhorf)[12] functionals as implemented in the GGA (Generalized Gradient Approach)[13] method. The Brillouin zone was sampled with a 5 x 5 x 1 Monkhorst Pack grid. All systems were optimised until the total force is reduced to 0.02 eV/atom. A vacuum of 30 $\mathring{A}$ was maintained in the non-periodic direction to prevent deluding interlayer interactions and the supercell length was chosen to be 15 $\mathring{A}$ to avoid Coulombic interactions in the periodic direction. All geometric structures were visualised using XCRYSDEN[14] software.

For As QD's, Density Functional Theory as implemented in Quantum Espresso 6.0 Package[15,16], with a plane wave basis set was used. Exchange correlations were treated using the PBE[12] functional under GGA (Generalized Gradient Approximation)[13]. An energy cutoff of 300 eV was used to represent valence electrons. Vanderbilt's Ultrasoft pseudopotentials[17] were chosen to approximate the interactions between core electrons and the atomic nucleus. To avoid spurious interactions, a vacuum of 30 $\mathring{A}$ was created in the non-periodic z direction and a distance of 15 Angstroms was maintained between the molecules under the supercell consideration. The Brillouin Zone was sampled using a Monkhorst Pack grid of 4 x 4 x 1. For electronic calculations, a 21 x 21 x 1 grid was considered. All systems were optimised until the total force reduced to 0.02 eV/atom. Time Dependent Density Functional Theory (TD-DFT) calculations were carried out in Gaussian16[10] set of codes to estimate the optical response of arsenene, under

the Tamm-Dancoff approximation[18,19]. CAM-B3LYP[20] hybrid exchange correlation functional was used to treat long range interactions in the system. All geometric structures were visualised using XCRYSDEN[14] software.
Charge transfer interactions with donor acceptor molecules, namely TTF (tetrathiafulvalene) as the electron donating moiety to phosphorene nanocluster and TCNE (tetracyano-ethylene) and TCNQ (tetracyanoquinodimethane) as electron accepting groups were studied, using Mulliken Population Analysis.

Optical Calculations

The optical properties are described by the complex dielectric function[21] :

$$\epsilon(\omega) = \epsilon_1(\omega) + i\epsilon_2(\omega) \tag{2.3}$$

which can be further extrapolated to give the absorption coefficient $\alpha(\omega)$

$$\alpha(\omega) = \frac{\sqrt{2}\omega}{c}\left\{\left[\epsilon_1^2(\omega) + \epsilon_2^2(\omega)\right]^{1/2} - \epsilon_1(\omega)\right\}^{-1/2} \tag{2.4}$$

Calculations on the imaginary part of the dielectric function yield the absorption coefficient as a function of Energy, from where we can deduce the maximum wavelength of absorption.
TD-DFT calculations enable us to study the lowest excitations from the ground state. The dipole strength function $S(\omega)$ measures the excitation induced a system by a particular frequency, as the fast Fourier transform of the dynamic polarizability.

$$S(\omega) = \frac{4m_e}{e_h^2}\omega Im\alpha(\omega) \tag{2.5}$$

where α is the dynamic polarizability.

2.3 Structural Characteristics

Black Phosphorene is known to have a puckered structure with a non-symmorphic space group of base-centered orthorhombic . The unit cell consists of 4 Phosphorus atoms. The lattice parameters are **a=3.31 Å**, **b=4.38 Å**. A vacuum of **20 Å** was maintained in the non-periodic z-direction to avoid spurious interlayer interactions. To study the size dependence of the optical properties of the BPQD's supercells of varying sizes were taken, from 40 to 100 Phosphorus atoms. All calculations were performed considering AA type stacking.

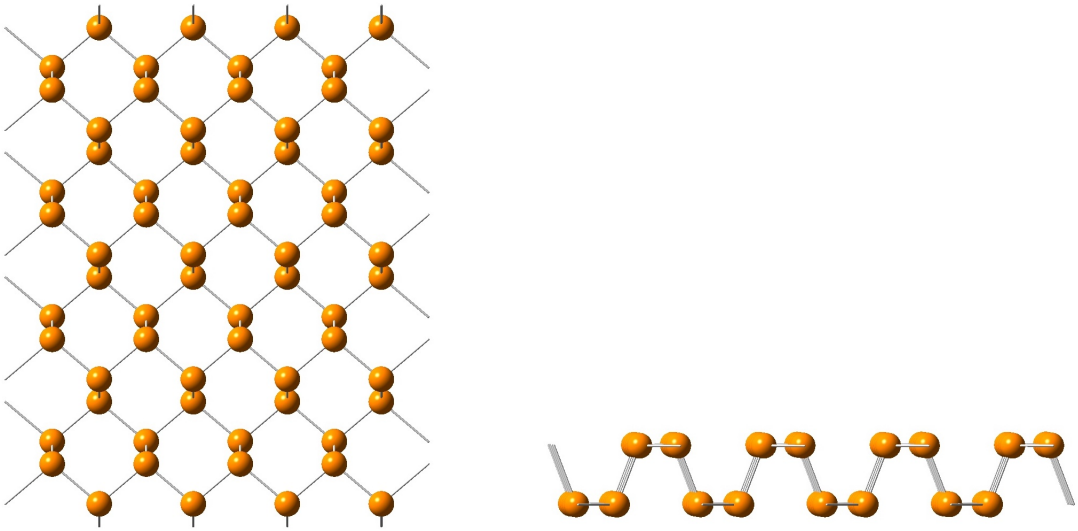

Figure 2.4: (a) A 4×4 supercell of BPQD with 64 P atoms (b) Puckering in Black Phosphorene

The buckled(β-form) of Arsenene has a honeycomb structure with the space group of P3m12 and its unit cell has 2 As atoms. The optimized As-As bond distances were found to be 2.503 Åand the As-As-As bond angle is 91.98 de-

grees. The crystal structure has isotropy along a and b directions, thus the lattice parameters are equal; **a = b= 3.61 Å**. The buckling height is 1.40Å, which is in good agreement with previously reported data[2,6].

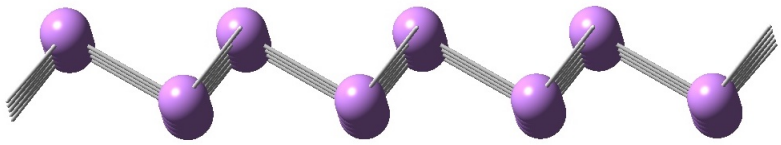

Figure 2.5: Buckling in Arsenene

2.4 Results and Discussion

2.4.1 Optical Properties

BPQDs show absorbance in the region of 300-500 nm of the electromagnetic spectrum. A red shift is observed in the absorption wavelength, on increasing the size of BPQDs. The size dependence of the absorption wavelength can be attributed to quantum confinement effect, which is stronger for smaller sizes and creates discretely spaced energy levels, as described in Equations 2.3 - 2.5. The intensity of absorption peaks depends crucially on the surface to bulk ratio of atoms. It increases with increase in size and saturates eventually as the ratio tends to a negligible value. In fact, such quantum confinement effects can also be described in terms of Tight-Binding model, within which every consecutive level has opposite parity.

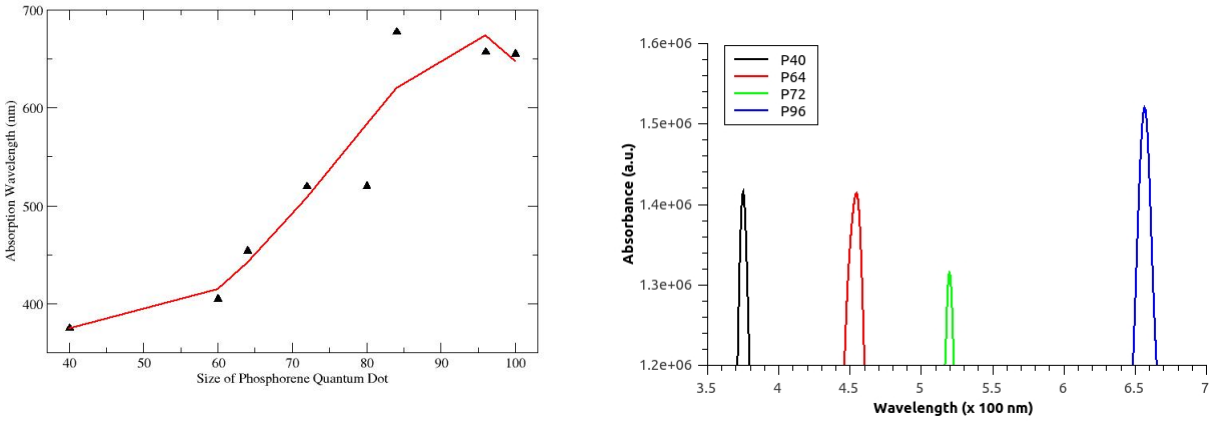

Figure 2.6: (Trends in the absorption spectra of BPQDs with increase in size

Time dependent Density Functional Theory (TD-DFT) studies on the optimized ground state of the BPQDs show that the max for the emission spectra depends crucially on the size of the nanocluster. As reported in [2], it is found that, for BPQDs of sizes from 40 to 60 atoms the emission max is Anti-Stokes shifted from the absorption max , precisely due to change in spatial geometry. However, for sizes beyond 60, the shift in emission is Stokes shifted with little change in the geometry. It should be pointed out here that for experimental systems, since they correspond to more than 500 atoms, the photoluminescence spectra show Stokes shift with increase in nanoparticle diameter.

For AsQD's, we observe an Absorption maxima at : 354.09 nm and the Emission wavelength at 431 nm for 32 atom systems. There is a red shift in the emission spectra on increasing the size of the AsQDs. This is due to the increased stability of the optical excitation with increase in the size of the system, as the excitonic volume expands and thereby gains stability. Arsenene quantum dot with 24 atoms has an Emission at 300 nm, as opposed to the quantum dot with 50 atoms, which has emission peak at 477nm. These spectra conform well with experimental reports on AsQDs.

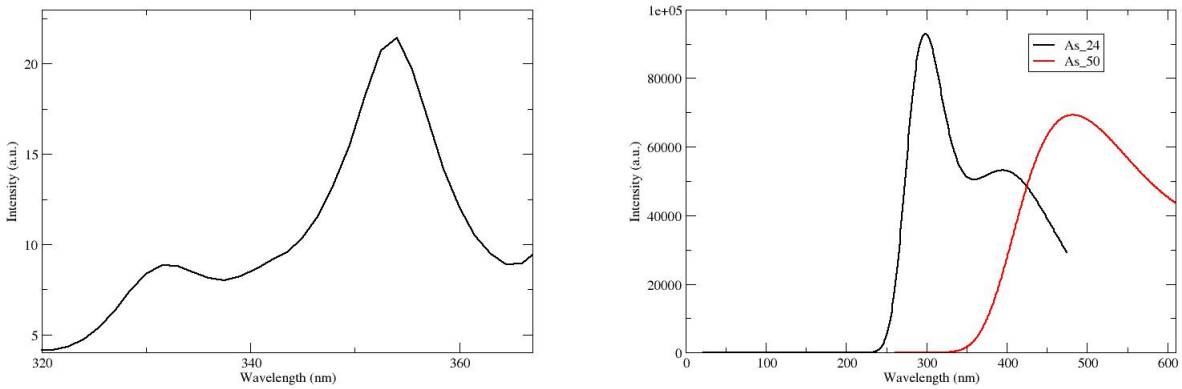

Figure 2.7: (a) Absorption spectra of AsQDs (b) Absorption spectra of AsQDs of increasing size.

2.4.2 Charge-Transfer Studies

From the optimized structures, it is observed that TTF and TCNE molecules lie at a distance of 3.5 Åfrom the monolayers.

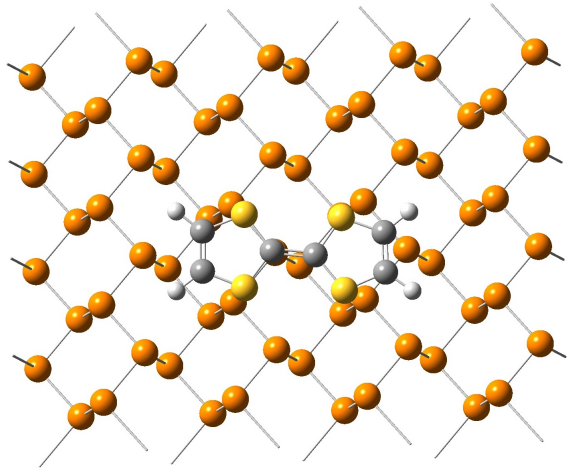

Figure 2.8: BPQDs with TTF molecule

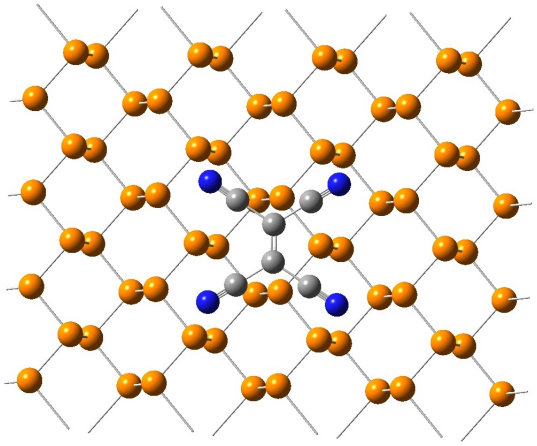

Figure 2.9: BPQDs with TCNE molecule

Mulliken Population study is an effective tool for studying partial atomic charges that can offer a qualitative insight into the net charge of the system. A differential population analysis of the orbitals proves that BPQD's accept electrons from TTF into the empty 3d bands of P atoms, and donates electrons to TCNE/TCNQ from the 3p bands of P, as observed from the rise and fall in electronic charge density of the corresponding orbitals respectively.

Charge Transfer is also evident from the absorption spectra of the QDs in the presence of donor-acceptor molecules, TTF, TCNE and TCNQ as given in Figures 2.10(a),(b) and 2.11(a),(b) . On increasing the ratio of concentration of TCNE/TCNQ to BPQDs, a red shift is observed in the absorption spectra, but a blue shift occurs in case of TTF, since TTF is a donor while TCNE and TCNQ are acceptor moieties.

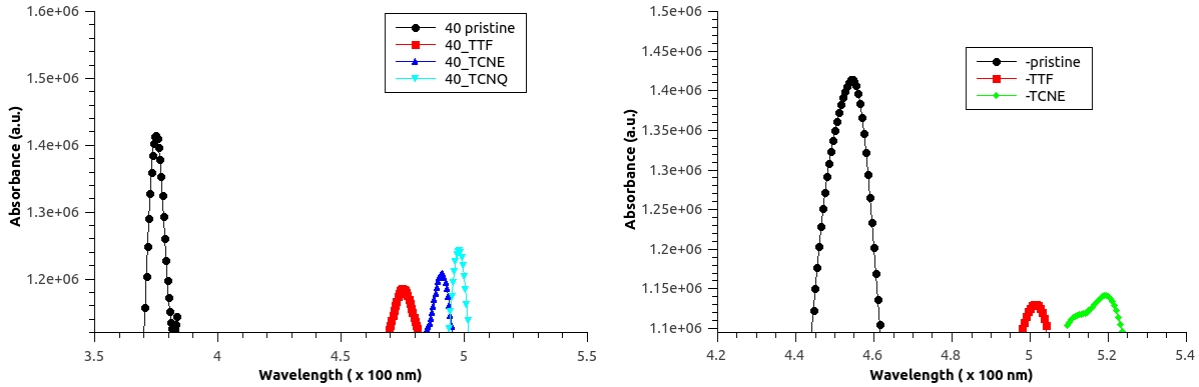

Figure 2.10: (a) Absorption spectra of BPQD's(P40) in pristine and charge transfer states. (b) Absorption spectra of BPQD's(P60) in pristine and charge transfer states..

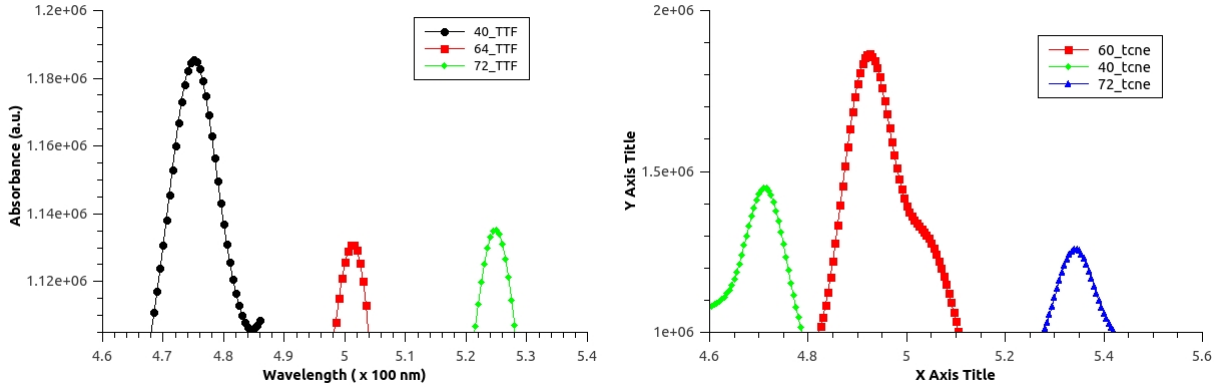

Figure 2.11: (a) Absorption spectra of BPQD's with donor TTF molecule (b) Absorption spectra of BPQD's with acceptor TCNE molecule..

2.5 Conclusion

In this chapter, theoretical calculations have been carried out on Quantum Dots of Black Phosphorene and Arsenene. Like other Group 15 elements, both Phosphorene and Arsenene are known to have puckered and buckled structures. The puckered form is more stable for Phosphorene whereas the buckled form is preferred in Arsenene. TD-DFT calculations were performed

to study their optical activities and a generic increase in absorption and emission wavelengths was observed on increasing the size of the quantum dots, which agrees fairly well with experimental reports of BPQDs and theoretical predictions of AsQDs. This is expected as the gaps between energy states start decreasing on increasing the size of the quantum dots and thus reducing the Quantum confinement effects. Charge transfer studies were also carried out on BPQDs with donor and acceptor molecules, TTF, TCNE and TCNQ. Photoluminescence was found to be quenched by donor and acceptor molecules, as indicated by a red shift in the optical spectra, with the acceptors having more pronounced quenching effects.

References

[1] J.N.Tiwari, R.N. Tiwari, K. S.Kima, *Progress in Materials Science*, 2012, **57**, 724.

[2] X. Niu, Y. Li, H.Shu, J.Wang *J.Phys.Chem.Lett.* 2016, **7**, 370.

[3] L.K. Li, Y. Yu, G.J. Ye, Q.Q., X.D. Ou, H Wung, D. Feng, H.X. Chen, Zhang, Y.B., ti.Nanotenhol 2014, **9**, 372.

[4] X. Zhang, H. Xie, Z.L. C. Tan, Z. Luo, H.L.J. Lin, L. Sun, W.Chen, Z. Xu, L. Xie, W.Huang, H. Zhang, *Angew. Chem. Int. Ed.* 2015, **54**, 3653.

[5] Y. Xu, Z. Wang, Z. Guo, H. Huang, Q. Xiao, H. Zhang, Xue?Feng Yu, *Adv. Optical Mater.* 2016, **4**, 1223.

[6] M. Lee, Y.H. Park, E.B. Kang, A. Chae, Y. Choi, S. Jo, Y. J. Kim, S-J

Park, B. Min, T.K. An, J. Lee, Su-Il In, S.Y. Kim, S.Y. Park, I. In, *ACS Omega* 2017, **2**, 7096.

[7] J.Dai, X.C.Zeng, *J. Phys. Chem. Lett.* 2014, **5**, 1289.

[8] C. Kamal, M.Ezawa, *Phys. Rev. B*, 2015, **91**, 085423.

[9] J. M. Soler, E. Artacho, J. D. Gale, A. Garca, J. Jun-quera, P. Ordejn, D. Snchez-Portal, *J. Phys.Condens. Matter* 2002, **14**, 2745.

[10] M.J. Frisch, G.W. Trucks, H.?B. Schlegel, G.?E. Scuseria, M.A. Robb, J.R. Cheeseman, G. Scalmani, V. Barone, B. Mennucci, G.A. Petersson, H. Nakatsuji, M. Caricato, X. Li, H.P. Hratchian, A.?F. Izmaylov, J. Bloino, G. Zheng, J.L. Sonnenberg, M. Hada, M. Ehara, K. Toyota, R. Fukuda, J. Hasegawa, M. Ishida, T. Nakajima, Y. Honda, O. Kitao, H. Nakai, T. Vreven, J.A. Montgomery Jr., J.?E. Peralta, F. Ogliaro, M. Bearpark, J.J. Heyd, E. Brothers, K.N. Kudin, V.N. Staroverov, T. Keith, R. Kobayashi, J. Normand, K. Raghavachari, A. Rendell, J.C. Burant, S.S. Iyengar, J. Tomasi, M. Cossi, N. Rega, J.M. Millam, M. Klene, J.E. Knox, J.B. Cross, V. Bakken, C. Adamo, J. Jaramillo, R. Gomperts, R.E. Stratmann, O. Yazyev, A.J. Austin, R. Cammi, C. Pomelli, J.W. Ochterski, R.L. Martin, K. Morokuma, V.G. Zakrzewski, G.A. Voth, P. Salvador, J.J. Dannenberg, S. Dapprich, A.D. Daniels, O. Farkas, J.B. Foresman, J.V. Ortiz, J. Cioslowski, D.J. Fox, Gaussian 09, Revision C.01, **Gaussian Inc.**, Wallingford CT, 2010.

[11] N. Troullier, J. L. Martins *Phys. Rev. B* 1991, **43**, 1993.

[12] J.P.Perdew, K. Burke, M. Ernzerhorf, *Phys. Rev. Lett.* 1996, **77**, 3865.

[13] S. Grimme, *J. Comput. Chem.* 2006, **27**, 1787.

[14] A. Kokalj, *Comput. Mater. Sci*, 2003, **28**, 155; XCRYSDEN code; http://www.xcrysden.org

[15] P. Giannozzi, S. Baroni, N. Bonini, M. Calandra, R. Car, C. Cavazzoni, D. Ceresoli, G. L. Chiarotti, M. Cococcioni, I. Dabo, A. Dal Corso, S. Fabris, G. Fratesi, S. de Gironcoli, R. Gebauer, U. Gerstmann, C. Gougoussis, A. Kokalj, M. Lazzeri, L. Martin-Samos, N. Marzari, F. Mauri, R. Mazzarello, S. Paolini, A. Pasquarello, L. Paulatto, C. Sbraccia, S. Scandolo, G. Sclauzero, A. P. Seitsonen, A. Smogunov, P. Umari, R. M. Wentzcovitch, J.Phys.:Condens.Matter 21, 395502 (2009) http://dx.doi.org/10.1088/0953-8984/21/39/395502.

[16] P Giannozzi, O Andreussi, T Brumme, O Bunau, M Buongiorno Nardelli, M Calandra, R Car, C Cavazzoni, D Ceresoli, M Cococcioni, N Colonna, I Carnimeo, A Dal Corso, S de Gironcoli, P Delugas, R A DiStasio Jr, A Ferretti, A Floris, G Fratesi, G Fugallo, R Gebauer, U Gerstmann, F Giustino, T Gorni, J Jia, M Kawamura, H-Y Ko, A Kokalj, E Kkbenli, M Lazzeri, M Marsili, N Marzari, F Mauri, N L Nguyen, H-V Nguyen, A Otero-de-la-Roza, L Paulatto, S Ponc, D Rocca, R Sabatini, B Santra, M Schlipf, A P Seitsonen, A Smogunov, I Timrov, T Thonhauser, P Umari, N Vast, X Wu and S Baroni, *J.Phys.Condens.Matter*, 2017, **29**, 465901.

[17] D. Vanderbilt, *Phys. Rev. B*, 1990, **41** 7892.

[18] M.E. Casida, 1995, *Journal of Molecular Structure: THEOCHEM*, 2009, **914**, 3-18.

[19] S. Hirata, M. Head-Gordon, *Chemical Physics Letters*, 1999, **314**, 291?299.

[20] T. Yanai, D.P. Tew, N.C. Handy, *Chemical Physics Letters*, 2004, **393**, 51?57.

[21] J-H.Lin, H.Zhang, X-L. Cheng, *Front.Phys.*, 2015, **10**, 107301.

3

Electronic and Optical Properties of a Few Layered Semiconducting Materials*

The successful exfoliation of Graphene in 2004 marked the birth of an era of exploring 2D nano-systems. In recent years, synthesis of 2D NSM(nanostructured materials)s has become a focal area in materials research, owing to their many unique properties. Their shape-dependent characteristics allow them to be utilized as building blocks for the key components of nanodevices. 2D materials can either be allotropes of various elements or compounds (having covalent linkages). Layered combinations of different 2D materials called van der Waals heterostructures are also extensively studied [1–4]. These systems have interlayer interactions governed by van der Waals forces. Inspired from Graphene, 2D systems of different elements have been realised such as, Phosphorene, Borophenes, Boron Nitride, Germanane, Bismuthene.

**Work done in this chapter has been submitted as "Arsenene Nanosheets and Quantum Dots" , Pratap Vishnoi, Madhulika Mazumder, Swapan K. Pati, C.N.R. Rao (2018).

Compounds like TMDs(Transition Metal Dichalcogenides, like MoS_2, WS_2, $MoSe_2$, etc.) Borocarbonitrides, MXenes are also gaining a lot of interest. A number of methods have been developed for the generation of 2D systems - *Scotch Tape Exfoliation*, *Chemical Vapour Deposition*, *Colloidal Synthesis* to name a few.

Applications

The fast growing field of 2-D systems find applications in a wide range of fields. Efficient light harvesting, sensitive photo-detection, and low-threshold lasing make them promising materials for the next generation electronics and opto-electronic devices. The tunability in their electronic structure which can be achieved by band engineering can generate systems with band gaps matching the solar spectrum, which will find use in solar cells and photovoltaics. Carrier mobility and density may also be regulated, for field effect transistors (FETs) and p-n junctions. Moreover, these materials can withstand large amounts of strain without degradation, and thus are excellent choices for use in flexible, wearable electronics, and portable electronic gadgets.

3.1 Germanane and Arsenene Nanosheets

Group 14 layered lattices are known to have appreciable conductivities when the atoms are in sp_2 state. But the conductivities may be maintained considerably, even when the atoms are sp_3 hybridized. Germanane is a single layer crystal composed of Germanium atoms bonded with Hydrogen in the z-direction. It is actually a result of passivation of Germanene[5,6], and Ge here is in an sp_3 hybridized state. It has an electron mobility 10 times that of Silicon and 5 times that of bulk Germanium. Passivation makes it physically

and chemically stable on exposure to air and water.

The synthetic route of Germanane has been inspired from the proof of existence of layered Zintl phases like $CaSi_2$ and $CaGe_2$ that can be topochemically deintercalated in aqueous HCl at low temperatures to produce layered Silicon and Germanium solids[7,8]. Hydrogen-terminated Germanane was exfoliated successfully for the first time by Elisabeth Bianco et al[5,6], in 2013, from topochemical deintercalation of $CaGe_2$ in aqueous HCl. The Calcium sites in the Zintl phases of $CaGe_2$ interchange with the H atoms in the HCl solution to leave behind GeH and $CaCl_2$. Theoretical predictions performed on electronic, optical and transport properties[9] of Germanane suggest its efficiency in nanoelectronic devices.

Recently, Group 15 elemental layered structures have also aroused a lot of interest for their potential applications in the fields of electronics and optoelectronic materials. Besides Phosphorene, Arsenic and Antimony have been extensively studied in different structural phases theoretically and experimentally[10,14]. Two dimensional Arsenene sheets were first studied theoretically by Kamal and Ezawa[10] and this study was followed up by many more analyses, including the effect of strain[10], carrier mobility[13] and doping[14].

3.2 Computational Details

Density Functional Theory as implemented in Quantum Espresso 6.0 Package[15,16], with a plane wave basis set was used to study electronic properties. Exchange correlations were treated using the PBE[17] functional under GGA (Generalized Gradient Approximation)[18]. An energy cutoff of 300 eV was used to represent valence electrons. Vanderbilt's Ultrasoft pseudopotentials[19] were chosen to approximate the interactions between core electrons and the atomic nucleus. To avoid spurious interactions, a vacuum of 30 Angstrom

was created in the non-periodic z direction and a distance of 15 Angstroms was maintained between the molecules under the supercell consideration. The Brillouin Zone was sampled using a Monkhorst Pack grid of 4 x 4 x 1. For electronic calculations, a 21 x 21 x 1 grid was considered. An HSE[20,21] calculation was performed to estimate the correct band gap. All systems were optimised until the total force reduced to 0.02 eV/atom. All geometric structures were visualised using XCRYSDEN[22] software.

For Arsenene sheets, charge transfer interactions with donor acceptor molecules, namely TTF (tetrathiafulvalene) as the electron donating moiety to phosphorene nanocluster and TCNE (tetracyano-ethylene) and TCNQ (tetracyanoquinodimethane) as electron accepting groups were studied, using Mulliken Population Analysis.

3.3 Structural Features

Germanane has a planar honeycomb structure (Space group $P6m3c$)with the unit cell having 2 Ge atoms. The crystal structure has isotropy along a and b directions, thus the lattice parameters are equal (a = b= 4.4 Å).

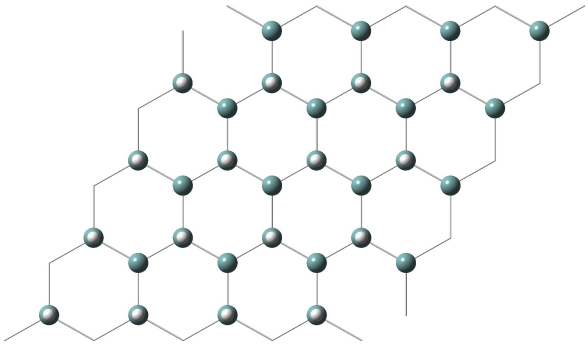

Figure 3.1: Ge-H, Ge-Cl, Ge-Br sheets *(Blue balls - Ge, White balls - H or Cl or Br)*

In the surface modified Germanane, H is replaced by Cl, Br, CH_3, NO_2, NH_2

and OH, as described in Figures 3.1, 3.2, 3.3, 3.4 and 3.5 respectively.

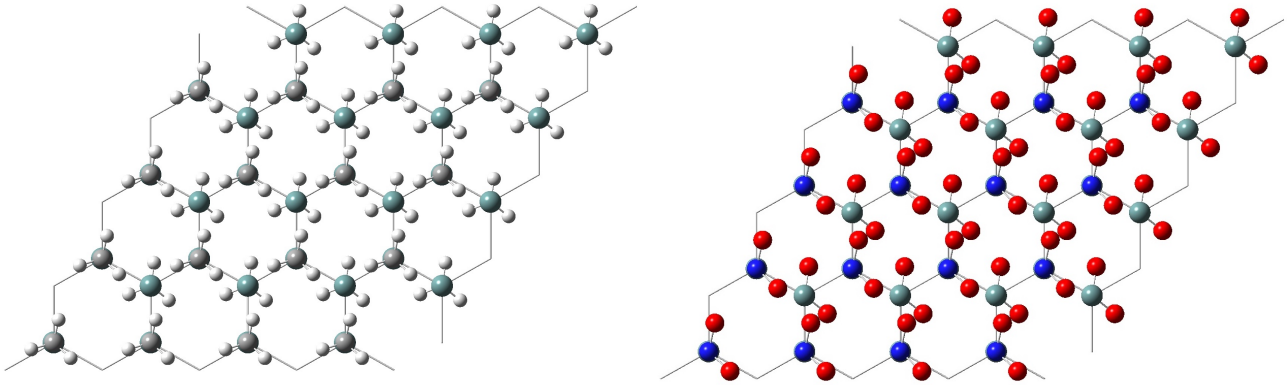

Figure 3.2: (a)Ge $-$ CH_3 sheets *(Blue balls - Ge, Grey balls - C, White balls - H)*, (b) Ge $-$ NO_2 sheets *(Light Blue balls - Ge, Dark Blue balls - N, Red balls - O)*

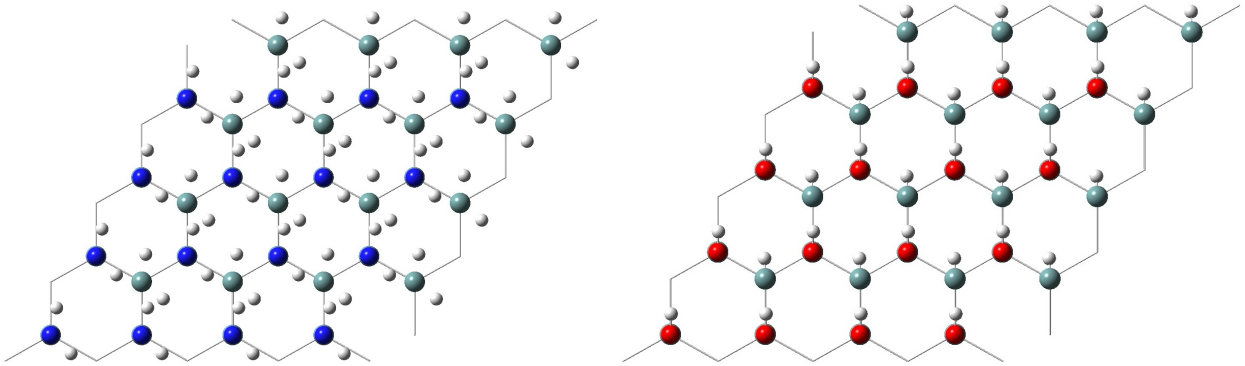

Figure 3.3: (a)Ge $-$ NH_2 sheets *(Light Blue balls - Ge, Dark blue balls - N, White balls - H)*, (b) GeOH sheets *(Light Blue balls - Ge, Red balls - O, White balls - H)*

The buckled(β-form) of Arsenene has a honeycomb structure with the space group of P3m1 structure, where the unit cell has 2 As atoms. The optimized As-As bond distances were found to be 2.503 Åand the As-As-As bond angle as 91.980. The crystal structure has isotropy along a and b directions, thus the lattice parameters are equal (a = b= 3.61 Angstroms). The buckling height is 1.40 Angstroms, which is in good agreement with previously reported data[9]. A 4 x 4 supercell with 32 atoms was studied.

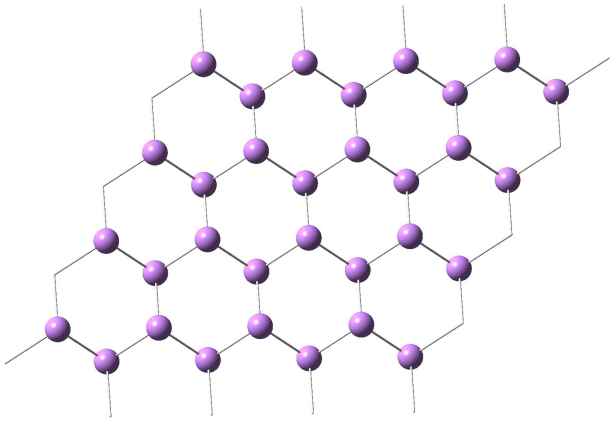

Figure 3.4: Arsenene sheet

3.4 Results and Discussion

3.4.1 Electronic Properties

Band Structure

Band structure calculations on the pristine and doped Germanane sheets revealed interesting results. Pristine Germanane is a direct band gap semiconductor with a band gap of 1.41 eV, which bears good agreement with the reported values[9].

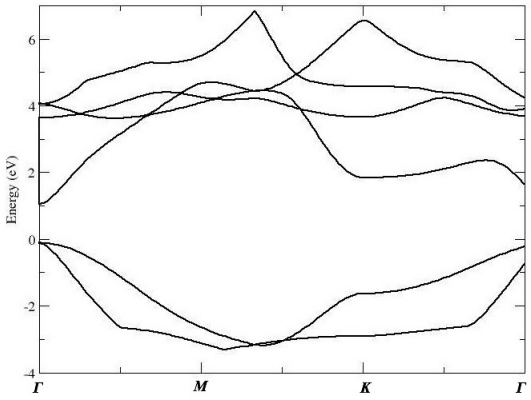

Figure 3.5: GeH band structure

Surface modification of pure germanane sheets proves to be an important approach in tuning the band gap. It is observed that nitration increases the

band gap whereas chlorination, bromination, alkoxylation, animation and hydroxylation has a reverse effect, as evident from the band diagrams(Figures 3.7 - 3.10).

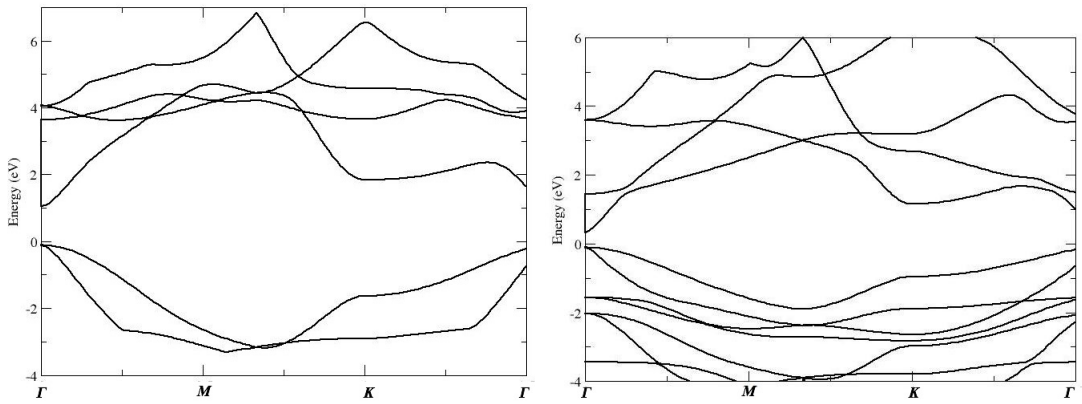

Figure 3.6: (a) GeCl band structure. (b) GeBr band structure

It is observed that the band gaps of GeBr, GeCl, $GeNH_2$ and GeOH are considerably lower than GeH and also fall within the energy range corresponding to the mid-IR zone of the electromagnetic spectra. This suggests that these materials can be effectively utilized in IR absorbing systems.

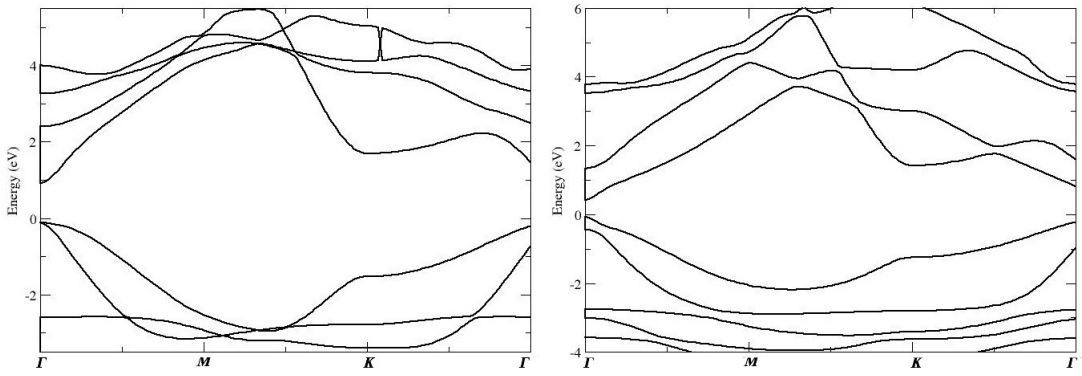

Figure 3.7: (c)GeCH3 band structure. (d) GeOH band structure

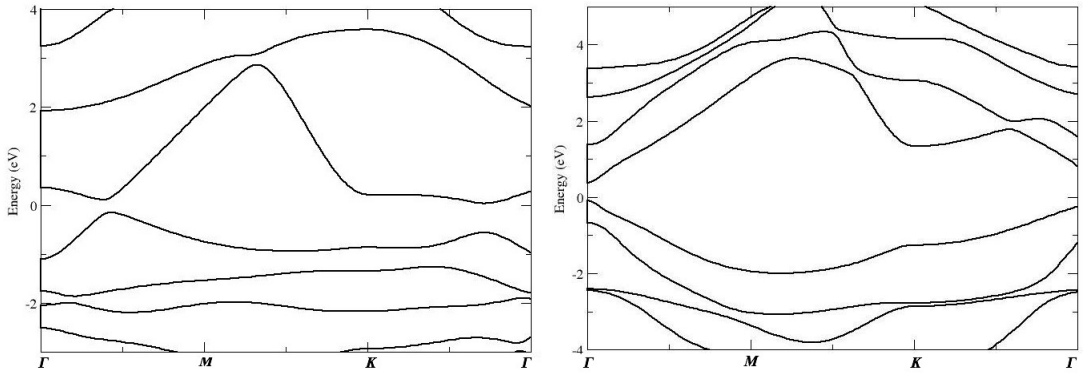

Figure 3.8: (e)GeNO2 band structure. (f) GeNH2 band structure

Morphology	**Band Gap (eV)**
GeH	1.41
GeCl	0.61
GeBr	0.45
$GeCH_3$	1.02
$GeNO_2$	1.47
$GeNH_2$	0.46
GeOH	0.51

Table 3.1: Band gaps of Pristine and Doped Germanane structures

For Arsenene sheets, Band Structure calculations were performed using the PBE functional, taking Spin-Orbit Coupling (SOC) effect into account, as the As atoms have spin orbit coupling. The band gap was found to be 1.96 eV. However, when we changed the functional from PBE to HSE06 and calculated the band structure, the band gap turned out to be 2.06 eV at the point.

Further elucidation of the band formation and contributions from different orbitals is achieved through projected density of states (pDOS) calculations. As found from the pDOS plots, the Fermi level has contributions from both s and p orbitals, but the contribution from p orbitals is higher, at the top of

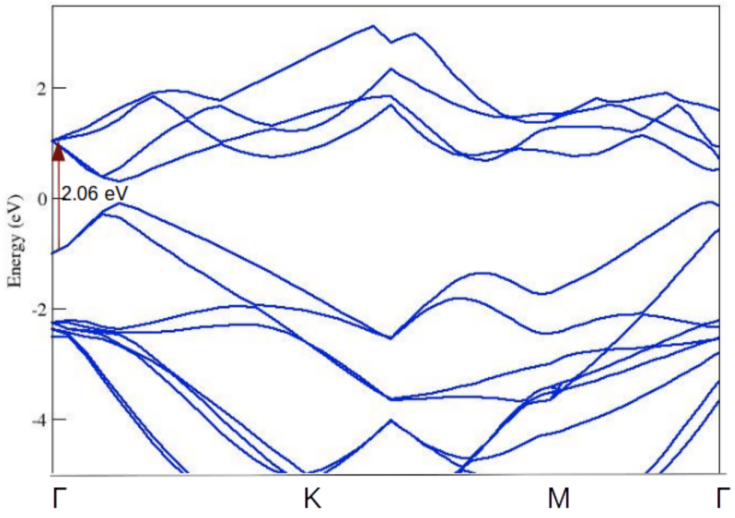

Figure 3.9: Arsenene band structure

valence bands and bottom of conduction bands. In fact, the s-orbital does not contribute at all in the conduction band of Arsenene. This is a common observation in monolayer sp_2 hybridized honeycomb structures (non-planar).

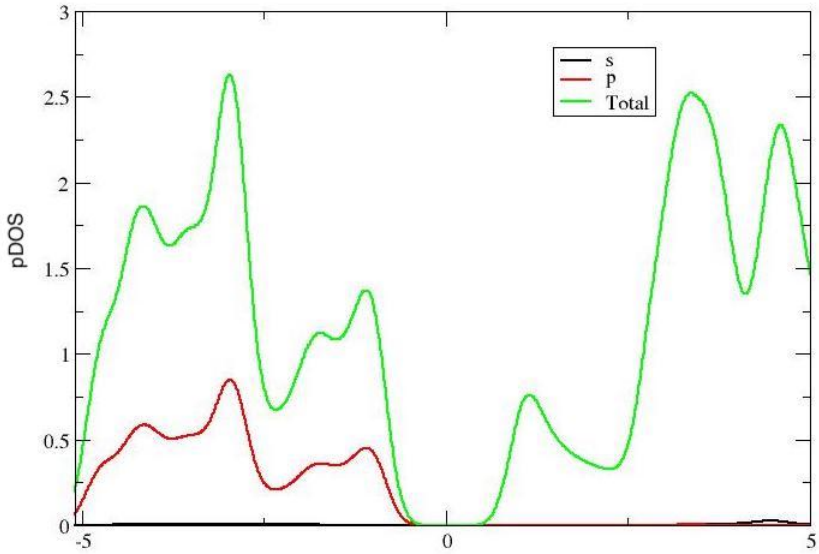

Figure 3.10: Arsenene band structure

3.4.2 Optical Properties

From TD-DFT calculations on the 4 × 4 Arsenene nanosheet, we observe an Absorption maxima at : 354.09 nm and the Emission wavelength at 431 nm of the electromagnetic spectrum, which indicates that Arsenene absorbs in the UV region and emits in the visible light range.

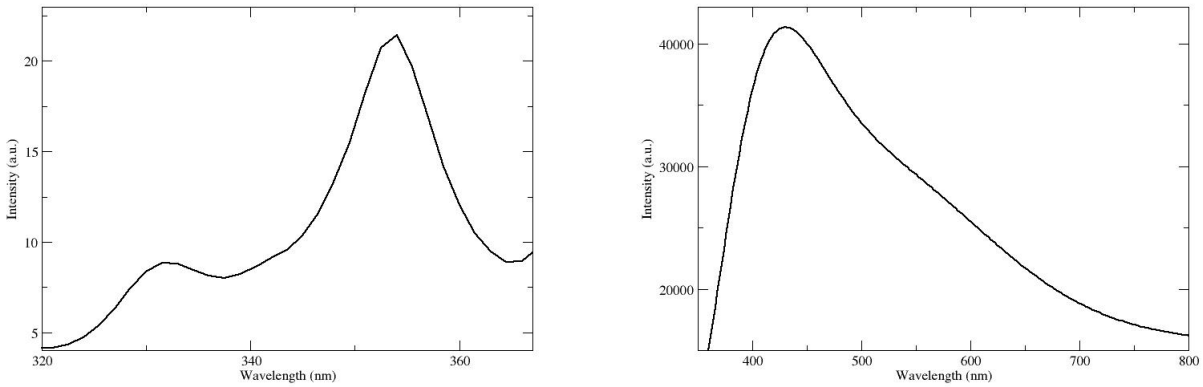

Figure 3.11: (a) Absorption spectra of Arsenene nanosheet. (b)Emission spectra of Arsenene nanosheet

3.4.3 Charge Transfer Studies

Mulliken Population study is an effective tool for studying partial atomic charges that can provide a qualitative insight into the net charge of the system. Figures 3.12 (a) and (b) show the optimized structures of TTF and TCNE molecules on Arsenene nanosheets.

A differential population analysis of the orbitals proves that there is significant electron transfer from TTF into the empty 4d bands of As atoms, and to TCNE from the 4p bands of As, as observed from the rise and fall in electronic charge density of the corresponding orbitals respectively. There

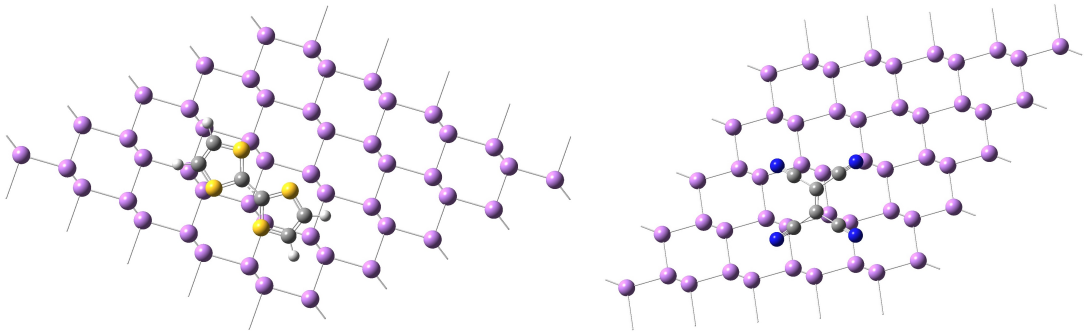

Figure 3.12: (a) Arsenene nanosheet with TTF molecule. (b)Arsenene nanosheet with TCNE molecule

is a charge transfer of 0.128e from TTF to Arsenene nanosheets into the 4d orbitals of As atoms and a transfer of 0.095e from Arsenene to TCNE from the 4p orbitals of As atoms.

3.5 Conclusion

In this chapter, nanosheets of Hydrogen-passivated Germanane and Arsenene were studied under computational frameworks. The effect of functional group substitution in Germanane by Cl, Br, CH_3, NO_2, NH_2andOH were also looked at. Electronic calculations mainly band structure calculations and projected density of states reveal how geometrical structure and composition affect the physical properties of the nanosheets. Tunability in band gap can prove to be promising in building devices with specific absorption properties, especially in the near-mid IR range. Ongoing calculations may elucidate the intrinsic details behind these observations and how they can be applied in real materials. Optical calculations on Arsenene nanosheets prove that it can be used as a material with visible light absorption. Further calculations involving the use of GW and BSE frameworks, which are improvements upon Density

Functional Theory, will correctly estimate optoelectronic properties. Charge transfer studies were performed on Arsenene nanosheets by Mulliken Population analysis which shows that the extent of charge transfer is more from the donor molecule TTF to the Arsenene sheet rather than from the sheet to the acceptor molecule TCNE.

References

[1] A.K. Geim, I.V. Grigorieva, *Nature*, 2012, **499**, 419.

[2] V Zólyomi, J. R. Wallbank and V.I. Fal'ko, *2D Mater.*, 2014, **1**.

[3] A. O'Hare, F.V.Kusmartsev, K.I. Kugel, *Nano Lett.* 2012, **12**, 1045.

[4] S.Cahangirov, M. Topsakal, E. Aẗurk, H. Sahin, S. Ciraci, *Phys. Rev. Lett.*, 2009, **102**.

[5] E.Bianco, S.Butler, S.Jiang, O.D.Restrepo, W.Windi, J.E.Goldberger *ACS Nano*, 2013, **7**, 4414.

[6] S.S. Jiang, S. Butler, E. Bianco, O.D. Restrepo, W.Windl, J.E. Goldberger, *Nat. Commun*, 2014, **5**, 3389.

[7] G. Vogg, M.S. Brandt, M. Stutzmann, *Adv. Mater.* 2000, **12**, 1278.

[8] H. Okamoto, Y. Kumai, Y. Sugiyama, T. Mitsuoka, K. Nakanishi, T. Ohta, H. Nozaki, S. Yamaguchi, S. Shirai, H. Nakano, *J. Am. Chem. Soc.* 2010, **132**, 2710.

[9] J. Zhao, H. Zeng, *RSC Adv.*, 2016, **6**, 28298.

[10] C. Kamal, M.Ezawa, *Phys. Rev. B*, 2015, **91**, 085423.

[11] Y. Xu, B. Peng, H. Zhang, H. Shao, R. Zhang, H. Lu, D.W. Zhang, H. Zhu, 2016, *arXiv:1604.03422 [cond-mat.mtrl-sci]*

[12] D. Kecik, E.Durgun, S.Ciraci, *Phys. Rev. B*, 2016, **94**, 205410.

[13] Y. Wang, Yanli, Ding, *Nanoscale Research Letters*, 2015, **10**, 1.

[14] M-Y Liu, Y. Huang, Q-Y. Chen, C. Cao, Y. He, *Scientific Reports*, 2016, **6**.

[15] P. Giannozzi, S. Baroni, N. Bonini, M. Calandra, R. Car, C. Cavazzoni, D. Ceresoli, G. L. Chiarotti, M. Cococcioni, I. Dabo, A. Dal Corso, S. Fabris, G. Fratesi, S. de Gironcoli, R. Gebauer, U. Gerstmann, C. Gougoussis, A. Kokalj, M. Lazzeri, L. Martin-Samos, N. Marzari, F. Mauri, R. Mazzarello, S. Paolini, A. Pasquarello, L. Paulatto, C. Sbraccia, S. Scandolo, G. Sclauzero, A. P. Seitsonen, A. Smogunov, P. Umari, R. M. Wentzcovitch, J.Phys.:Condens.Matter 21, 395502 (2009) http://dx.doi.org/10.1088/0953-8984/21/39/395502.

[16] P Giannozzi, O Andreussi, T Brumme, O Bunau, M Buongiorno Nardelli, M Calandra, R Car, C Cavazzoni, D Ceresoli, M Cococcioni, N Colonna, I Carnimeo, A Dal Corso, S de Gironcoli, P Delugas, R A DiStasio Jr, A Ferretti, A Floris, G Fratesi, G Fugallo, R Gebauer, U Gerstmann, F Giustino, T Gorni, J Jia, M Kawamura, H-Y Ko, A Kokalj, E Kkbenli, M Lazzeri, M Marsili, N Marzari, F Mauri, N L Nguyen, H-V Nguyen, A Otero-de-la-Roza, L Paulatto, S Ponc, D Rocca, R Sabatini, B Santra, M Schlipf, A P Seitsonen, A Smogunov, I Timrov, T Thonhauser, P Umari, N Vast, X Wu and S Baroni, *J.Phys.Condens.Matter*, 2017, **29**, 465901.

[17] J.P.Perdew, K. Burke, M. Ernzerhorf, *Phys. Rev. Lett.* 1996, **77**, 3865.

[18] S. Grimme, *J. Comput. Chem.* 2006, **27**, 1787.

[19] D. Vanderbilt, *Phys. Rev. B*, 1990, **41** 7892.

[20] Heyd, Scuseria, and Ernzerhof *J. Chem. Phys.*,2003, **118**, 8207

[21] Heyd, Scuseria, and Ernzerhof, *J. Chem. Phys.*, 2006, **124**, 219906.

[22] A. Kokalj, *Comput. Mater. Sci*, 2003, **28**, 155; XCRYSDEN code; http://www.xcrysden.org

4

NASICON Type Cathode Materials for Sodium Ion Batteries

Energy is omnipresent and drives everything. Our modern lives, both individual and societal, have come to depend on its abundance, convenience, and potential. It is the motive force within our bodies, propelling our vehicles, lighting our world, making our lives more convenient. We are in the midst of a continuous cycle of acquiring and returning energy from and to our global environment. But the demand for energy is insatiable and unending. And perhaps one of the most important and indispensable forms of energy today is electricity. Talking of supplies, the historically state-owned electricity sector in developing countries is dependent on state subsidies for operating expenses, and has limited ability to generate resources for investment in modern equipments. Developing countries undertook sweeping reforms of their electric sectors in the 1990s. A key motivation for these reforms was to attract private investment to increase supply and provide universal access to electricity

at affordable prices.

The last few decades have been witness to an exponential rise in the consumption of electricity on a global scale, notwithstanding the fact that still 60% of the total population has no access to electricity. Technology-enabled urban lifestyles demand more electricity. The growth of the middle class, rising incomes, and more electricity-enabled appliances and machines contribute to the increasing electricity demand. Experts believe that the demand for electricity will double by 2060. Meeting this demand with more sustainable and cleaner energy sources will require substantial infrastructure investments and systems integration to deliver benefits to to all consumers.

Bearing the above in mind, quite naturally, a lot of research is put into efficient Electrical Energy Storage (EES). The roles of such EES devices are manifold. Firstly, EES reduces electricity costs by storing electricity obtained at off-peak times when its price is lower, and use is lesser, for use at peak times. Secondly, in order to improve the reliability of the power supply, EES systems support users when power network failures occur due to sudden unavailability like, natural disasters. Their third role is to maintain and improve power quality, frequency and voltage. They are also alternative cleaner replacements for conventional energy sources.

A Ragone plot is used for performance comparison of various energy-storing devices. On such a chart the values of specific energy (in Wh/kg) are plotted versus specific power (in W/kg).

$$\text{Specific Energy} = \frac{(V \times I \times t)}{m}$$

$$\text{Specific Power} = \frac{(V \times I)}{m}$$

where V = voltage, I = current t = time, m = mass

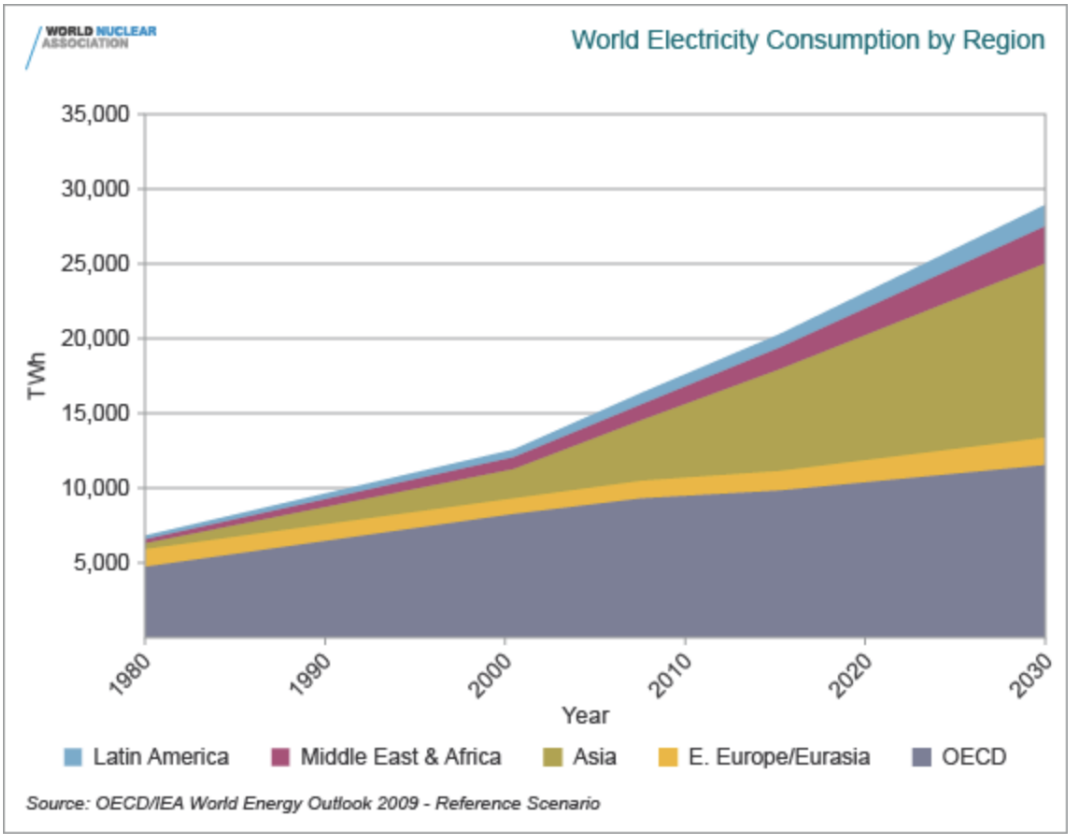

Figure 4.1: Global Electricity Consumption.
(Adapted from :*World Economic Forum. www.weforum.org*)

Batteries have been a fundamental source of electricity before the development of electric generators and electrical grids since the end of the 19th century. They are promising storage technologies for stationary applications because of their maturity, and the ease with which they are designed and installed compared to other technologies. The best EES device is the one which produces maximum specific energy by consuming minimum power.

Batteries are rated in terms of their nominal voltage and ampere-hour capacity. And there is a constant thirst to increase these parameters

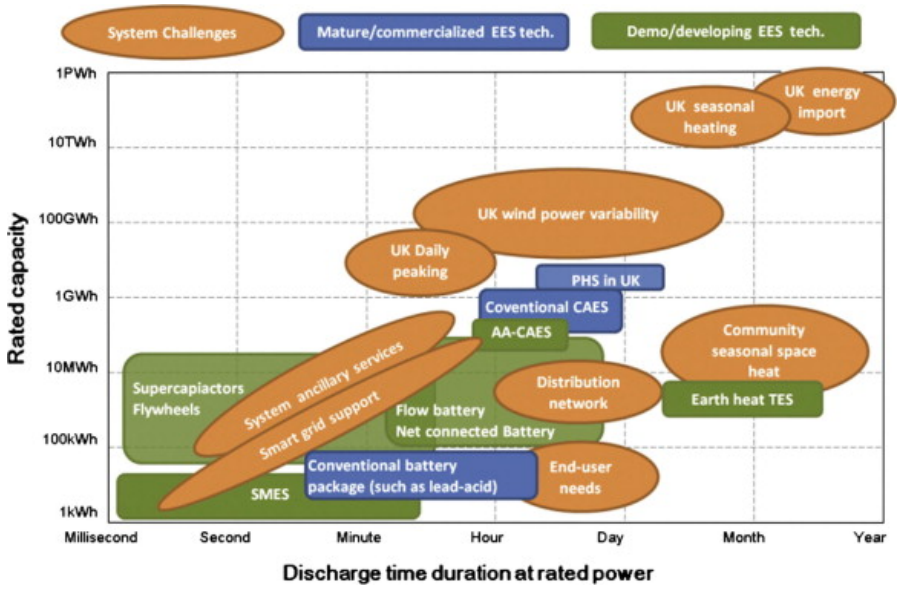

Figure 4.2: Available EES systems with Discharge Capacity.

for more sophisticated application. There has been significant research devoted to improve the same by modulating the choice of electrodes and electrolyte. And we have indeed come a long way from the pre-historic Baghdad batteries and Alessandro Volta's voltaic piles to the ubiquitous Alkali Metal Ion Batteries, with the Lithium Ion overshadowing most other candidates because of its high capacity and recyclability.

4.1 Lithium Ion Batteries

Ever since Prof. John B. Goodenough's successful construction[1,2] and commercialization of the Lithium Ion Battery, in 1991, technology has moved in leaps and bounds achieving high performance rechargeable batteries. The LIB offers significantly high energy and power density, making it a numero-uno choice for all kinds of applications ranging from nano-devices to daily handheld electronic gadgets to high-power consuming

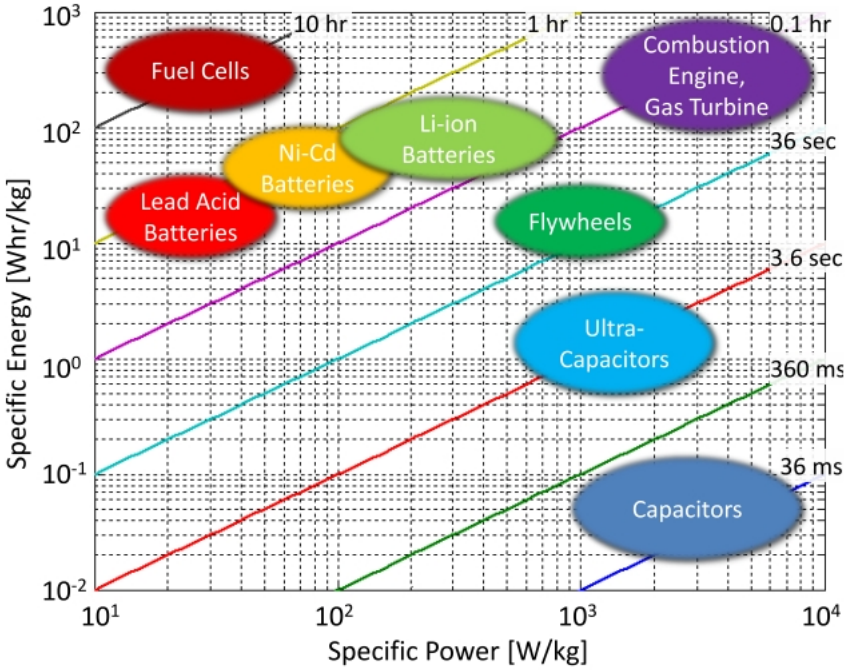

Figure 4.3: Ragone Plot for EES Devices.

grids. Li-ion batteries have certain fundamental advantages over other chemical systems. Firstly, Li has the lowest reduction potential of any element, allowing Li based batteries to have the highest possible cell potential and cell capacity of **372** $mAhg^{-1}$. Also, Li is the third lightest element and has one of the smallest ionic radii of any single charged ion. These factors allow Li-based batteries to have high gravimetric and volumetric capacity and power density. Finally, although multivalent cations allow for higher charge capacity per ion, the additional charge significantly reduces their mobility. Also, a significant shortage of Li is unlikely in the near future. Overall, the LIB technology is a real success story. Since its commercialization, the energy density continuously increased by about 7-8 Wh/kg per year, now reaching about 250 Wh/kg on the cell level (18650-type cells)[3,4].

The present day market for lithium ion batteries is far more complicated

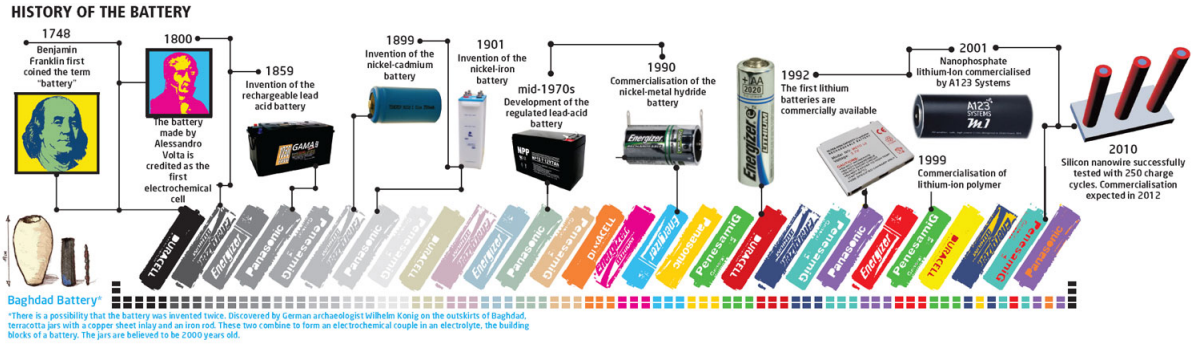

Figure 4.4: Evolution of EES Devices.

than the original small electronic devices. Many additional markets have been opened for small electronic devices such as lighting (LCD and fluorescent lights), medical devices, and many others. While high energy cells now have as much as 3.4 Ah, the high power cells have sacrificed some capacity to obtain 20A or higher continuous discharge capability in the same cell size. While some cells claim as high as 2.5 Ah capacity, it is difficult to sustain such a high capacity during cycling. The advantages and disadvantages of the LIB are summarized in the Table 4.1 [5,6].

Advantages	**Disadvantages**
1. Smaller and Lighter	1. Expensive
2. High Energy Density	2. Sensitivity to higher temperatures
3. Low self-discharge	3. Deep discharge
4. Zero to low memory effect	4. Aging Effects
5. Quick charging	5. Safety Issues
6. High Open Circuit Voltage	5. Environmentally unfriendly

Table 4.1: Advantges and Disadvantages of LIBs.

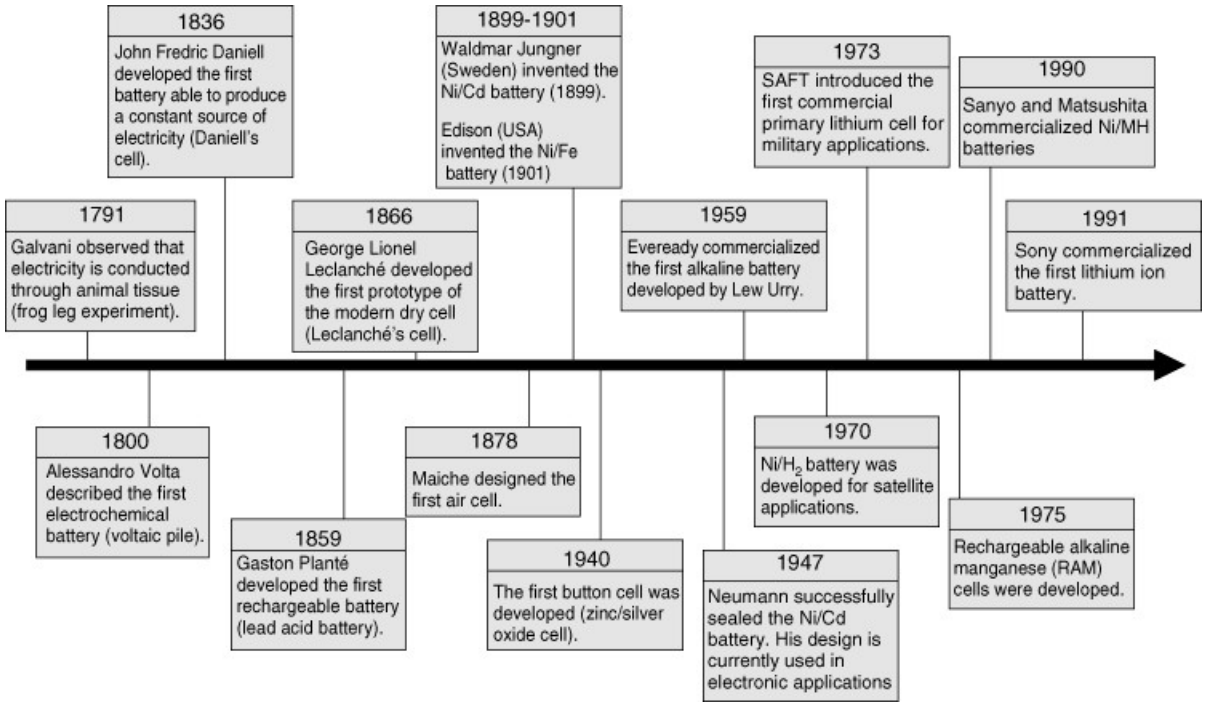

Figure 4.5: Timeline of Important Events in the Development of Batteries.

4.2 Advent of Sodium Ion Batteries

As our oceans and dinner-table shakers show, salt is everywhere, and its ability to carry a charge makes it a perfect low-cost energy storage candidate. Sodium-based batteries are making in-roads in various forms, from the standard 18650 format used in laptops, to a quirky design with an anode made of a carbonized oak leaf. Sodium, the **fourth most abundant** element on earth, has a seemingly unlimited distribution. SIBs (Sodium Ion Batteries) were initially studied when the development of LIBs began in the 1970s and 1980s, but due to rapid advances in the development and success of commercial applications of LIBs, SIBs were largely abandoned. However, in the search for newer battery technologies, sodium shows good potentiality. Sodium has a normal electrode potential of approximately **0.3V** higher or, in terms of ion volume, twice or greater

than lithium. Sodium is also cheaper, less toxic and more abundant than Lithium. If sodium ion secondary batteries can be made practical, there will be an approximately a three digit relaxation in the constraints on reserves accompanying this, and we can expect that the environmental impact and cost will be greatly reduced.

Currently, one of Na-ion's largest drawbacks is that the batteries take a long time to charge and discharge, and a slow discharge rate does not supply enough power density for high-power applications. In general, there is a tradeoff between the charge/discharge rate and capacity, so that attempts to increase the charge/discharge rate have resulted in severely reduced capacity. The new Na-ion batteries can operate at a current density (a measure of the charge/discharge rate) that is 1000 times higher (10 A/g vs. 10 mA/g) than most previously reported organic Na-ion batteries while retaining a much higher capacity (72 mAh/g).

	lithium	sodium
ratio of reserves	1	1,000
cost (for carbonate)	$ 5,000/t	$ 150/t
atomic weight	6.9 g/mol	23 g/mol
ionic volume	1.84 Å^3	4.44 Å^3
theoretical capacity	3,829 mAh/g	1,165 mAh/g
normal electrode potential vs. SHE	–3.045 V	–2.714 V

Figure 4.6: Lithium vs Sodium (Adapted from *Development of a Sodium Ion Secondary Battery*, Sumitomo Kagaku, 2013)

Like every battery, SIB consists of two electrodes of sodium insertion materials for positive and negative electrodes and they are ionically connected by sandwiching electrolyte which is generally a Na salt dissolved in organic solution. As sodium is the second-lightest and -smallest alkali

metal next to lithium, the sacrifice in energy density is expected to be minimized since electrochemical Na insertion/deinsertion is same as that of Li-system. Furthermore, contrary to Li-Al alloy formation in LIB's, a copper current collector for a negative electrode is able to be replaced with much inexpensive aluminum because Na metal does not form alloy with Al, which is definitively advantageous of SIBs.

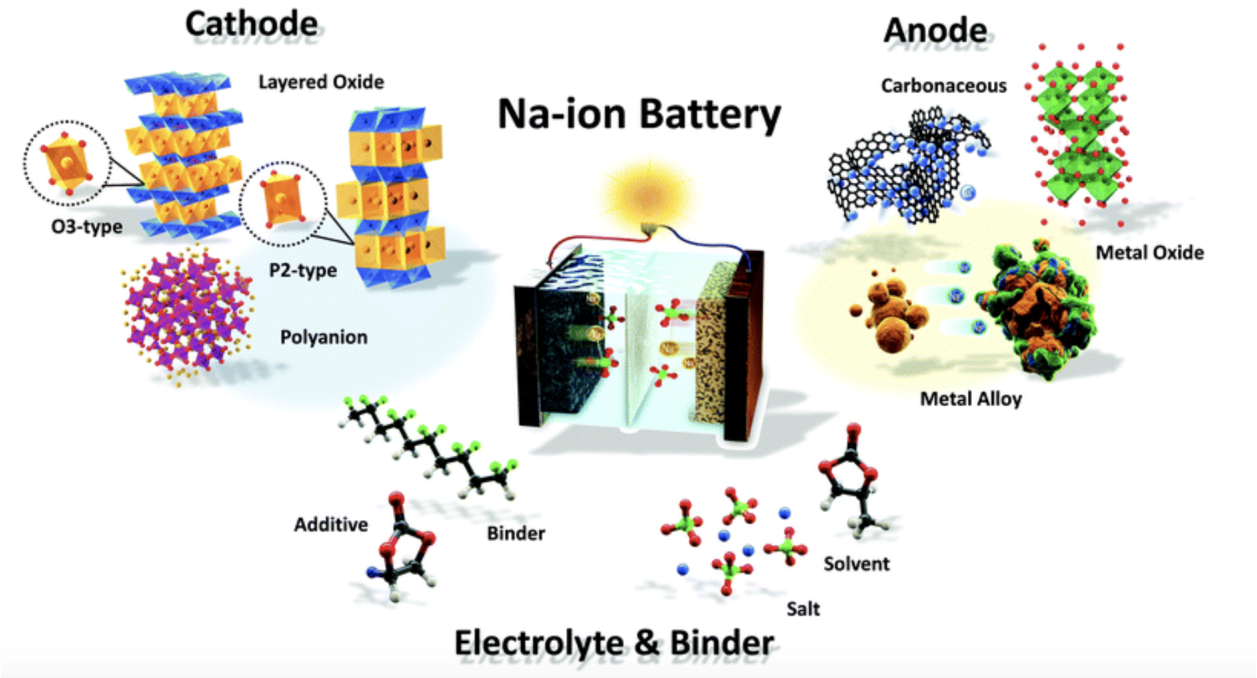

Figure 4.7: Sodium Ion Battery Scheme (Adapted from *Sodium-ion batteries: present and future*; Jang-Yeon Hwang et al; *Chem.Soc.Rev.*2017)

Following the scheme of existing lithium-ion batteries, a intercalation sodium battery could consist of an anode made of a high-capacity, dense Na-metal alloy (e.g. Na metal, Na_4Sn or Na_xC) and a high-capacity cathode. Research is still in its initial phase regarding the design of SIB's, with the focus on organic electrolytes which provide higher cell voltages. Following is a brief summary of what has been achieved so far in the SIB

technology.

Cathodes

Metal oxide cathode materials are promising candidates for SIBs because there are several processing techniques (e.g. sol-gel method, co-precipitation, solid state reaction, etc.) that can be used to obtain these stoichiometric layered structures. Many of these materials are nano-sized, which offer large surface area and short diffusion paths for ions during de/sodiation upon cycling. For most of the oxide materials, the amount of sodium deintercalated from the cathode material ranges from **0.5 to 0.85**[7]. This is dependent on the initial stoichiometry and phase transitions that occur with respect to the change in oxidation states of the metals within the active material. Understanding the electrochemical behavior of the active materials at these different stages will enable the determination of the acceptable Na content range for alkali ion layers.

It has been observed that crystal structure plays an important role in the functionality of SIBs. Also, significant differences arise while using pure crystal systems and mixed ionic solids. The use of substitution or doping of other transition metals in the layered oxide structures can offer multiple advantages over oxides with a single transition metal component, including-

1. Better stability of the material,
2. Increased capacity by adding more redox active substitutes
3. Removal of Jahn-Teller distortions
4. Reduction in volume change of the active material
5. Higher cycling numbers with better capacity retention.

Three types of Na-insertion materials have been explored so far - layered oxides or sulfides, cyanoperovskites and framework oxides. Currently, mixed oxides like $NaFeO_2$, $Na(Ni_{1/3}Fe_{1/3}Mn_{1/3})O_2$ are being explored for their high charge-discharge cycle rates.

Anodes

The lower energy density and limited cycling life of SIBs are still the main challenges impeding their wide application. Tremendous work has been done on anode materials for SIBs, and rational structural design is considered as an effective way to enhance their electrochemical performance. The anode materials for SIBs can be categorised into three groups, based on the reaction mechanism during sodiation/desodiation processes[7]:

(1) the insertion reaction materials, which include carbonaceous materials and titanium-based oxides; (2) the conversion reaction materials, represented by transition metal oxides or transition metal sulphides; and (3) the alloying reaction materials, including Na-metal alloying compounds containing elements of Group 14-15. There are some characteristic benefits and drawbacks for each type, which fosters extensive research for finding appropriate anodic materials. Nano-sized materials constitute a big group, which includes nano particles, nano cubes, nano fibers or nano sheets, these different structures could also make up 3D network morphology. The advantage of nanostructured materials is that they have robust structures with short diffusion path for both Na-ions and electrons.

Some other hierarchical structures are also useful, such as core-shell or

yolk-shell structure, which contain shell that could suppress particle aggregation and volume change effectively, the space in yolk-shell structure could be considered as wonderful buffer zone as well. However, these two kinds of structures are more complicated to be synthesized. Therefore, anode materials for SIBs can be categorized into these three groups: (1) nanostructures; (2) porous or hollow structures; (3) layered structures and (4) core-shell or yolk-shell structures.

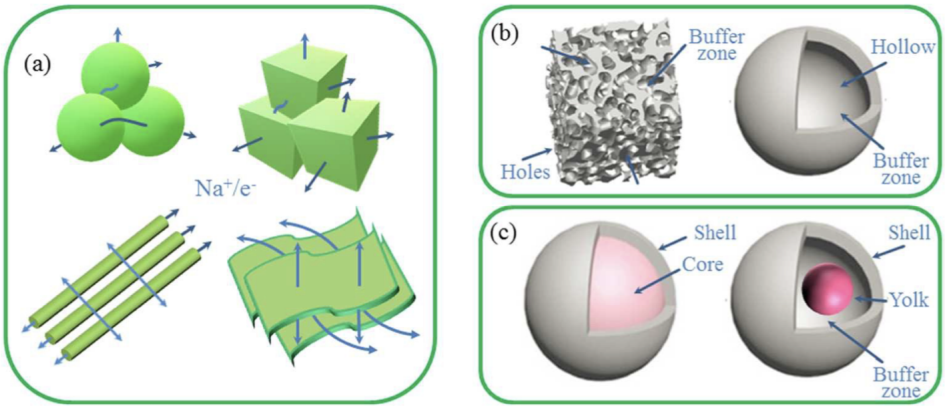

Figure 4.8: Schematic figures of (a) Nanostructures (spheres, cubes, fibers and sheets), (b) porous and hollow structures, (c) core-shell and yolk-shell structures. (Adapted from *Structural Design of Anode Materials for Sodium-Ion Batteries, Journal of Materials Chemistry A*)

Electrolytes

Electrolyte design or functional development is very effective at promoting the performance of sodium-ion batteries. The electrolyte plays a key role in balancing and transferring charges in the form of ions between the two electrodes. It basically determines the electrochemical window of a cell according to the LUMO and HOMO energies of the mixture, which reflect the thermodynamic stability. Additionally, operational

kinetics control of SIBs is closely connected to Na^+ transference numbers of the electrolyte and the solid-electrolyte interface (SEI) on the anode, which is related to the electrolyte composition. As previously reported, the optimal electrolyte will form a suitable SEI layer on the anode and improve cycling and rate performance of the cells.

Generally, the choice of electrolyte decides or affects energy density, safety, cycle life, storage performance, operating conditions, etc. Furthermore, as is well known, electrode materials determine the specific capacity of batteries and thus attract more research attention than the electrolyte, while the reversible capacity of active materials is influenced by the electrolyte. The interaction between electrolyte and electrodes in all electrochemical processes significantly influences the SEI interface state and internal structure of active materials. Therefore, good compatibility between the electrolyte and electrode enhances the performance of electrode materials and even that of the whole battery. As of now, a few studies have been done on comprehensively investigating electrolyte formula or new electrolyte systems.

Popular choices for the SIB electrolyte are

(1) Non-aqueous Liquid Electrolytes:

Organic solvents meet the following conditions:

- Sufficient dissolving capacity of the salt. This means that a solvent with a high dielectric constant will ensure a high ionic conductivity.

- Relatively low viscosity over a wide temperature range. This is required so that the resistance to ionic migration is small and the solvent remains as a stable liquid over a wide temperature range.

- High electrochemical and chemical stability. High electrochemical stability of the solvent and good compatibility between solvents and electrodes are a precondition to developing a high energy density cell with excellent electrochemical performance.

- Low cost, simple preparation, and environmental benignity are the main reasons why non-aqueous liquid electrolytes are intensively investigated not only for commercial LIBs but also for emerging SIBs.

Ethylene carbonate (EC), dimethyl carbonate (DMC), and an ethyl methyl carbonate (EMC)/ diethyl carbonate (DEC) mixture have been presented as effective liquid electrolytes in SIB's as of now.

(2) Aqueous Liquid Electrolytes :

Aqueous electrolytes offer many advantages, such as low cost, high inherent safety, and eco-friendliness. Na_2SO_4 with various concentrations in deionized water is the most widely-used electrolyte. It has also been observed that by adjusting the electrolyte pH, the potentials of Na intercalation and de-intercalation of some materials could be controlled in the stable range of water.

(3) Solid State Electrolytes : Unlike liquid SIBs, solid-state SIBs can completely address the safety issue because they can employ non-flammable solid- state electrolytes, which eliminate the leakage or flammability problems for liquid SIBs. In addition, a solid-state electrolyte with a wide electrochemical window makes possible the use of a metal sodium anode and high-potential cathode for high- energy-density batteries. Additionally, mechanical properties, flexibility, and simple

assembly processes (since electrolytes act both as the ion transport pathway and the separator) make them especially attractive. Nowadays, solid polymer electrolytes and conductive inorganic electrolytes (glasses and ceramics) are the common solid-state electrolyte materials that are studied and used in SIBs.

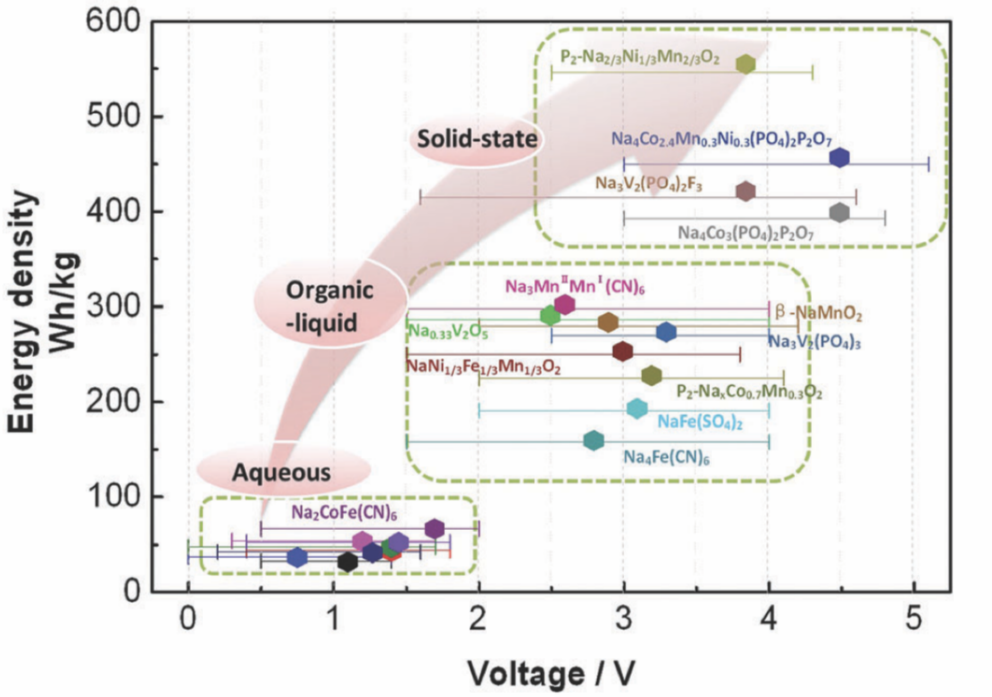

Figure 4.9: The energy density of various SIBs based on different electrolytes. (Adapted from *Electrolyte design strategies and research progress for room-temperature sodium-ion batteries, EnergyEnviron.Sci.*,2017)

Research on electrochemical Na intercalation in battery system has been reported since the early 1980s but Na-ion batteries have not been commercialized as well Lithium Ion Batteries. Since 2010, with the slogan of beyond lithium, research trends in SIBs have been intensively focused on electrode materials. There is enough room for improving the currently present prototypes, especially in materials suited for the cathode. Apart from inherent thermodynamic disadvantages, SIBs have to over-

come multiple kinetic problems, such as fast capacity decay, low rate capacities and low Coulombic efficiencies.

Special attention is now being diverted to a class of compounds termed as **NASICON** (Sodium **S**uper **I**onic **CON**ductor) materials, as they exhibit exceptionally high ion conductivity, coupled with structural stability - rendering them most promising for sodium storage. Moreover, the flexibility of the NASICON structure allows the accommodation of transition metal ions, by which electronic conductivity is induced and Na^+ - storage is enabled. Before diving into the technical aspects of our calculations, it would be beneficial to conceptually get acquainted with this class of materials.

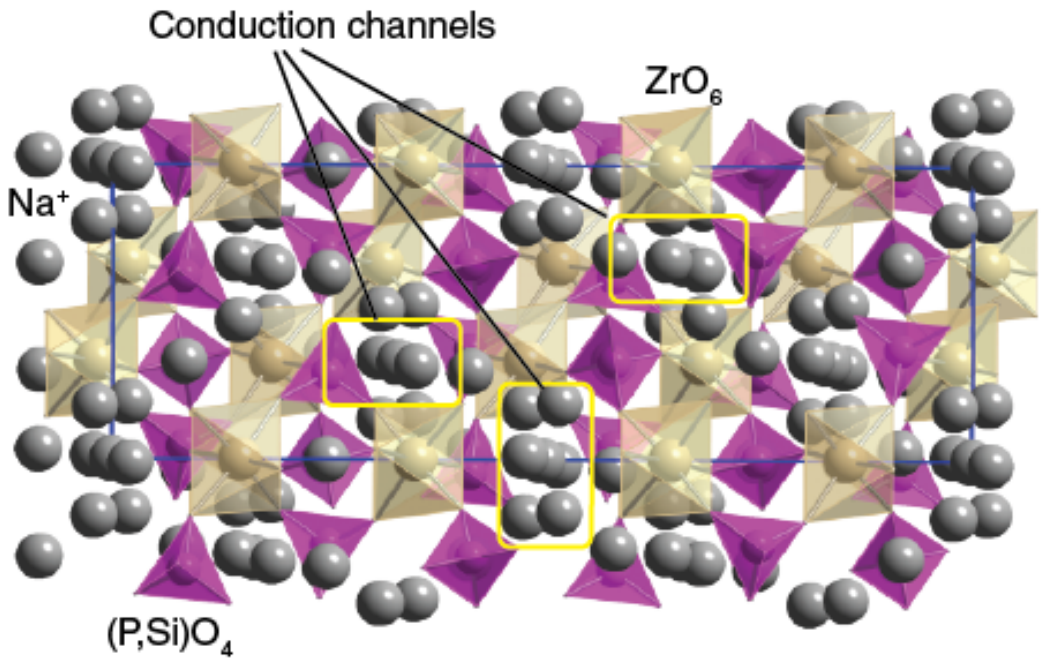

Figure 4.10: Generic crystal structure of NASICON. (Image courtesy : *http://www.chemtube3d.com*)

4.3 The NASICON Class of Materials : A Brief Overview

In the middle of twentieth century (before 1960s), ionic conductors like a-AgI, Ca^{2+}, or Y^{3+} substituted ZrO_2 were studied[9]. In 1960s, an excellent Na^+ conductor, β-Alumina ($Na_2O.11Al_2O_3$), was prepared[10,11]. β-Alumina has a layered structure and Na^+ ions migrate between two-dimensional conductive planes only. To overcome this restriction, *Hong* and *Goodenough* et al[12,13]. proposed a framework structure with suitable tunnel size for Na^+ migration in a three dimensional network of $Na_{1+x}Zr_2P_{3-x}Si_xO_{12}(0 < x < 3)$. They were termed as NASICON - an acronym for sodium (Na) Super Ionic CONductor.

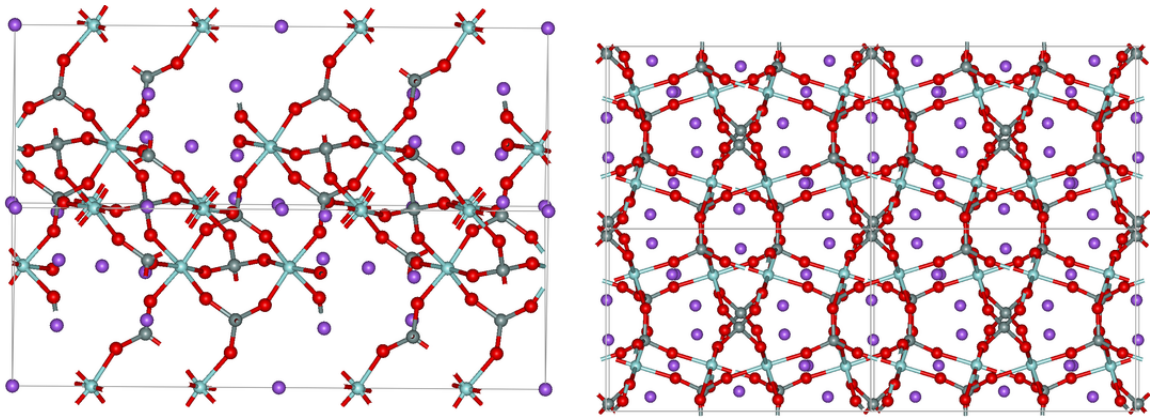

Figure 4.11: (a) Unit cell of $Na_{1+x}Zr_2P_{3-x}Si_xO_{12}$ (x = 1) (b) 2 x 2 cell of $Na_{1+x}Zr_2P_{3-x}Si_xO_{12}$ (x = 2). (red: O, purple: Na, light green: Zr, dark green: sites shared by Si and P) (*Image Courtesy : www.wikipedia.org*)

They are a class of structurally isomorphous 3D framework compounds possessing high ionic conductivity, often comparable to that of liquid electrolytes at higher temperatures. The high ionic conductivity (10^{-3}S/cm) of these materials is used in making devices such as membranes, fuel cells, and gas sensors. In addition, their low thermal expansion behaviour, host

for radioactive waste, fairly large surface area (hence used in catalytic conversions), and ability to accommodate ions in the lattice make them worthy of investigation. The high conductivity is due to hopping of Na ions among interstitial sites of the NASICON crystal lattice.

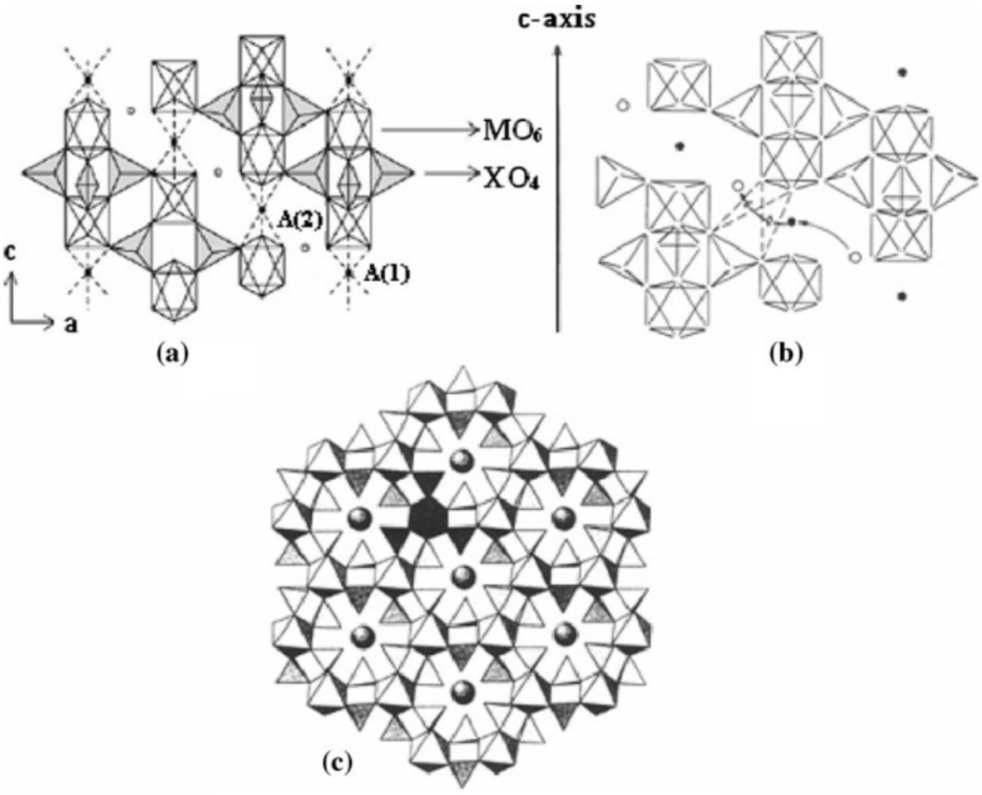

Figure 4.12: The structure of Nasicon showing a The A1 (type 1) and A2 sites (type 2), b conduction pathway, and c hexagonal array of the [A2(XO4)] groups in the plane (001) [15]

4.4 Structure and Composition

The crystal structure of NASICON compounds was elucidated in 1968 [14]. It is a covalent network consisting of ZrO_6 octahedra and PO_4/SiO_4 tetra-

hedra that share common corners. The NASICON electrical conductivity, depends on the NASICON composition, on the site occupancy, and on the oxygen content in the surrounding atmosphere.

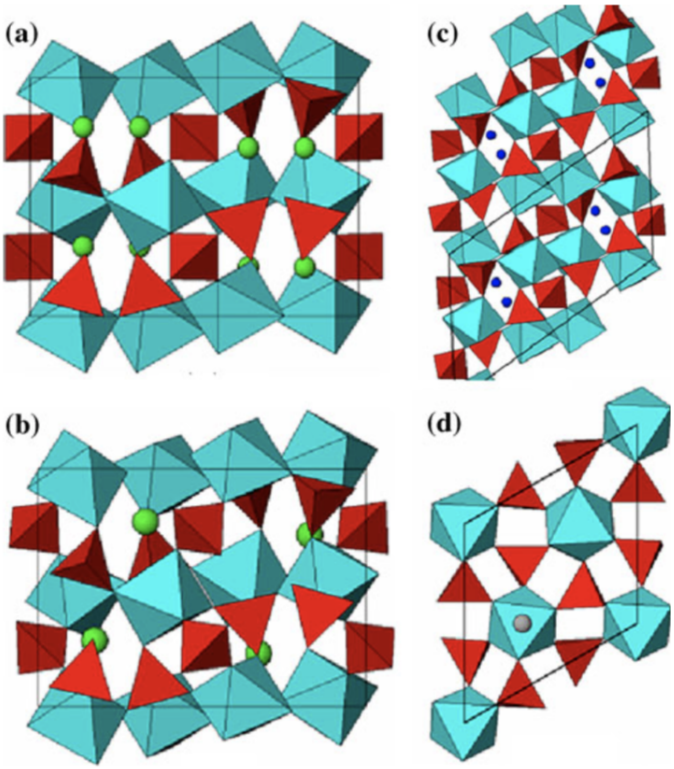

Figure 4.13: Structures of Nasicon polymorphs: a orthorhombic (Pbna), b monoclinic (P2 /c), c triclinic (C1), and d Corundum-like.[15]

The general formula of Nasicon composition can be written as $AMM'P_3O_{12}$ (or $AM_1M_2P_3O_{12}/AM_1M_2(PO_4)_3$) where the site A can be occupied by alkali ions (Li^+, Na^+, K^+, Rb^+, Cs^+, alkaline earth ions (Mg^{2+}, Ca^{2+}, Srg^{2+} etc.), and H^+, H_3O^+, $Ln^{3+}(Ln = rare - earth)$, Zr^{4+}, or it can also be vacant. The M and M' sites are occupied by di (Zn^{2+}, Cd^{2+}, Ni^{2+}, Mn^{2+} ,Co^{2+}), tri (Fe^{3+}, Sc^{3+}, Ti^{3+},V^{3+}, Cr^{3+}...), tetra (Ti^{4+}, Zr^{4+}, Sn^{4+}, Si^{4+}, Ge^{4+}), and penta (V^{5+}, Nb^{5+}, Ta^{5+}, Sb^{5+}, As^{5+}) valent transition metal ions to balance the charge suitably[15].

Phosphorus can be partially substituted by Si or As. Depending on the composition, the crystal structure can be **rhombohedral** (for many Nasicon systems), **monoclinic, triclinic, orthorhombic, Langbeinite, Garnet, SW type** (orthorhombic scandium wolframate Sc2(WO4)3), and **corundum-like**. The rhombohedral structure (Figure. 4.10) consists of a three-dimensional rigid framework with $M(M')O_6$ octahedra and $PO_4(SiO_4)$ tetrahedra sharing common corners. This 3D framework contains interconnected channels in which the mobile conducting ions are encapsulated at A sites. The interstitial space of the tunnels provides the conduction pathway for the mobile ion as shown in Figure 4.12 . The ions present in A position can have two different sites: type I sites situated between two $M(M')O_6$ octahedra along the c-axis (ribbons of $O_3MO_3AO_3M'O_3$) with a distorted octahedral coordination and type II sites (Figure 4.12.) located between the ribbons perpendicular to c-axis with a trigonal prismatic coordination. The ribbons are connected by PO_4 tetrahedra along the a-axis. All these compounds sharing the same topology in their framework are called Nasicons irrespective of its magnitude of conductivity.

4.4.1 Properties

NASICON materials are known for their unique characteristics like -

1. Ionic Conductivity : NASICON has 3D channels which allows far better ionic conductivity than that in Na- β-Alumina. The conductivity is often comparable to liquids at high temperatures. The highest ionic conductivity is usually obtained for x = 2, because at x

= 2, the relative partial molar enthalpy of $Na_2O$is minimum and the relative partial molar entropy of Na_2O on the other hand is maximum, hence Na^+ ions are more mobile in this composition.

2. Thermal Conductivity : NASICON shows low thermal expansion behaviours which depend on the composition and the lowest value occurs at x = 0.33. There is no information about crack formation in NASICON upon heating and cooling or due to thermal shock.

3. Storage Kinetics : storage kinetics is not just transport controlled. This is due to the heterogeneity of the situation and also due to the superposition of migration and diffusion. The situation can be grossly simplified if the electrode is either predominately ionically or electronically conductive, which is normally the case. Given sufficiently fast access of ions (liquid electrolyte) and electrons (current collecting phase) to the electroactive particles (including fast phase transfer), the storage kinetics is then a chemical diffusion problem, where the chemical diffusion coefficient is given by[15,16] :

$$D^{\delta} \propto \frac{\sigma_{ion} \times \sigma_{e}on}{\sigma}\left(\frac{\chi_{ion}}{c_{ion}} + \frac{\chi_{eon}}{c_{eon}}\right) \tag{4.1}$$

where c_{eon} and c_{ion} are the concentration of the electronic and ionic carriers. The χ?factors describe internal trapping reactions, which are usually crucial at the temperature of operation. If we assume $\sigma_{ion} > \sigma_{eon}$ and $c_{ion} > c_{eon}$ for NASICON materials,

$$D^{\delta} \propto \chi_{eon} D_{eon} \tag{4.2}$$

which means that D^{δ} is determined by the electronic mobility (proportional to D_{eon}) and trapping reactions (χ factors).

4.5 Electrode Materials from NASICON materials

The choice of cathode is a critical component in making the SIB competitive. The Nasicon class of materials has been explored for both Electrolytic and Electrodic performances, and their framework-oxide type morphology has fuelled a deep interest utilising them for building cathodes. The highly covalent 3-dimensional network has a large number of interstitial spaces, through which Na ions can diffuse. $Na_3V_2(PO_4)_3$ is by far the best NASICON type material, delivering a highly reversible specific capacity of 110 $mAhg^{-1}$ and two voltage plateaus of 3.3 - 3.4 V associated with the V^{4+}/V^{3+} couple and 1.6 V, associated with the V^{3+}/V^{2+} couple[18]. So it can be used as both cathode and anode; the higher voltage rendering it applicable as a cathode and the lower potential allowing it to be an anode. This multifunctionality can be beneficial in diverse situations that have material specificity over a voltage range. $Na_3V_2(PO_4)_3$ has been synthesized by solution-based carbothermal reduction (S-CTR) method 17 and also by solid state reaction method, employing Citric acid as the source of carbon to reduce the oxidation state of Vanadium.

Based on time-dependent experiments, an outside-in self sacrificed morphological evolution mechanism from microsphere to 3D nanofiber network has also been proposed W. Ren et al. The $Na_3V_2(PO_4)_3$ exhibits a superior cycling ability and rate capability. The discharge capacity re-

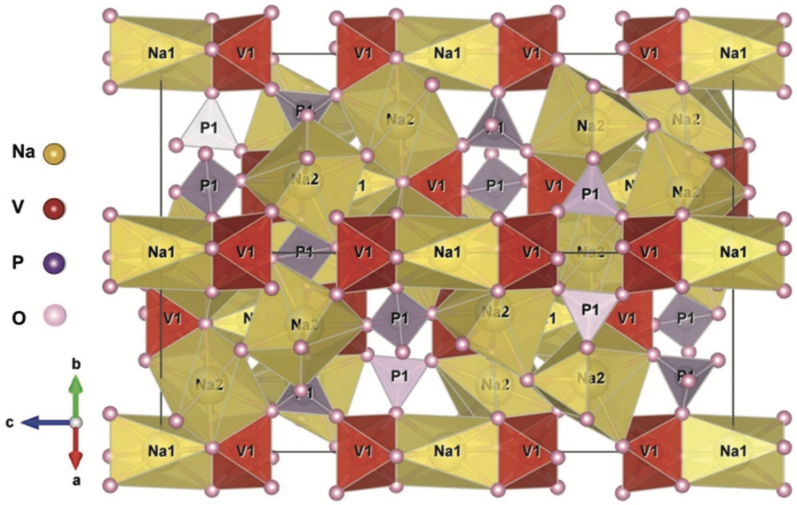

Figure 4.14: Crystal structure of NVP (*Adapted from Challenges and Perspectives for NASICON-Type Electrode Materials for Advanced Sodium-Ion Batteries, Shuangqiang Chen et al; Advanced Materials 2017*

tains 74.3% of the discharge capacity of its first cycle with coulombic efficiency of 99.3% after 100 cycles. The discharge capacity of $Na_3V_2(PO_4)_3$ at 10 C is 48.87 $mAhg^{-1}$,4 which is 58.4% of the cell cycled at 0.1 C. Furthermore, the structure of $Na_3V_2(PO_4)_3$ is stable for a considerable amount of Na^+ ions (2 mol of Na+ ions) insertion and extraction with only 0.42% difference of unit-cell volume between fully charged and discharged states.

It is obvious that the capacity will be affected by the number of Na ions migrating from the interstitial sites, though there are multiple possibilities for the occupation of these sites.

4.5.1 Structure of NVP

The **rhombohedral** $Na_3V_2(PO_4)_3$ (NVP) is characterized by space group R3c and offers an open framework via NASICON structure. The basic constituents of the framework structure are $[VO_6]$ octahedra and

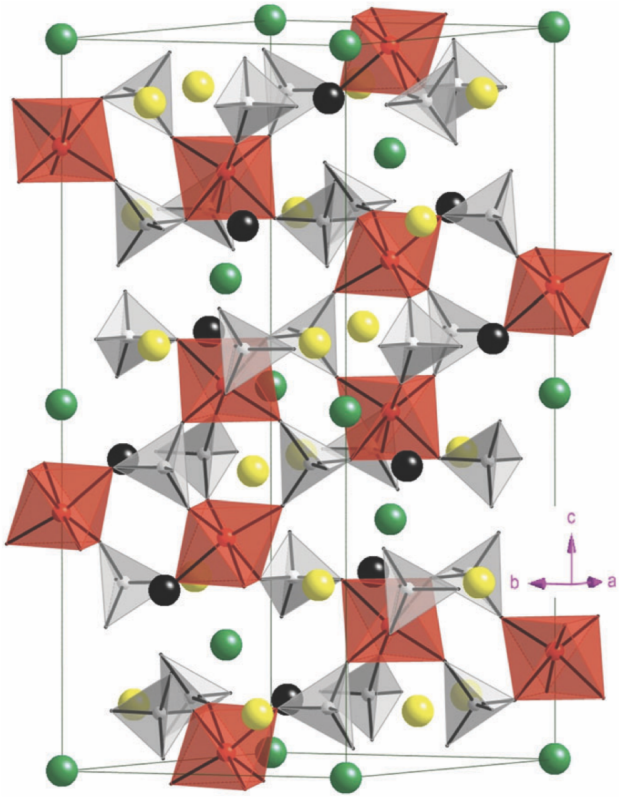

Figure 4.15: Crystal structure of NVP. Na at the Na(1) site are shown by green balls, Na at the Na(2) site by yellow balls and the empty Na sites by black balls. The V octahedra are shown in red and the P tetrahedra in grey. (*adapted from Hybrid functional study of the NASICON-type* $Na_3V_2(PO_4)_3$*: crystal and electronic structures, and polaron-Na vacancy complex diffusion, K.M Bui et al. PCCP, 2015 [19]*)

.

[PO4] tetrahedra interlinked via corner-sharing to form the polyanion $[V_2(PO_4)_3]$ units along the c-axis. (Figure 6.14 displays the structure of NVP with the lattice parameters a = b = 8.728 and c = 21.804). The octahedral $[VO_6]$ and corner shared [PO4] create ***Lantern units*** which offer a three-dimensional route for the Na ions to migrate.

Each primitive cell of NVP contains 6 formula units built from the $[V_2(PO_4)_3]$ and 2 different Oxygen environments for Sodium - 6-fold co-ordinated Na(1) site between two adjacent $[V_2(PO_4)_3]$ units along the z-axis and 8-fold coordinated Na(2) site at the same z value as the P

atoms between two PO_4 tetrahedra.

Houria and Soo report[19], that if all of the Na(1) and Na(2) sites are occupied by Na ions (one Na(1) and three Na(2) sites), 4 cations could be hosted in the voids per formula unit of $Na_4V_2(PO_4)_3$. Theoretically the capacity of such an arrangement would be pretty high - 236 $mAhg^{-1}$, with respect to the extraction of 4 Na ions. However, the oxidation state of V in $Na_4V_2(PO_4)_3$ is +2 which is highly unstable. Thus, $Na_3V_2(PO_4)_3$ having a stable V^{3+} state is more favourable with respect to synthesis. This structure has one Na(1) and two Na(2) sites, i.e. 3 mobile Na sites.

4.5.2 Na Ion Migration in NVP Crystal

It was proposed by K.M. Bui[19] for the first time that the ion diffusion mechanism in NVP crystal can be explained by a polaron-Na vacancy complex model. The bound polaron forms at the first nearest V site to the Na vacancy. Consequently, the movement of the Na vacancy will be accompanied by the polaron. Therefore, the Na diffusion should be treated as diffusion of the polaron-Na vacancy complex. There can be three preferable diffusion pathways -two intra-layer diffusion pathways and one inter-layer pathway. The activation barriers for the intra-layer and inter-layer pathways are 353 meV and 513 meV, respectively[19]. Theoretical calculations using hybrid functionals like HSE06 and onsite Coulomb Hubbard corrected GGA functionals have confirmed the same[17].

Despite many advantages associated with $Na_3V_2(PO_4)_3$, such as high stability and relatively high voltage, low conductivity is still the key drawback to its commercial application. In the past few years, researchers have investigated many different ways to overcome this

problem, mainly concentrating on optimizing the synthetic strategies, surface conducting modifications, element doping, and so forth. To improve the rate capability and cycling ability of $Na_3V_2(PO_4)_3$, various strategies, such as doping other elements, coating carbon using various carbon resources, and reducing the particle size, have been suggested. Lim et al. reported that substituting a part of sodium by potassium can enhance the cycling ability of $Na_3V_2(PO_4)_3$. Using glucose as a carbon precursor to synthesize $Na_3V_2(PO_4)_3$ helps reduce the particle size to $<$ 300 nm, which dramatically increases rate capability, and the material continues to retain discharge capacity of 60 mAh g 1 at 30 C.

In our work, we begin with the simulation of the template system $Na_3V_2(PO_4)_3$ and perform fundamental electronic calculations on it. This is followed by systems having the same morphology as NVP, but significant amount of doping. First principles calculations have been performed on $Na_3FeV(PO_4)_3$, $Na_3FeV(PO_4)_3$, $Na_4MnV(PO_4)_3$, $Na_3TiV(PO_4)_3$ and $Na_3NbV(PO_4)_3$, to check their relative stabilities, intrinsic electronic properties and also Na ion diffusion.

4.6 Computational Methods

First principles Density Functional Theory calculations as implemented in Quantum Espresso 6.2[20,21] set of codes was used to study the class of NASICON systems. All atoms were treated under a plane wave basis set, with an energy cutoff of 300 Ry to represent valence electrons. PBE (Perdew-Burke-Ernzerhorf)[22] functional under GGA(Generalized Gradient Approximation)[23] was used to treat exchange correlations. Ultrasoft pseudopotentials developed by Vanderbilt[24] was used to

approximate the interactions between core electrons and nucleus of Na, V, Fe, Mn, Ti, Nb and P atoms and Ultrasoft pseudopotentials was used for O atoms. A Monkhorst Pack grid of $3 \times 3 \times 3$ was used to sample the Brillouin Zone. All structures were designed and visualized using GaussView 5.0 and XCRYSDEN[25]software. All the systems were optimized until the total force reduced to 0.02eV/atom.

The unit cell taken for calculations consists of 126 atoms, with 12 V atoms and 24 Na atoms.

4.7 Structure

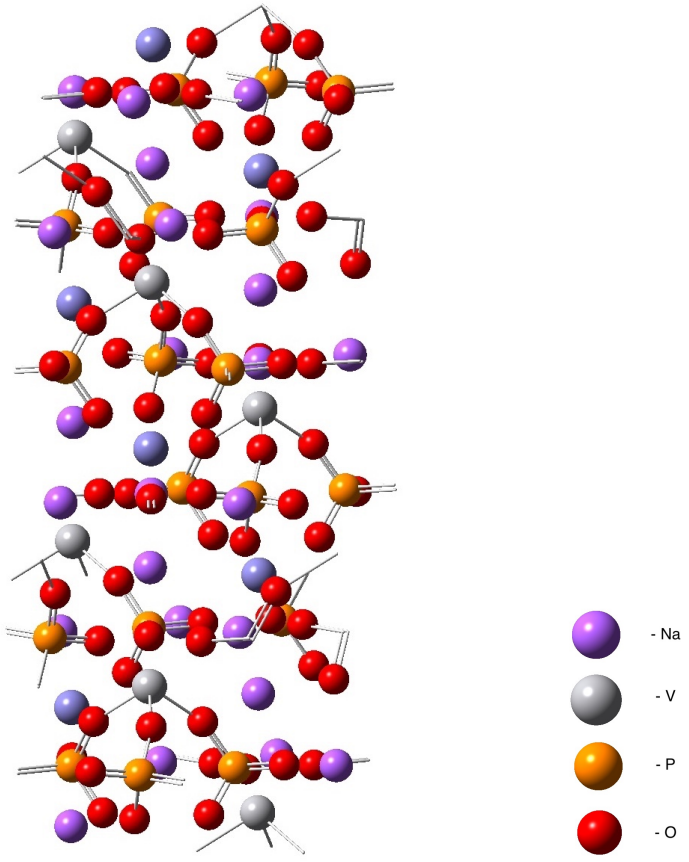

Figure 4.16: Optimized structure of $Na_3V_2(PO_4)_3$

The geometrical parameters of the structures obtained from optimization

of the crystal systems are **a = b = 8.7288 Å** and **c= 21.804 Å** which bears good resemblance with previously reported structures. A total of 8 $V_2(PO_4)_3$ units were discernible. Figure 4.16 describe the optimized crystal structures of $Na_3V_2(PO_4)_3$.

After obtaining the optimized structure of $Na_3V_2(PO_4)_3$, the structures were doped by replacing 6 of the V atomic sites by Fe,Mn,Ti and Nb atoms respectively, to maintain a 1:1 concentration ratio between V and the dopant atoms. The resultant structures were further optimized to obtain stable crystal systems as shown in Figure 4.17 (a) and (b) for $Na_3FeV(PO_4)_3$, $Na_4MnV(PO_4)_3$, and Figure 4.18 (a) and (b) for $Na_3TiV(PO_4)_3$ and $Na_3NbV(PO_4)_3$ respectively.

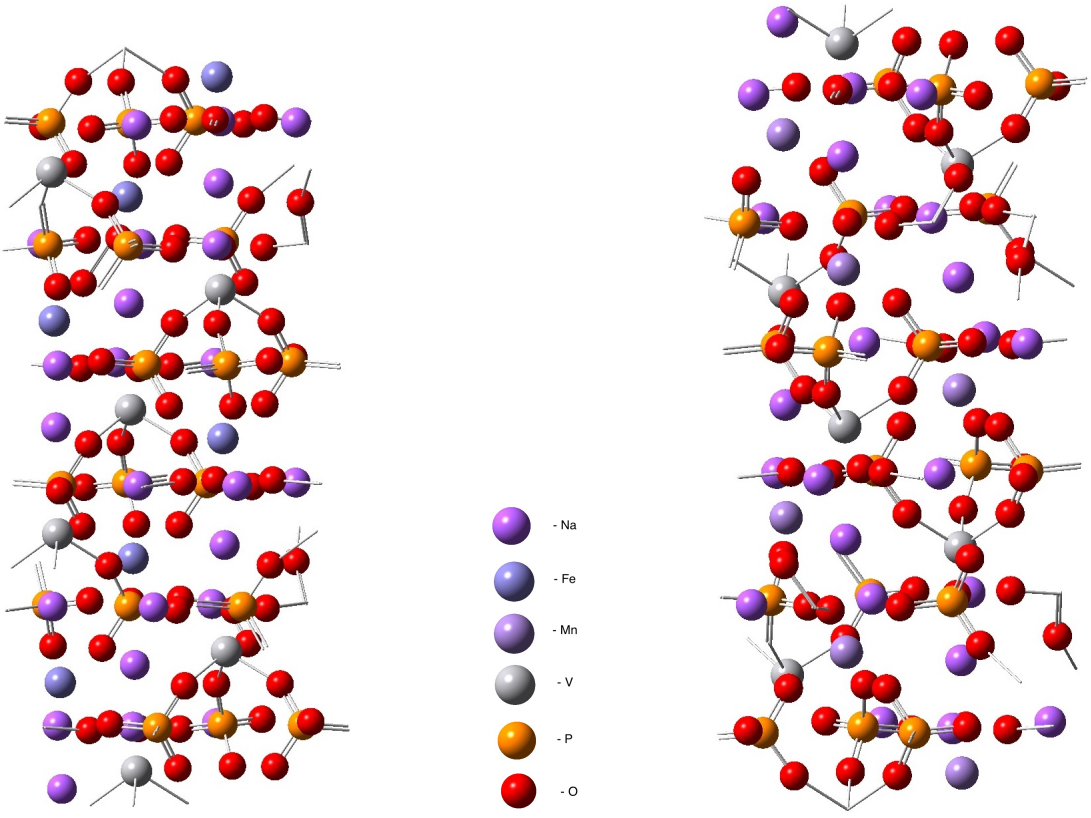

Figure 4.17: (a) Optimized structure of $Na_3FeV(PO_4)_3$ (b) $Na_4MnV(PO_4)_3$

It should be noted here that the stable oxidation state of Fe, Ti and Nb atoms is +3 while that of Mn is +2 in the respective crystal systems, to maintain charge neutrality with V atom in the +3 state.

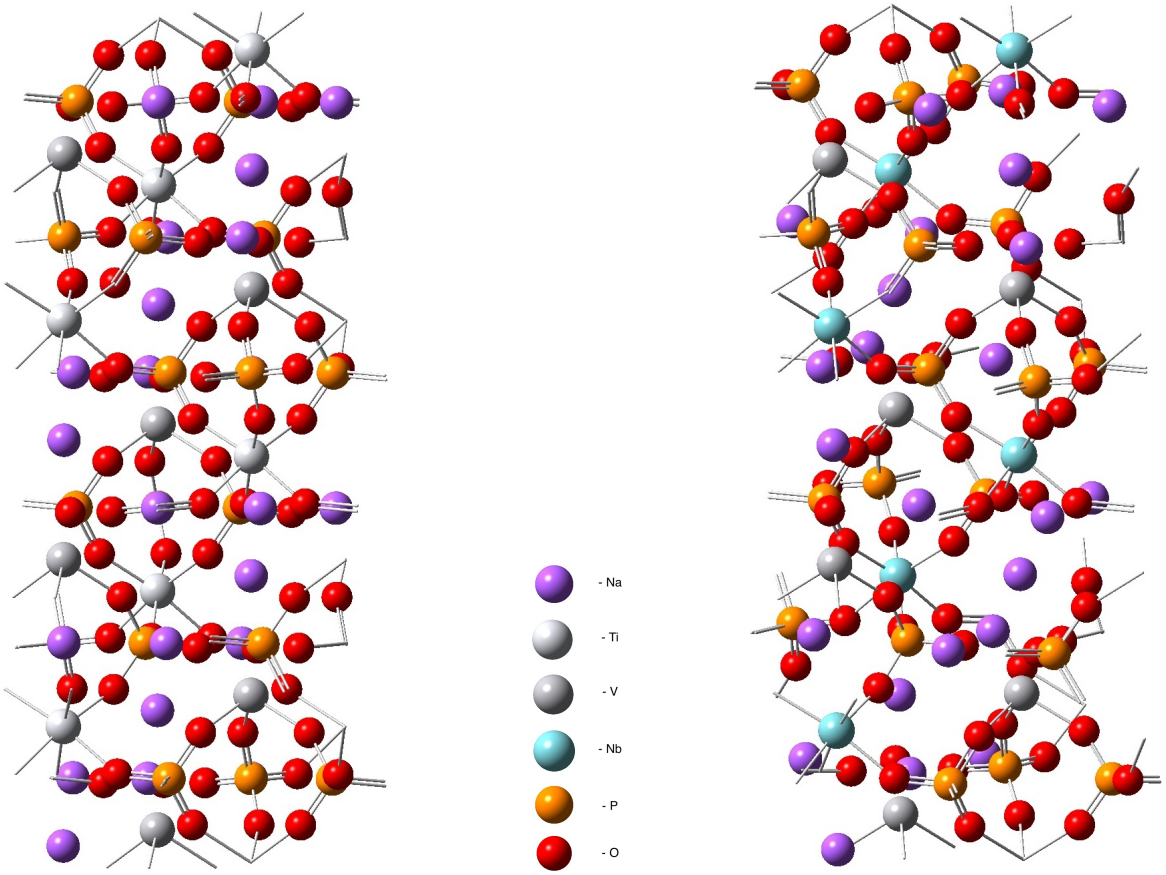

Figure 4.18: (a) Optimized structure of $Na_3TiV(PO_4)_3$ (b) $Na_3NbV(PO_4)_3$

4.8 Results and Discussion

4.8.1 Electronic Properties

In terms of stability, the ground state energies were seen to decrease on moving from Ti to Fe. From GGA calculations the band gaps are

observed to vary from 3.1 to 1.75 eV, as one moves across the period from Ti to Fe.

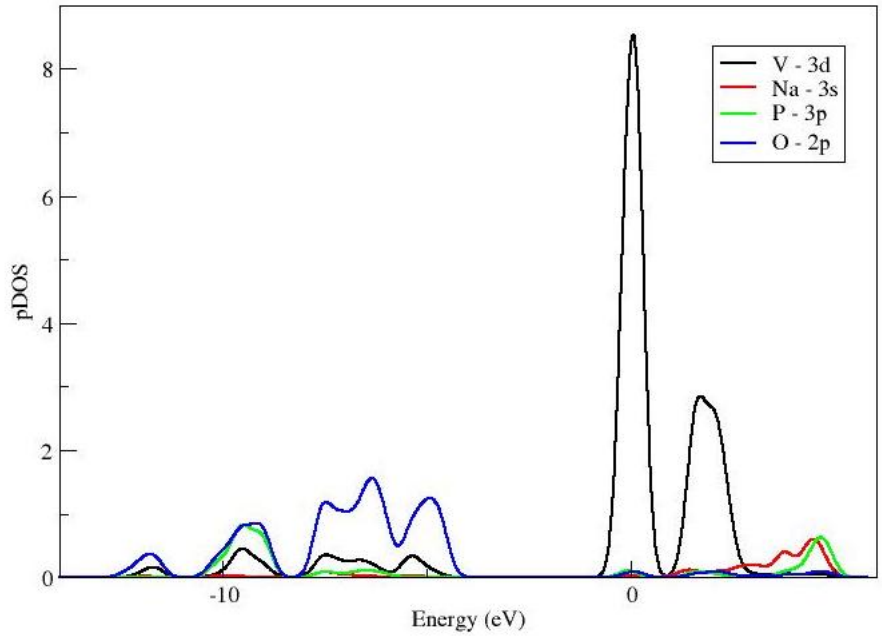

Figure 4.19: Projected Density of States for $Na_3V_2(PO_4)_3$ crystal system.

To elucidate the contribution of each atom near the Fermi Level, the projected density of states (PDOS) is a useful tool. It is evident from the pDOS plot in Figure 4.19 that, the low-lying energy states of $Na_3V_2(PO_4)_3$ have fair amounts of contribution from the 3d orbitals of Vanadium, 3s orbitals of Sodium, 3p orbitals of Phosphorus and 2p orbitals of Oxygen atoms. However at the Fermi Level (scaled as Zero of energy) and beyond (i.e. the conduction states), the density of states of the 3d orbitals of the Vanadium atoms, shoots up. There is partial contribution from the orbitals of Phosphorus and Oxygen atoms. But the contribution from the outer 3s orbital of Sodium is almost negligible. This indicates that the system is electronically metallic, the metallicity

owing to the Vanadium electrons solely.

Most importantly, the pDOS plots help to shed light on the nature of bonding present in the system and it suggests that the Na atoms are loosely bound to the crystal near the Fermi level. In other words, the Na atomic sites can be called "labile", and Na atoms can be easily extracted. This is a useful observation, since the performance of any electrode depends on the rate of intercalation/de-intercalation, or diffusion of the active species.

On doping the $Na_3V_2(PO_4)_3$ crystal system with Fe, Mn, Ti and Nb, the general nature of the pDOS plots (Figures 4.20, 4.21, 4.22, 4.23) does not vary significantly. The sole difference lies in the fact that along with Vanadium, the dopant metal also becomes responsible for metallicity, as proved by the prominent peaks owing to the 3d orbitals of V and the dopant metal atoms at the Fermi level.

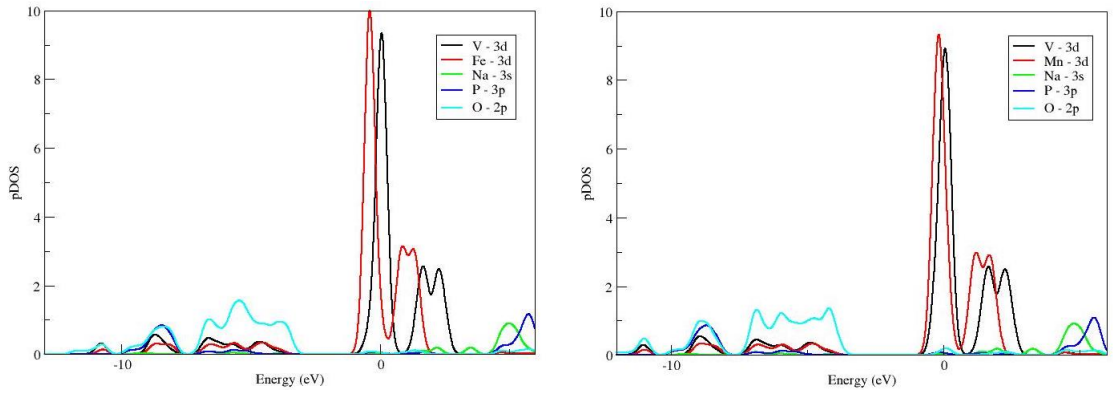

Figure 4.20: Projected Density of States Plots of (a) $Na_3FeV(PO_4)_3$ (b) $Na_4MnV(PO_4)_3$

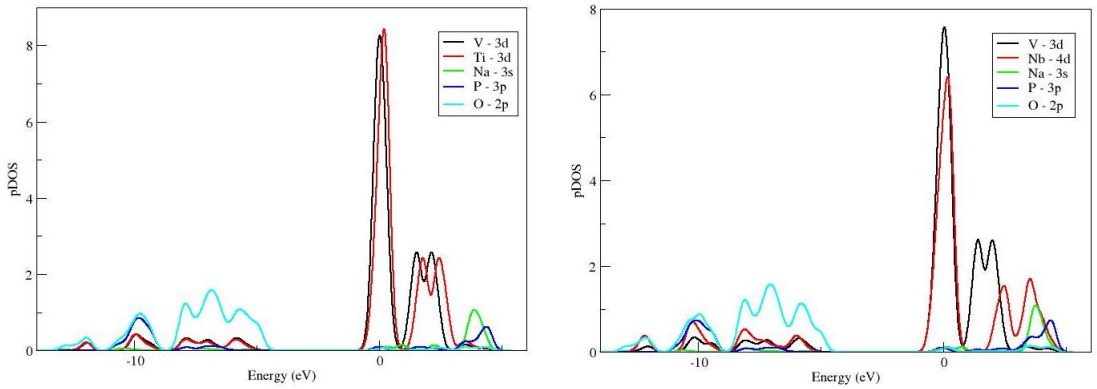

Figure 4.21: Projected Density of States Plots of (a) $Na_3TiV(PO_4)_3$ (b) $Na_3NbV(PO_4)_3$

Another important observation from the pDOS plots is that the density of states of the 3d orbitals of Vanadium and the other transition metals become more segregated and distinct as we move from Ti to Fe doping. While the peaks corresponding to the 3d orbitals of Ti and Nb have a maximal overlap with that of V, the overlap reduces in Mn and the peaks become distinctly separate in case of Fe. This is a natural transition, owing to the electronegativity difference existent across the period from Vanadium, with Ti and Nb having lesser difference and Mn and Fe having a greater difference. The metallic nature of atoms reduce from left to right, which is also evident from the position of the 3d peaks. For Fe and Mn, a shift of the peaks toward the left of the peak corresponding to V 3d orbitals, is discernible, whereas the peaks of Ti and Nb are at the same position as that of V.

4.8.2 Energetics of Sodium Diffusion

As previously mentioned, there are 12 sites for Transition Metal atoms and 24 Sodium atomic sites, out of which 8 phosphate units can be discerned. It is known that there are 2 types of sodium sites :

1. Na(1) between two $V_2(PO_4)_3$ sites and

2. Na(2) having the same z coordination as two P atoms. There is one site (A) of type 1 and three sites (B,C,D) of type 2. We find 4 Na atoms corresponding to each of the A,B,C and D sites and begin to extract Na atoms from each site successively. The energy change in each process is calculated as :

$$\Delta E = E(M - Na_n) - E(M - Na_{n-x}) - x \times E(Na) \tag{4.3}$$

where $E(M - Na_n)$ is the ground state energy of the initial system with all Na atoms intact; $E(M - Na_{n-x})$ is the energy of the system after extracting x Na atoms and $E(Na)$ is the energy of the stablest state of Na. As Na is known to crystallize in a BCC (body-centred cubic) lattice, it is expected to be the stablest morphology of Na. The ground state energy of a Na BCC crystal was calculated and halved, to get a per-atom energy value. Then, using Equation (5.3), an estimate of the diffusion energy was obtained.

Additionally, voltage of these systems was calculated using equation 4.4, in which the diffusion energy was divided by the number of Na atoms removed (x) multiplied by the charge on a single electron (e).

$$V = \frac{\Delta E}{x \times e} = \frac{E(M - Na_n) - E(M - Na_{n-x}) - x \times E(Na)}{x \times e} \tag{4.4}$$

On removing one Na atom from $Na_3MV(PO_4)_3$ to make $Na_2MV(PO_4)_3$, (M=V, Fe, Mn, Nb, Ti), to maintain charge neutrality, the oxidation state of V changes from +3 to +3.5; there might be another scenario, that out of the 2 V atoms, (in $Na_3V_2(PO_4)_3$) one V^{3+} is oxidized to V^{4+}, and the other one remains as V^{3+}. This can also occur in the doped

systems, and the feasibility would be determined by the Ionization Potentials of both the Transition metals in the formula units.

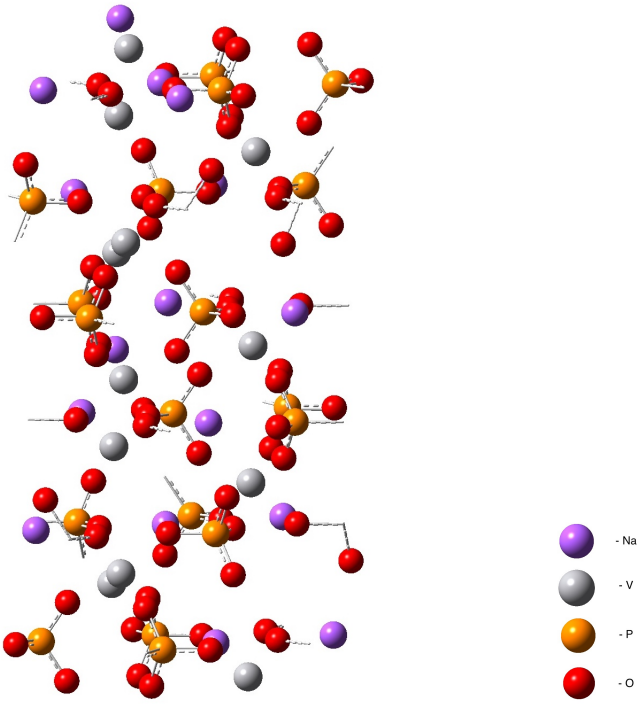

Figure 4.22: Structure of $Na_3V_2(PO_4)_3$ after removing 8 Na atoms from A and C sites.

On removing two Na atoms from $Na_3MV(PO_4)_3$ to make $NaMV(PO_4)_3$, the oxidation state of V changes from +3 to +4 and on removing all three Na atoms from $Na_3MV(PO_4)_3$ to make $MV(PO_4)_3$, the oxidation state of V changes from +3 to +4.5. We looked at each transition and calculated the change in energy involved. It is noteworthy to mention here, that the total number of Na atoms that could be possibly removed is 12 (4 $\times$ 3 Na per formula unit). So, for each transition, a total of 4 Na atoms would be involved. However for the $Na_4MnV(PO_4)_3$ system, in order to observe the transition from V^{3+} to V^{4+}, an additional Na atom should be removed (i.e. 3 Na atoms per formula unit), so 12 Na were removed.

Crystal System	ΔE_1(eV)	x_1	(V_1)	ΔE_2(eV)	x_2	(V_2)	ΔE_3(eV)	x_3	(V_3)
$Na_3V_2(PO_4)_3$	0.473	1	1.61	25.02	2	3.13	-	-	-
$Na_3FeV(PO_4)_3$	0.264	1	0.90	27.88	2	3.48	-	-	-
$Na_4MnV(PO_4)_3$	0.344	1	1.17	42.43	2	2.68	3.12	3	3.54
$Na_3TiV(PO_4)_3$	0.644	1	2.19	33.05	2	4.13	-	-	-
$Na_3NbV(PO_4)_3$	0.711	1	2.42	35.77	2	4.47	-	-	-

Table 4.2: Diffusion energy changes, Number of Na atoms removed and Voltage of the 5 NASICON systems.

Since there are three types of Na(2) sites, B,C and D there can be six possible mechanisms of Na extraction. These would be from sites A-B, A-C, A-D, B-C, B-D and C-D. We performed extractions from A-B, A-C and A-D sites respectively and optimized the resultant structures. It was found that, the structures with Na(A-B) and Na(A-D) extractions were more stable than the those with Na(A-C) removals. So, it is suggested that the B and D sites are more stable compared to the C sites and thus, less favourable for Na extraction. The Na at C-site is more labile and can easily diffuse in and out of the system. For $Na_4MnV(PO_4)_3$, 3 Na were removed from A, B and C sites respectively.

The energy changes and the net voltage corresponding to each transition were calculated and are reported in Table 4.2, with ΔE_i corresponding to the energy change in each transition, x_i being the number of Na atoms removed per formula unit and V_i being the net voltage generated.

The above values clearly indicate that the voltage delivered can be improved by doping the pure $Na_3V_2(PO_4)_3$ by transition metal dopants. While it is understandable, that for pure $Na_3V_2(PO_4)_3$, removal of each Na atom results in a redox transition of 0.5 units ($3 \rightarrow 3.5 \rightarrow 4 \rightarrow 4.5$), the scenario for the doped systems remains debatable, as to which redox transition takes place precisely. The electronic environment created by

the dopants can be different from the pure system, which is our further quest of investigation. Doping with Fe or Mn is observed to generate voltages that compare well with previously reported experimental results[26]. However, the voltages generated with Ti and Nb doping, are significantly higher. We suggest that the additional 1.34 V (4.47 V - 3.13 V) obtained from Nb doping, corresponds to a Nb^{4+}/Nb^{3+} redox couple.[?]. Further calculations on the electronic transitions, kinetics and mobility of Na species in these systems are ongoing and are expected to shed more light on the electrochemistry of these systems. At this level, it is recommended that Ti and Nb doping on V bear the prospect of designing cathode materials with better outputs.

4.9 Conclusion

In this chapter, we studied 5 NMV type NASICON crystal systems, pure $Na_3FeV(PO_4)_3$ and doped $Na_3FeV(PO_4)_3$, $Na_4MnV(PO_4)_3$, $Na_3TiV(PO_4)_3$ and $Na_3NbV(PO_4)_3$. Calculations on Projected Density of States reflect upon their intrinsic electronic structure. Although in terms of structural stability, the Fe-doped system is the most promising, having the lowest energy, it might not prove to be as efficient as the other systems with respect to cathodic functions, i.e. active species migration. Interestingly enough, calculations on changes in energy in the initial and final Na-extracted systems, reveal that Ti and Nb doping generates a high voltage of 4.13 V and 4.47 V respectively, which is the highest among reported voltages in NMV type NASICON cathodes. From this juncture, more advanced levels of theoretical calculations and efficient experimental strategies, are thus required to design a high-performance electrode suitable for Sodium-ion batteries.

References

[1] K. Mitzushima, P.C. Jones, P.J. Wiseman, J. Goodenough, *Materials Res. Bull.*, 1980, **15**, 783.

[2] J.B. Goodenough, K-S Park, *J.Am.Chem.Soc.*, 2013, **135**, 1167.

[3] T.W. Johnson, D.J. Grzybowski, M.A. Kubale, J.J. Rosenbecker, K.F. Scheucher, G.D. Meyer, J.M. Zeller, K.L.Glasgow, ?Lithium based battery pack for a hand-held power tool?, U. S. Pat. 7,554, 290, 30 June (2009).

[4] www.molicel.com/hq/.

[5] http://www.radio-electronics.com/info/power-management/battery-technology/lithium-ion-battery-advantages-disadvantages.php

[6] http://www.versiondaily.com/lithium-ion-battery-advantages-disadvantages/

[7] M.Sawicki, L.L.Shaw, *RSC Adv.*, 2015, **5**, 53129.

[8] J-Y.Hwang, S-T.Myung, Y-K.Sun, *Chem. Soc. Rev.,* 2017,**46**, 3529-3614.

[9] H. Aono, N. Imanaka, G. Adachi *Acc Chem Res*, 1994, **27**: 265 and references there in

[10] N. Weber, J.T. Kummer, *Proc. Annu. Power Sources Conf.*, 1967, 21:37

[11] M.S. Whitingham, R.A. Huggins, *J.Che.Phys.*, 1971, **54**, 414.

[12] H.Y.P. Hong, *Mater.Res.Bull.*, 1976, **11**, 173.

[13] J.B. Goodenough, H.Y.P Hong, J.A. Kafalas, *Mater. Res. Bull.*, 1976, **11**, 203.

[14] H.L. Ove, K. Peder, *Acta Chem Scand*, 1968, **22**, 1822.

[15] N. Anantharamulu, K. Koteswara Rao, G. Rambabu, B. Vijaya Kumar, Velchuri Radha, M. Vithal, *J. Mater. Sci.* 2011, **46**, 282.

[16] J.Maier, *J.Am.Ceram.Soc.*, 1993, **76**, 1212

[17] S. Chen, C. Wu, L. Shen, C.Zhu, Y.Huang, K.Xi, J.Maier, Y.Yu, *Adv. Mater.*, 2017, **29**.

[18] W.Song, X. Cao, Z.Wu, J.Chen, K.Huangfu, X.Wang, Y.Huang, X.Ji, *Phys.Chem.Chem.Phys*, 2014, **16**, 17681.

[19] K.M.Bui, V.A.Dinh, S.Okada, T.Ohno, *Phys.Chem.Chem.Phys.*, 2015, **17**

[20] P. Giannozzi, S. Baroni, N. Bonini, M. Calandra, R. Car, C. Cavazzoni, D. Ceresoli, G. L. Chiarotti, M. Cococcioni, I. Dabo, A. Dal Corso, S. Fabris, G. Fratesi, S. de Gironcoli, R. Gebauer, U. Gerstmann, C. Gougoussis, A. Kokalj, M. Lazzeri, L. Martin-Samos, N. Marzari, F. Mauri, R. Mazzarello, S. Paolini, A. Pasquarello, L. Paulatto, C. Sbraccia, S. Scandolo, G. Sclauzero, A. P. Seitsonen, A. Smogunov, P. Umari, R. M. Wentzcovitch, J.Phys.:Condens.Matter 21, 395502 (2009)
http://dx.doi.org/10.1088/0953-8984/21/39/395502.

[21] P Giannozzi, O Andreussi, T Brumme, O Bunau, M Buongiorno Nardelli, M Calandra, R Car, C Cavazzoni, D Ceresoli, M Cococ-

cioni, N Colonna, I Carnimeo, A Dal Corso, S de Gironcoli, P Delugas, R A DiStasio Jr, A Ferretti, A Floris, G Fratesi, G Fugallo, R Gebauer, U Gerstmann, F Giustino, T Gorni, J Jia, M Kawamura, H-Y Ko, A Kokalj, E Kkbenli, M Lazzeri, M Marsili, N Marzari, F Mauri, N L Nguyen, H-V Nguyen, A Otero-de-la-Roza, L Paulatto, S Ponc, D Rocca, R Sabatini, B Santra, M Schlipf, A P Seitsonen, A Smogunov, I Timrov, T Thonhauser, P Umari, N Vast, X Wu and S Baroni, *J.Phys.Condens.Matter*, 2017, **29**, 465901.

[22] J.P.Perdew, K. Burke, M. Ernzerhorf, *Phys. Rev. Lett.* 1996, **77**, 3865.

[23] S. Grimme, *J. Comput. Chem.* 2006, **27**, 1787.

[24] D. Vanderbilt, *Phys. Rev. B*, 1990, **41** 7892.

[25] A. Kokalj, *Comput. Mater. Sci*, 2003, **28**, 155; XCRYSDEN code; http://www.xcrysden.org

[26] W.Zhou, L.Xue, X.Lu, H.Gao, S.Xin, G.Fu, Z.Cui, Y.Zhu, J.B. Goodenough, *Nano Lett.* 2016, **16**, 7836.

[27] S. Y. Lim, H. Kim, R. A. Shakoor, Y. Jung and J. W. Choi, *J. Electrochem. Soc.*, 2012, **159**, A1393.

[28] L. Kong, C. Zhang, J. Wang, W. Qiao, L. Ling D. Long, *Scientific Reports*, 2016 ,**6**.

5

Summary and Future Outlook

The science of materials is really a "multi-dimensional" arena encompassing several disciplines. The role of a material scientist is to intelligently amalgamate diverse attributes of already existing, available or synthesized materials and develop them into new advanced systems, that could be tailored to suit specific applications in modern technology. The fascinating reality of materials is the fact that their nature varies significantly when they are allowed to explore different dimensions, but at the fundamental atomistic level, the subatomic particles constituting any material remain the same. This intricate relationship between the microscopic structure and macroscopic manifestations is a rather demanding subject of study.

Ever since Max Planck's proposition of Quantum theory, as the science that deals with the smallest imaginable scales of energy levels of atomic/subatomic particles, the field has been met with both intrigue and skepticism. Under quantum mechanics, objects can never have well defined positions, much in contrast with the classical systems surrounding us. However, it succeeds in holding up to many experiments that classical mechanics cannot explain. Quantum theory of materials

has been expanding ever since its birth in the 1920s, and Yale Prof Jack Harris's remark, in this regard *"Quantum effects aren't really a limitation. They're a resource to our knowledge. "* bears enough proof of the eminence of this theory.

On this train of thought, quantum mechanistic studies find huge application in the design of materials that can be embraced by future predicaments. From the past few decades, extensive research is being carried out to generate solutions for our demanding lifestyles. From the nano to macro scales, these solutions are aimed at efficient utilization of resources, conservation techniques and development of alternate, sustainable technologies that have minimum detrimental impacts on our environment. Theoretical predictions often help to ease and fasten this pursuit.

As described generically in the title, this thesis recounts computational investigations of some materials at different dimensions. While low dimensional systems exhibit many exciting phenomena, the study of materials in higher dimensions will help to quickly bridge the gap between the predicted and the perceivable. Our investigations on low dimensional Black Phosphorene Quantum Dots, Arsenene Quantum Dots and sheets and Germanane nanosheets, project these systems as functional materials. Having high flexibility, absorption in the mid-IR to visible region and optimum band gaps, they can find potential applications in semiconductor devices, light-operated electronics, IR absorbers, energy harvesters and photocatalysts. The studies on three dimensional materials were carried out with the aim of developing productive EES (Electrical Energy Storage) systems and our findings suggest new routes which need further exploration.

In the light of the present conclusions drawn from our work, it is safe to disclaim that only a fundamental framework has been established so far. It is a belief that ongoing calculations based on detailed electronic scenario and photophysical aspects would shed more light on the layered semiconducting systems; ion transport mechanisms, electrochemical capacities, and migration kinetics would help us to establish this class of Nasicon systems as reliable and effective components of energy storage devices.